Abstract

Durability and safety of concrete structures are fully governed by mechanical properties. This is especially true at early age, when cement matrix is not yet fully developed, and phase arrangement becomes critical for understanding mechanical behavior. This factor can be thouroughly examined only with the use of numerical models.

This study is specifically focused on the prediction of effective elastic properties of cement paste by Finite Element method (FEM) based on its microstructure. The 3-D microstructure is an output of a vector microstructural model. Up to 5 million of overlapping spheres can exist in the computational volume of cement paste. The geometrical representation for FEM computation therefore becomes a challenge.

In this study, at first, specific aspects of the FEM are investigated with respect to the early age microstructure. Mesh for such a complex microstructure poses a challenge, simplifications of the geometry have to be accepted. Sensitivity to mesh type, resolution, integration scheme and size of computational volume is tested. The most important factor in the prediction is identified as artificial connectivity, which is a result of insufficient resolution. It causes substantial overestimation of elastic properties at the beginning of hydration. A scheme to partially treat this effect is presented.

In the second part of the work, the model is applied to study variations of microstructural parameters. These include the effect of flocculation, water/cement ratio, particle size distributions and number of hydrate clusters. It is shown, that the model is able to capture the differences in microstructural arrangements despite the resolution limitations, verified experimentally. As such, the model has the capability to be used for explanation of anomalies in the material structure.

Keywords: Finite Element method, microstructure, cement paste, elastic properties

Zusammenfassung

Die Dauerhaftigkeit und Sicherheit von Betonbauten werden durch die mechanischen Eigenschaften von Beton bestimmt. Dies ist besonders der Fall in frühen Alter, wenn die Zementmatrix noch nicht voll entwickelt ist. In diesem Stadium ist die Phase Anordnung kritisch für das Verständnis der mechanischen Verhalten. Numerische Modelle bieten für die gründliche Analyse solche Probleme vielversprechende Möglichkeiten.

In dieser Arbeit wird eine auf Finite-Elemente-Methode (FEM) basierende Methode beschrieben, die speziell auf die Vorhersage der effektiven elastischen Eigenschaften von Zement-Paste auf der Grundlage ihrer Mikrostruktur angestimmt ist. Die dazu benötigte 3-D Mikrostruktur wird von einem 3-D Modellprogramm erzeugt. So ein Modell kann von bis zu 5 Millionen überlappenden Sphären bestehen. Die Verarbeitung von solchen riesigen Datenstrukturen kann für die FEM-Berechnung eine echte Herausforderung werden.

Im ersten Teil dieser Arbeit, werden die spezifische Aspekte der FEM in Bezug auf die Mikrostruktur im frühen Beton Alter untersucht. Die erste Schwierigkeit ist die Maschenerzeugung für eine so komplexe Mikrostruktur. Deshalb muss man Vereinfachungen der Geometrie akzeptieren. In dieser Arbeit werden verschiedene Parameter der Modellierung wie Maschentyp, Auflösung, Integrations System und die Grösse der Berechnungsvolumen, untersucht. Diese Untersuchung zeigte das der wichtigste Faktor bei der Vorhersage von elastischen Eigenschaften, infolge unzureichender Auflösung enstehende künstliche Verbindungen sind. Diese Verbindungen verursachen erhebliche Überschätzung der elastischen Eigenschaften am Anfang der Hydration. Ein Verfahren dass dieses Problem teilweise behandelt, wird auch vorgestellt.

Im zweiten Teil der Arbeit wird das Modell angewandt, um Variationen der mikrostrukturellen Parameter zu untersuchen. Dazu gehören die Wirkung der Flockenbildung, Wasser-Zement-Verhältnis, Partikelgrössenverteilung und die Anzahl der Hydrat-Gruppen. Es wird gezeigt, dass das Modell in der Lage ist, die Unterschiede in der Mikrostruktur Parameter, trotz der begrenzten Auflösung zu erfassen. Damit bietet dieses Modell die Möglichkeit, für die Erklärung von Anomalien in der Beton

Strukturen zum Einsatz zu kommen.

Schlagwörter: Finite Element Methode, Mikrostruktur, Zement-Paste, Elastische Eigenschaften

Acknowledgments

The author is grateful to the European Community under the Marie Curie Research Training Network MRTN-CT-2005-019283 - Fundamental understanding of cementitious materials for improved chemical physical and aesthetic performance - (http://www.nanocem.org/MC-RTN/) for the full support.

I also acknowledge Triazza, Plavna, Tasna, Rims, Arina, Nuna and Tina.

Contents

Chapter 1

Introduction

Mechanical properties of concrete, especially at early age play an important role for safety and future durability of structures. Efforts to predict them simply from the amount of components date back to the end of 19th century.

Today we know much more about concrete, we understand its multiscale nature and simultaneously a thorough background of solid mechanics is established for prediction of mechanical properties of heterogeneous materials. Yet, concrete differs from the majority of construction materials, because when put into construction, its mechanical properties are not fully developed and its behavior is therefore dependent on age. Therefore it is important to study its mechanical properties.

As soon as concrete is mixed during the construction process, it starts a rapid development phase which gradually slows down after few days and concrete reaches its safe phase. The first few days of concrete development are commonly referred to as the early age. While for the purpose of safety the knowledge of mechanical properties is needed at early age (1 - 7 days), mechanical properties of concrete are usually described by the compressive and bending strength at 28 days.

Efforts to explain mechanical properties by relating them to simpler properties, such as porosity, are rather unsuccessful. Dramatic variation of compressive strength for the same porosity were observed many times. Moreover, increasing demand exists on the use of supplementary cementitious materials (SCMs) - silica fume, fly ash and slag - the early age behavior of which is not very well understood. Therefore it is necessary to develop mechanical models, which will be able to explain the behavior

in terms of phase arrangement.

Elastic properties are responsible for short term deformation. Although elastic properties are not sufficient to explain mechanical behavior, they can help us understand the effects of microstructural properties more easily, because their prediction does not involve many unknown parameters.

To be able to improve overall properties of concrete, we should understand its multiscale nature. Concrete is studied in four different levels depending on the scale: concrete (centimeter scale), mortar (millimeter scale), cement paste (micrometer scale) and hydration product calcium-silicate-hydrate (nanometer scale). The physical properties are best examined at the lowest levels, however higher levels are needed to explain the structural behavior. The challenge is to extract the parameters from the lower levels to provide the input for the higher levels.

Physical properties are best explained with analytical expressions. For the late age, analytical schemes have been extensively used to predict the elastic properties. However, analytical schemes rely on a stable morphology, which is during the early ages still under development and therefore is not well-suited for analytical approaches. Moreover, analytical approaches have limited capabilities to distinguish between different material distributions within the same volume. The lack of a regular structure makes it very challenging to find analytical expressions to describe early age geometry. In this sense, numerical methods, specifically Finite Element method (FEM), represent an attractive alternative. The prediction methods for effective elastic properties of heterogeneous materials based on FEM are quite well developed.

1.1 Motivation and Objective

Finite Element method has been extensively used to study the properties of heterogeneous materials. Until recently, only few applications of FEM modelling at the cement paste level existed, and even fewer were used for the early age. To the best of my knowledge, the problems connected with determining early age properties by FEM are still unaddressed. This work is focused on the prediction of effective elastic properties on the cement paste level, at early age by Finite Element method.

In the Finite Element method a small volume of the material is taken and subdivided into finite elements. The number of subdivions effectively determines the resolution of the analysis. Since the volume is in 3-D, the problem scales in the cube of the resolution. The consequence is, that the limits of the practical computational cost are quickly reached.

The long-term goal of this study is to establish a methodology that will allow us to understand anomalies, such as higher porosity and simultaneously higher strength for certain cement blend mixes.

The objective of this work is to find out whether the elastic properties of cement paste can be extracted reliably within practical computational limits. The effect of Finite Element modelling parameters, such as resolution, mesh type, effect of porosity, size of the computational volume are studied.

1.2 Description of the approach

The Finite Element analysis in this work consists of three main parts - microstructural model, mesher and solver. The microstructural model μic, which has been developed at LMC EPFL, creates a series of microstructures over time. The microstructure - specific and optimised mesher and solver have been developed as a part of this work in an object-oriented language. Fig. 1.1 shows the flow used to evaluate the elastic properties.

Different parameters specific to Finite Element method and microstructure were studied and their effect was systematically determined. The study can be roughly divided into two main parts. In the first part of the study, the specifics of the FEM with regard to the complex early age microstructure are studied and evaluated. In the second part of the study, the focus is put on the investigation of the microstructural variations, taking into account the results of the previous part. The effect of individual parameters is verified using experiments (static and dynamic measurements).

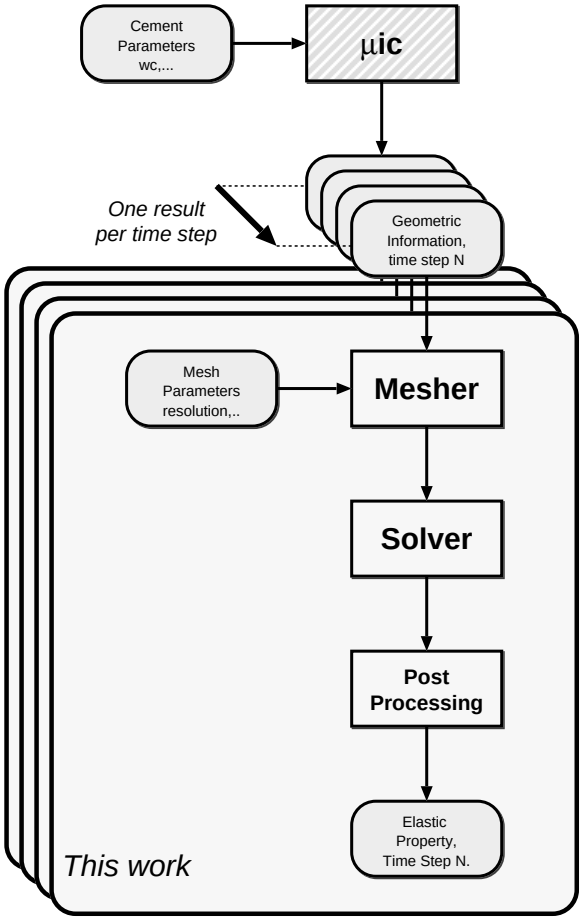

Figure 1.1: Simplified diagram showing different parts of the elastic property extraction methodology.

1.3 Structure of the thesis

In Chapter 2, an overview of the techniques for the prediction of effective elastic properties of heterogeneous materials is presented. Later, focus is put on the description of the approaches for the cement paste microstructure. Both analytical and numerical studies at high and low porosity ranges and their implications are presented.

Chapter 3 deals with the specifics of the Finite Element method resulting from complex geometry of the early age microstructure. Focus is put on resolution, meshing approaches, treatment of porosity and size of computational volume. The results from this chapter form the basis of the computations in the Chapter 4.

In Chapter 4, virtual microstructures are created and the effect of various parameters, such as flocculation, w/c ratios, particle size distribution, density of the C-S-H hydration product and number of hydrate clusters is studied. Implications of this chapter are directly reflected in Chapter 5.

Experimental validation on several cement mixes is presented in Chapter 5. The variation of the microstructural parameters and experimental results are discussed.

Finally, Chapter 6 provides the discussion of the results both in terms of FEM specific and microstructural parameters.

Chapter 2

State of the Art

Although concrete is one of the most used building materials, we still do not understand how its mechanical behavior is linked to its microstructure in detail. Many length scales which have to be considered for modelling of even basic mechanical properties and the complex microstructure, pose an enormous challenge for the prediction process. Approaches developed for other heterogeneous materials, can only be applied to cement with considerable limitations. The objective of this chapter is to summarize these modelling approaches which have been studied for heterogeneous materials and focus on their applications and limitations in the field of cementitious materials, specifically on the cement paste level.

2.1 Microstructure-mechanical properties relationships of composites

The modelling of heterogeneous materials is having an increasing impact on our understanding of the behavior of materials and one of the challenges of the theoretical analysis of the microstructure-strength relationships of materials is the necessity to consider several length scales. Direct numerical analysis of the material behavior, which takes into account both macroscopic boundary conditions and microstructural details would require unattainable computational resources. To overcome this problem, homogenization and/or multiscale modeling has been used.

The objective of micromechanics is to link the macroscopic properties of hetero-

geneous materials to their microstructural parameters. The microstructure of the heterogeneous materials is generally stochastic, the sizes and spatial distributions of the reinforcing inclusions are random and so are the resulting physical fields. Homogenization is a method, which determines the mean values of these fields by external loadings, simultaneously determining effective elastic properties of the medium. A whole area of Solid Mechanics has been developed in the past fifty years to predict theoretically the effective properties of heterogeneous materials from the properties of their phases and their distribution. Most of the progress has been made in the field of linear elastic constitutive behaviour. The pioneering contributions of Hill [32], Hashin and Shtrikman [27] are well known.

The prediction of the effective properties of a heterogeneous material assumes that the problem contains two scales which are well separated. The microscopic scale should be small enough for heterogeneities to be separately identified and the macroscopic scale should be large enough for the heterogeneities to be smeared out. The most common methods for bridging scales are rigorous bounds, effective medium and effective field methods and asymptotic theory of periodic microstructures.

2.1.1 Bounds and analytical schemes for heterogeneous materials

An estimation of the effective properties can be obtained by rigorous bounds. Early work on them was carried out by Voigt [78] and Reuss [57]. Although both sought for an exact solution of the elastic properties with random microgeometries, Hill [33] showed that their estimations only give upper and lower bounds. The use of variational principles for the calculation of bounds was introduced by Hashin and Shtrikman [27], [28]. The bounds are quite wide for materials with high contrast of the individual properties of the phases - Fig.2.1, nevertheless, the approach turned out to be the basis for construction of approximate solutions of the homogenized problems by means of trial fields.

The most used analytical schemes are based on the work of Eshelby (1957) [22], who obtained a relatively compact solution which has been a basis for many approximation methods. He worked on the stress field of an isolated ellipsoidal inclusion in an elastic infinite matrix, which undergoes a transformation and changes its shape or size. The basic scheme developed on the top of this idea is a dilute

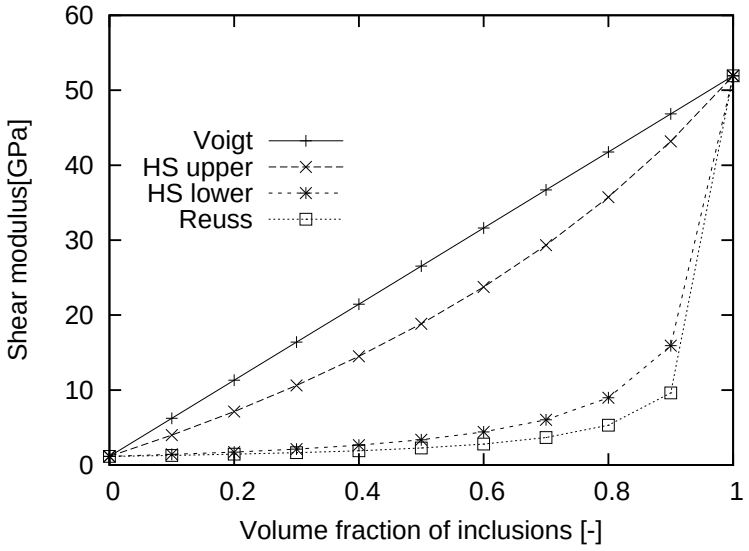

Figure 2.1: Bounds on shear modulus, $E_1 = 135$ GPa, $E_2 = 3$ GPa, $\nu = 0.3$

distribution model, which assumes that if the volume fraction of particles is small (ideally less than 3%), their interactions can be neglected.

Eshelby's scheme was taken as a basis for other schemes, which focused on the multi-particle problems. Two principal approaches exist in this area - effective field and effective medium methods, which reduce the complex nature of the multiple-particle problems, to a problem of one particle.

A combination of Eshelby's approach and the effective field method is the basis of the Mori-Tanaka (MT) model [49], [9]. In this approach, each inclusion behaves as an isolated one and is subjected to the averaged stress fields invoked by all other inclusions. The stresses invoked by other inclusions are superimposed on the applied external stress. This way the method accounts for the interactions between inclusions. When the matrix is the softer phase, the method leads to the same formulae as the lower Hashin-Shtrikman bound. The method has a very good performance for lower volume fractions of inclusions 10 - 30%, but underestimates severely the effective moduli for particle concentrations larger than 30% (in case particles are the reinforcing phase). This is possibly because only one pattern is used to build the localization relation [43]. Although the Mori-Tanaka approach takes into account the stress perturbation inside the matrix due to the presense of other inclusions, it is not able to account for the spatial distribution. This can be solved by newer an-

alytical schemes, which model such distribution by an ellipsoidal cell, called double inclusion, surrounding the inclusion - e.g. IDD [82].

The most used scheme within effective medium methods is the Self-Consistent (SC) scheme. The method was originally developed by Hershey [31] and Kroner [42] for single crystals and polycrystals, and then extended by Budiansky [15]. In this method, the reference medium has the effective properties of the microstructure and the field acting on each inclusion is the external field applied to the medium. The Self-Consistent approach allows microstructures with some degree of regularity to be described well, but not clustered structures or microstructures with large differences between properties of the phases.

Unfortunately, most of these analytical models can only give estimates for the effective properties, and simplifying assumptions result in considerable difference in the predictions, mainly at high porosities. More sophisticated schemes are needed to obtain the effective elastic properties. This is a task of an asymptotic homogenization theory, developed in 1970s and 1980s by Sanches-Palencia [61], which deals with heterogeneous materials with a periodic distribution of components. Material is modelled as an infinite series of unit cells under far field load. This is a more rigorous analysis than the effective field approaches. It not only permits equivalent properties to be obtained, but it also solves the stresses in the constituents at microscale. In the framework of this theory, the homogenization is reduced to a standard problem of the representative cell, on which effective elastic properties can be computed by analytical or numerical methods. In the next section we will concentrate on numerical methods, which are able to simulate complex microgeometries and provide a numerical solution of the boundary value problem of a representative volume element.

2.1.2 Numerical modelling of heterogeneous materials

The real microstructure of a material is often complex and inhomogeneous and the prediction of its effective properties becomes a nontrivial problem, even in the case of microstructures with linear elastic properties of the individual phases. In such cases, the relationship between microstructure and mechanical properties can be obtained via discretized numerical models.

Direct numerical simulations by the Finite Element method for composites with periodic microstructures were developed at the end of the 1960s and opened the way to numerous studies [53], [2]. More recently, efforts have been made to consider composites with more complex microstructures [14], [50].

A numerical method based on Fast Fourier Transform has been developed by Moulinec and Suquet [51] as an alternative to FEM. By using the exact expression of the Green's function for an elastic homogeneous comparison material, the problem is reduced to an integral equation which is solved iteratively. Typically, the method's convergence is dependent on the contrast between the phases. The method does not converge when the contrast of phases is infinite (for case of voids or rigid inclusions).

Special meshing and computation techniques have been developed over time. In order to include the specific effects of microstructural morphology on the homogenization analysis, Ghosh et. al utilized the Voronoi cells to represent the arbitrary distribution of inclusions and developed a novel numerical method, called the Voronoi Cell Finite Element [23]. In this method, FE meshes are created by Dirichlet tessellation of real microstructures. Each polygon formed by tessellation contains one inclusion and is used as a finite element.

Ostoja-Starzewski [55] introduced an attractive alternative to micromechanical FE analysis - spring network based model (lattice model). The inclusions are represented by single pixels or finite regions, which makes it possible to account for anisotropy. Compared to FEM, the method does not need remeshing and construction of the stiffness matrix.

The extended finite element method (XFEM) is a numerical technique that extends the classical FEM and solves problems which cannot be effectively resolved by mesh refinement - such as discontinuities, singularities and boundary layers. This is done by introducing a local enrichment of approximation spaces, realized through the partition of unity concept. The XFEM was developed in 1999 by Ted Belytschko et.al [7]. An advantage of the method is that the mesh does not need to updated upon problem evolution. The disadvantage are the numerical instabilities occuring with a large number of interacting enrichment features.

No matter what the prediction methods is, the computational cost associated with the prediction of effective elastic properties on 3D microstructures can be very

high and care must be taken, so that the reliability and stability of the results is ensured.

Within the numerical discretization techniques, several approaches exist in the analysis of microstructures:

Periodic microfield approaches - assume periodic cell arrangement, analysis of a repeating cell of a microstructure

Embedded cell approach - unit cell with a real microstructure is embedded into a region with effective material properties

Windowing approach - test windows are placed over the microstructure and are subjected to homogeneous boundary conditions, the result is obtained by averaging results of several windows

Modelling the full microstructure of a sample

The most common and least computationally intensive approach is the periodic microfield approach for regular microstructures and the windowing approach in case of random heterogeneous materials. Modelling the full microstructure of the sample requires the highest computational resources and is therefore rather rare.

2.1.3 Boundary conditions and size of the computational volume

Representative volume element (RVE) is defined as the smallest possible representation of the microstructure, which is statistically homogeneous. The choice of the boundary conditions generally should not influence the result of the prediction. However, due to computational constraints, the computational volume might not be sufficient and the boundary conditions come into play. Hori and Nemat-Nasser [35] indicated that the predicted effective elastic properties vary depending on the boundary conditions and that the homogeneous displacement and traction boundary conditions give the upper and lower bound of the elastic modulus. According to Hill [32], a computational volume is representative if the responses under uniform displacement and traction boundary conditions coincide.

Displacement boundary conditions, as an equivalent to the state in which the boundary planes remain flat after the deformation [1], seem to work only for symmetric volumes subjected to normal tractions. Many researchers later - e.g. [53], [68], [70] indicated that the plane-remains-plane boundary conditions are overconstrained.

Mixed boundary conditions have been proposed [30], [29] arising from experimental set-ups, in which it is very difficult to realise uniform boundary conditions (especially static). These works have shown that the mixed boundary conditions yield better approximations than the uniform (displacement or static) boundary conditions.

Suquet [70], Hollister and Kikuchi [34] and others [3] [74] concluded that more accurate results can be obtained by using periodic boundary conditions. Periodic boundary conditions should be applied to periodic media. For media with disordered microstructure there is no reason to assume that they will act as a periodic unit cell, much less that its boundaries will remain flat. This assumption can cause some boundary effects - the useful volume is smaller than the simulated volume, the response is stiffer than it should be [46].

Previous studies have reported that a RVE size of about two times the dimension of the heterogeneities (reinforcements) allows estimates of these properties for a two-phase material to be obtained with an error of the order of 5%, whereas an RVE over heterogeneities ratio of 5 provides predictions as close as 1%, whatever the inclusion concentration and phase contrast [21].

2.1.4 Geometry discretization

Discretization of the problem is an essential part in the process of its solution. A variety of convential meshing approaches has been used and can be divided into two categories - structured and non-structured meshing approaches.

Structured meshes can be created in two ways. The first approach involves creation of a mesh with regular polygons (or polyhedra) and then mapping the same object into the same topology, but with different shape. In the second approach (grid-based approach), regular grids of nodes and elements are constructed and object is meshed and inserted into the same space. Elements lying outside the geometry

of the object are removed, those on the boundary are shaped to capture the boundary. Pixel (voxel) meshes represent a special extension of grid-based approaches. In a pixel and voxel based design, a mesh is generated by assigning the property of the phase to the finite element in a prescribed grid. This allows direct introduction of digital images into FE models, as it was developed by Hollister and Kikuchi on bone microstructures [34]. The problem of this approach is that the smooth interfaces are transformed into jagged geometries. Refinement techniques in form of a quadtree (octree) are needed to accurately represent the geometry of the problem. Kim et al. developed a meshing technique that starts from a quadtree (octree) and then successive element splitting and nodal shifting is carried out in order to create an accurate mesh [41].

Unstructured meshes are generally based on Delaunay Triangulation and their most common representant is an Advancing Front Technique. While this method produces microstructure-aligned meshes, it has several disadvantages. The first problem of this technique is the nodal sequence, which must be chosen so that it is possible to distinguish between the interior and exterior of the domain. Starting from the exterior and going inward, the advancing front fills the interior with triangles using Delaunay triangulation. This approach is one-sided, since only the interior of the boundary is meshed and is therefore not suitable for the analysis of complex overlapping geometries. Another issue with the triangulation is ensuring that the elements have a reasonable aspect ratio, which strongly influences the convergence of the solution. The disadvantage of this method is that it can be very difficult to align the element boundaries along complex boundaries, or to fill interpenetrating phases with simple shaped finite elements. The resulting mesh may contain a large number of elements and nodes, especially when the size ratio between particles is high and the distance between the particles is low.

The lack of information about the microstructural geometry or the incapability of dealing with the geometrical complexity result in idealization. Errors are introduced in the precision of the microstructural morphology, its discretization, choice of the representative volume etc.

In the next section the application of the micromechanical theory with both analytical and numerical approaches to cement paste is presented.

2.2 Micromechanical theory for cementitious materials

The cement matrix is a complex material - both unreacted species and hydration products are present and agglomerated by an amorphous product, C-S-H gel. After hydration of the clinker, the main components formed are portlandite (CH), aluminates and C-S-H gel. The C-S-H gel is the most important hydration product, comprising up to 60% of the final volume, and is responsible for the cohesion and mechanical properties of cement pastes.

Very early hydration stages can be characterized by formation of hexagonal acicular ettringite crystals at the surface of the clinker particles, and of a colloidal C-S-H product which is deposited on the surface of the clinker grains. These hydration products may lead to an increase in viscosity but they do not build up a connected network. Therefore, cement paste remains a fluid at this stage. The transition from a fluid to a solid, referred to as setting, takes place at a cement paste age of 3 - 5 h. C-S-H grows on the surface of the clinker particles and into the water-filled interstitial spaces, and mutually penetrates. In this way a microstructure with an interconnected network of solid particles originates.

The constitutive behavior of hardened cement paste has been observed to be linear elastic right up to failure. The short-term deformation is controlled by the elastic properties. At ages of 14 days or older, cement paste is well-approximated as a linear elastic material, at least for short loading times. The development of elastic modulus with the degree of hydration was observed experimentally to be linear at very early ages by Boumiz [13]. Smilauer showed by FEM, FFT and analytical homogenization schemes that the common assumption of linearity between hydration degree and E modulus are appropriate only for w/c higher than about 0.35. Below that a concave shape of the E modulus development was found.

The final elastic stiffness of cement paste is the larger the smaller the w/c. This can be explained by the characteristic initial distance between the clinker grains of its microstructure. The smaller the w/c, the closer the initial packing of the clinker grains, and the easier the growing hydrates bridge the gaps between neighboring clinker grains and establish a connected network of solid particles. The smaller the w/c of cement paste, the faster the increase in the predicted macroscopic stiffness

of the material with increasing degree of hydration.

2.2.1 Simple approaches to the prediction of mechanical properties

Although elastic properties are what controls the short-term deformation for any construction, clearly much more focus has been concentrated on compressive strength because of its failure representation and convenience of measurement. All empirical relations exist for the prediction of Young's modulus from compressive strength, rather than the other way around.

An increase in elastic modulus is observed to go together with an increase of strength, but the relationship is not clear. This is not surprising as elastic modulus seems to be related more to intrinsic values of the individual phases and connectivity. The elastic modulus has been related to the degree of hydration by De Schutter et al. [19] and percolation by Ye [80]. It has been shown that static Young's modulus, in the vicinity of the percolation threshold, seems to obey a power law, which is a function of the percolation p, percolation threshold p_c and a structural parameter k.

$$E \sim (p - p_c)^k \tag{2.1}$$

These empirical relations do not take into account the underlying physical processes and microstructure, ignoring chemical and physical properties, temperature, air-content and in the case of compressive strength the formation of cracks. Powers, instead, related the strength to the concentration of hydrates of cement in the space available for these products and has determined the relationship between gel/space ratio and strength, which is approximately proportional to the cube of gel/space ratio [72]. The general relationship of porosity and strength is not unique for cementitious materials. It has been observed for ceramics and metalic materials, as well. It seems, that porosity defined as the total volume of the overall volume of pores larger than the threshold of gel pores is a primary factor influencing the strength of cement paste [59].

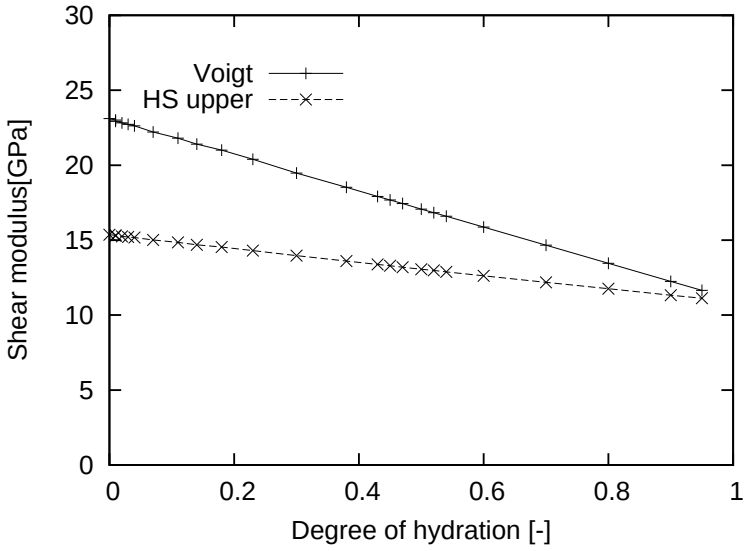

Figure 2.2: Voigt and HS upper bound with hydration

2.2.2 Rigorous bounds and analytical schemes applied to cementitious materials

Rigorous bounds and analytical schemes represent an established procedure for the prediction of effective properties of heterogeneous materials. Although they date back to more than 150 years, their proper framework for cementitious materials appears only in the last two decades. This could be due to the lack of information on the microstructural level (determination of the intrinsic properties of the phases, volume fractions evolving with hydration, morphological shape, mode of interaction of the microheterogeneities), which are an essential input for the prediction.

The use of rigorous bounds does not seem to say much about the elastic properties. Both the Reuss and lower Hashin-Shtrikman bound are very close to zero over the whole range of hydration, due to the presence of porosity. The Voigt and Hashin-Shtrikman upper bound decrease their values with the evolution of hydration - Fig.2.2 which indicates the convergence of the lower and upper bound at later ages due to the higher volume fraction of solid.

In the framework of cementitious materials, Ulm and co-workers [10], [17] started to explain stiffness evolution of cementitious materials by incorporating micromechanical theory in the early 2000s. Several other approaches based on this theory

have been developed in recent years, mostly focusing on how the shape of the individual phases influences the prediction of effective elastic properties - [56],[60].

Most of the analytical approaches at later ages assume matrix-inclusion morphology, in which C-S-H represents a matrix with embedded inclusions of unhydrated clinker, portlandite, aluminates and pores. The amount of inclusions generally exceeds 30 %, which immediately excludes the use of dilute distribution models, restricted to low volume concentrations - ideally less than 3 %. Both Self-Consistent and Mori-Tanaka based approaches are used for the prediction. On the other hand, studies at early ages with the focus on the estimation of percolation threshold use exclusively the Self-Consistent scheme [10], [56]. Based on the variation of the percolation threshold, the morphology on the micro and nano-level is adjusted. The morphology adjustment concerns e.g. the shape of low and high-density C-S-H, as well as the shape of other constituents on the microlevel or nanolevel. Mori-Tanaka is not used for early ages, because a continuous matrix has not yet formed.

2.2.3 Experimental basis

A proper base for the experimental data on elastic properties starts with the work of Powers [72], Thomson [75] and others, who used vibrational techniques to establish dynamic properties of cementitious materials.

Swamy and Rigby [58], who performed resonant frequency tests on hardened pastes for w/c 0.3, 0.4, 0.5, and 0.6, show that the elastic modulus decreases with increasing water content and that elastic moduli increases with age. In their study longitudinal and flexural modes produced almost the same values of Young's modulus (E) while the shear modulus (G) was about 40 % of the value of Young's modulus. Their experiments were performed on prisms (10x10x50 cm), cubes (10x10x10 cm) and cylinders (20 x 10 cm diam.) continuously cured in water. Similar conclusions were made by Sun et al. [69] who carried out tests on Portland cement paste samples of w/c 0.35, 0.50, and 0.60, from very early age to 96 hours, cured at constant temperature of 25° C. Specimens of 5x7, 5x23 cm were tested by a resonant frequency only in longitudinal and torsional mode. Their measurements also show that the shear modulus is approximately 40 % of the value of Young's modulus and the development can be described by a hyperbolic function.

Values of Poisson's ratio at early ages are quite sensitive to the values of E and G used, since they are so small compared to later ages. Haecker et. al [25] studied the elastic moduli at early degree of hydration. For this w/c 0.6, degree of hydration 0.219 cement paste, the experimental elastic moduli values were E = 1.7 GPa and G = 0.66 GPa (both with uncertainties of at least + 5%). He obtained Poisson's ratio 0.29, but choosing the value of E to be 5% higher and the value G to be 5% lower, he obtained Poisson's ratio of 0.423.

Ultrasound-technique appears to be well-suited for the estimation of setting time, which has the meaning of percolation threshold. Boumiz et al. [13] produced cement paste samples using white cement w/c of 0.35 and 0.40, respectively. The specimens were cured within an ultrasonics testing cell at constant temperature of 25°C, regulated by a water bath. From very early age on, ultrasonic velocities of both compressive waves and shear waves (sent through the samples with thickness equal to 1 cm) were measured every 10 min, up to sample ages of 24 h. He found a critical degree of hydration for the onset of the mechanical properties of cement paste w/c 0.35 at 0.015 and 0.4 at 0.021.

Constantinides et al. [17] measured the Young's modulus by UPV for later age microstructures. With his set-up, only the value of Young's modulus could be measured, values for Poisson's ratio were taken from literature.

2.2.4 Microstructural models

In order to investigate the development of microstructure with time and the change of its properties, particularly connectivity both in terms of mechanical and transport properties quantitative geometrical and topological description is needed. To achieve this, numerical microstructural models have been used in the past decades. The models generate the microstructure quickly, completely defined with the representation in 3D. Accurate simulation of the microstructure assumes that the kinetics of cement hydration and more importantly the distribution of products is understood and can be described. The kinetics depends on clinker composition, w/c, and on the curing conditions. Two basic types of models exist in this domain - vector and digital microstructural models.

The most used digital microstructural model is CEMHYD3D [8] based on dis-

cretization of computational volumes into cubic voxels, each occupied by a single phase of cement or a product. The hydration of cement particles and the microstructure developments are simulated through a cellular-automata approach operating on the entire collection of pixels. This approach permits a direct representation of multiphase, multisize and nonspherical cement particles using SEM images. However, only particles of particular sizes depending on the mesh-size can be modelled with increasing approximation as the particle size reaches the mesh size. Although this approach is known to be simple and effective in mechanical applications, it requires a trade-off between accuracy and speed or memory consumption, generally limiting the voxel size to about 1 μm. However, since many relevant features of cement microstructure are smaller than the voxel size, some information is irretrievably lost. Furthermore, an accurate representation of porosity and pore-connectivity might still not be possible as the average pore sizes continue to reduce with the progress of hydration.

The vector approach basically means that all particles are stored as centroid and radii of shells. Models essentially simulate cement hydration as particle growth with overlaps. The vector approach also allows the simulation of reactions of individual particles, based on the properties of each particle and their surroundings. The vector approach not only preserves the multi-scale nature of the cement particles, but also of the product with the possibility of identifying and modelling pores without resolution limit. This approach, however, faces a tremendous computational challenge as representative cement samples contain millions of discrete particles, limiting the capabilities of these models.

HYMOSTRUC3D [81] assumes that particles of same size react at the same rate. Hydration is basically simulated as an expansion of overlapping particles. Particle sizes are generated based on Rosin-Ramler distribution and the largest particle is placed at the center, others around it in a sphere. All particles are assumed equidistant and products are deposited on the grains. The limitations of HYMOSTRUC are that only one kind of product is modelled and all products deposit on the reacting cement grains. The model uses a look-up table approach - experimental results written as empirical equations are used to derive properties from results.

μic derives its basics from the work by Navi and Pignat [52] - Integrated Particle Kinetics Model. The model is evolutionary in nature, it helps the interpretation of experimental results and design of new experiments. The main difference between HYMOSTRUC and μic lies in the fact that while the former relies completely on product deposition on the surface of reacting particles, the latter can also model the nucleation and growth of products in the pore space.

Hain and Wriggers [26] attempted to generate digitally based microstructure from CEMHYD3D in order to compare it to the predictions on real microstructure but finally did not use it, as even for fully hydrated cement pastes (0.945 and 0.990) with w/c 0.45 and 0.55 the parts of microstructure in CEMHYD3D were distributed very evenly, unlike in real microstructures from computer tomography scans where accumulations of pores could be seen.

Smilauer [63] compared CEMHYD3D with the vector microstructural model of Pignat and concluded by the use of Fast-Fourier Transform that vector - concentrically grown microstructure is less stiff than the digital one. Though, he pointed out that this might not be the case for coarse cements of higher w/c, in which chunks of porosity are created by CEMHYD3D.

Haecker [25] used the microstructure generated by CEMHYD3D to predict elastic properties of several types of cement, with w/c varyiing from 0.25 to 0.6. The predictions at later age (higher than 0.5 degree of hydration) showed a good agreement with the experimental data from resonant frequency method, with a maximum error of 10 %. However, a simulation of an early age mix prepared with a w/c 0.6 (doh 0.219) showed a high overestimation of elastic properties. This was perhaps caused by the resolution (100 voxels per side) of the hydration process itself. Dropping the resolution in the hydration process showed an asymptotic convergence to the experimental data.

Differences between the microstructural models can be seen in terms of percolation threshold and will be discussed in the section Percolation threshold.

2.2.5 Elastic properties of the solid phases

Elastic properties of the phases present in cement are an essential input to the prediction of elastic effective properties. While properties of the crystalline phases are

known and their determination is straightforward, the properties of the amorphous C-S-H phase are constantly under dispute. Constantinides et. al [17] suggested that properties obtained by nanoindentation are intrinsic to all types of cement-based materials, and do not depend on w/c, admixtures etc.

Elastic properties of certain crystalline phases, which occur in cement paste, can be found in nature and have been documented in geological literature. Generally, elastic moduli of a crystal gives an anisotropic elastic moduli tensor which reflects the symmetry of the crystal lattice. An averaging by isotropic Voigt and Reuss bounds can be performed and results in an isotropic average elastic modulus tensor, which is perhaps more representative of what appears in real cement paste, where the crystalline phases are polycrystalline and randomly dispersed.

Obtaining elastic properties of clinker phases is straightforward. The Youngs' moduli of the other clinker phases, C_2S, C_3A, and C_4AF, have been measured via nanoindentation and have shown that the Youngs' moduli of these phases are all about the same within 15%.

The properties of portlandite seem to be as well quite well explored. Beaudoin [6] and Wittmann [79] measured the elastic modulus of CH compacts of different porosities. The elastic modulus of them was obtained from three-point bending tests and the intrinsic modulus of CH was found by extrapolating to zero porosity, log E vs. porosity curves. Monteiro [48] used the elastic stiffness coefficients of CH, determined by the use of Brillouin Spectrum. He used rigorous bounds, to obtain the range of elastic modulus and Poisson's ratio in range 39.77 - 44.89 GPa and 0.305 - 0.343, respectively.

Ettringite is also well characterised [40] and exhibits average values of Young's modulus 22.4 GPa and a Poisson's ratio 0.25.

C-S-H seems to exhibit a bi-modal distribution of Young's modulus. The first observations on this can be tracked back to Taplin [71]. Jennings [38] and Tennis and Jennings [73] proposed a model for the two types of C-S-H, with distinct volume fractions and geometry. The Young's modulus of C-S-H has been measured by nanoindenation by Constantinides et al. [17] and suggested the values of 21.7 and 29.4 GPa for low-density (LD) and high-density (HD) C-S-H. The average elastic properties determined by nanoindentation include the effect of porosity and of any

nanocrystalline CH or minor compounds present at smaller scales. Manzano et al. [44] calculated the elastic properties of C-S-H and other phases using an atomistic method. He found that the mechanical properties of 1.4 nm tobermorite and jennite were about twice as large as those of C-S-H gel. When applying characteristics such as intrinsic porosity and the finite chain length of the C-S-H gel to the crystals, the mechanical properties decreased and reached values in good agreement with nanoindentation measurements for C-S-H gels. Their simulations show that the longer the silicate chains, the better the mechanical properties.

The elastic moduli of some minor phases are not known independently. They are usually considered to have elastic moduli equal to a phase they structurally resemble.

To the best knowledge of the author, there are very few studies as how a span of elastic properties can influence the prediction. For fully hydrated microstructure, Hain and Wriggers [26] varied Youngs' moduli of the unhydrated part between 125 and 145 GPa and found very little influence of these stiffness parameters on the overall result. This seems to be reasonable in view of the small volume fraction of 2 %. The same authors found out, that air-filled porosity span (0 - 1000 MPa) has a negligible influence on the result.

2.2.6 Influence of shape on the prediction of elastic properties

The shape of the particles is an object of constant interest of several recent studies and it seems to be very influential for high porosity ranges. In the following, several morphologies of microstructural features will be discussed.

Bernard et. al [10] developed a multiscale micromechanics approach in which four levels were introduced - Fig.2.3. The first level (10^{-8} - 10^{-6} m) consists of two types of C-S-H matrix - low and high density, with different elastic properties. The second level (10^{-6} - 10^{-4} m) is the cement paste level with homogenized C-S-H matrix and inclusions of anhydrous, portlandite, etrringite and capillary porosity. The third level is the mortar level (10^{-3} - 10^{-2} m) with cement paste matrix, sand grains and ITZ. The last level is the concrete level (10^{-2} - 10^{-1} m) - aggregates with ITZ in a mortar matrix. The cement paste level was homogenized with the use of the SCS scheme, using the spherical assumption of particles. The percolation

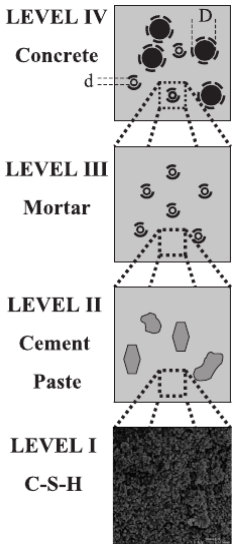

Figure 2.3: Bernard's multiscale model

threshold was defined at this level. In the following, only the studies of the cement paste level will be presented.

Pichler et. al [56] in the prediction of early age properties, represented clinker and pores by spherical shapes, with hydrates either by two limit shapes - spherical and acicular shape. Sphere represented the lower limit with aspect ratio equal to 1.0, a cylinder an upper limit with infinite aspect ratio - Fig.2.4.

Sanahuja et al. [60] proposed a morphological model consisting of two scales - Fig.2.5. At a lower scale, both inner and outer C-S-H were made from the same elementary bricks, differing only in porosity and morphology. The SCS was used for this level, modified to account for the non-spherical shapes of inner and outer product. At the paste scale, anhydrous cement surrounded by a layer of inner C-S-H were embedded into a matrix from outer C-S-H. Mori Tanaka was used to evaluate the elastic properties of this level.

Stora et al. [67] used an analytical scheme of Zheng and Du [82] - Fig.2.6 and introduced a morphological parameter, which accounts for the volume/surface ratio. Particles were represented by various shapes - ettringite as prolate needle shapes, portlandite as oblate disc shapes, clinker as a mixture between them. Their model adopted two levels - level I, with outer C-S-H matrix and inner C-S-H inclusions. At this level, the shape of inner C-S-H was considered spherical. At level II, homoge-

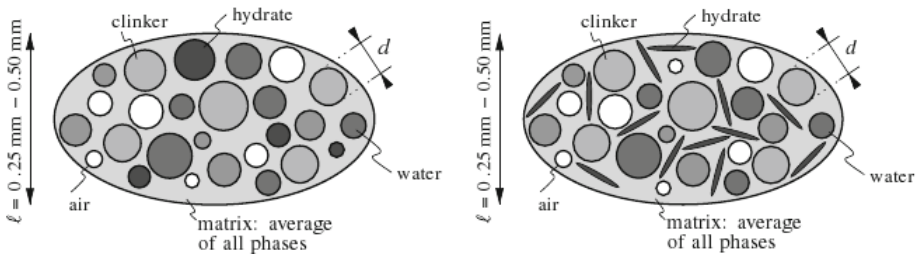

Figure 2.4: Pichler's model - spherical vs acicular hydrate shape

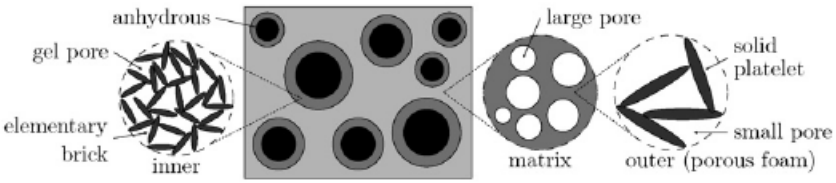

Figure 2.5: Sanahuja's model of inner and outer

nized C-S-H acted as a matrix for CH, capillary pores, unhydrated clinker, ettringite etc.

The shape of the particles seems to be influential only for early hydration stages, i.e. higher porosity ranges. Generally, for the same hydration degree, spherical hydrates predicted softer response than the elongated ones. This is because an assemblage of elongated hydrates and spherical clinker grains establishes a more effectively connected network of solid particles than in case of spherical hydrates and clinker grains. This effect is more pronounced with increasing w/c and lower degree of hydration [56].

Pichler [56] showed that the hydrate shapes matters for early ages of cement pastes with w/c larger than 0.45. Stora [67] concluded, that the real shape of

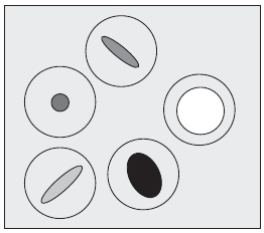

Figure 2.6: Stora's double inclusion model

clinker (aspect reatio 0.81, sphere is 1.0), has no effect on overall elastic properties in all porosity ranges. For leached pastes, the shape of CH seems to matter [67]. The effect of particle shape can be seen from FE simulations on aligned mesh [4] for fully hydrated cement pastes. For degraded pastes (higher porosity ranges), the results varied by 26 % for bulk modulus and 14 % for the shear modulus in case of different particle shape.

A comparison of analytical approaches vs. FEM seems to be in favour of FEM at early ages and higher porosity ranges. This is due to the fact that FEM intrinsically takes care of the geometry representation up to the resolution limits, unlike the analytical representation, which cannot take into account complex early-age microgeometries. For fully hydrated sound cement paste, analytical schemes and FE produce very similar results. For capillary porosities higher than 35 %, analytical schemes differ significantly from the FE results and it seems that, unlike FE, the analytical schemes completely fail to account for interactions between spherical inclusions [67]. Pichler [56] concluded that SC is reliable for mature pastes as well as for the early ages of pastes with w/c smaller than 0.45. Bary et al.[4] performed a study in order to evaluate the influence of the particle shape, samples were generated with a part of inclusions being prismatic (elongated ettringite, and flat hexagonal shapes of portlandite). Comparison of the numerical results to the analytical schemes, resulted in a good coherence for all the schemes (SCS, MT, IDD) for sound hydrated paste. Comparable results were obtained for MT, although it should not be used for volume fraction of inclusion exceeding 30 %. However, for degraded paste the SC scheme underestimates FE for both types of particles, since in the case of SCS neither of the phases is preferential, while the problem studied has a clear matrix-inclusion morphology.

2.2.7 Percolation threshold

Percolation is defined as a ratio of the volume of connected phase to the total volume of the solid phase in a sample. The percolation threshold is defined as a moment, when the first spanning cluster appears and a continuous path is formed. The discussion of the percolation threshold is mostly based upon the data of Boumiz et. al [13] who determined the percolation threshold with ultrasonic measurement

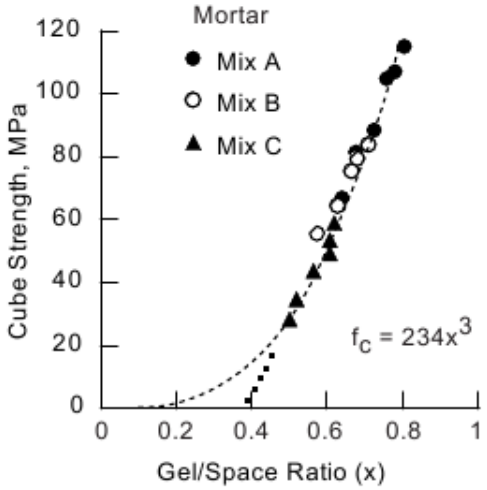

Figure 2.7: Extrapolation of the gel/space ratio curve. Taken from [45]

and calorimetry. The time of the percolation was assigned to a time when the first significant shear ultrasonic velocity occured. The thresholds were obtained for the cement paste of w/c 0.35 and 0.4, the degree of hydration being 0.015 and 0.021, respectively. Another source comes from the experimental work of Taplin, cited by Byfors [16]. His percolation threshold values are rather high - for a w/c 0.157 which required the degree of hydration of around 0.15 for a percolation threshold to occur. This seems to cause quite a confusion in the predictions, since Boumiz's and Taplin's data are rather far from each other [60] and most probably do not correspond to the same point. This is demonstrated on the Power's gel/space ratio curve - Fig.2.7. The linear upper part of the curve was most probably extrapolated back to zero in Taplin's work, while this is not what corresponds to the solid percolation threshold, which was observed by Boumiz.

The efforts to reproduce the percolation threshold by analytical schemes are carried out with the use of SC, which gives a percolation threshold of the volume fraction of solids higher than 50 % (under the assumption of spherical shapes of solids and pores).

The values of percolation threshold obtained by SC and its shape modifications are generally higher than the ones obtained by Boumiz. Bernard [10] studied a percolation threshold for w/c 0.35 and obtained 0.046 instead of 0.015 and for w/c 0.4 he obtained 0.11 instead of 0.021. The difference was explained by the experimental

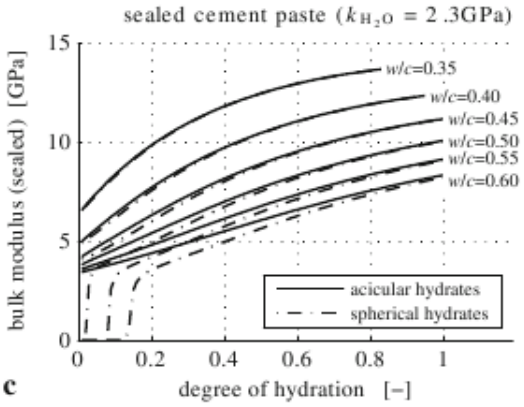

Figure 2.8: Pichler's percolation threshold for spherical vs. acicular hydrate shape

difficulty in the very first hours of calorimetric measurements and conclusion was made that an error between 0.03 and 0.06 could exist in the experimental data of Boumiz. The same refers to work of Sanahuja [60], whose prediction for undrained conditions and a non-spherical shape of outer C-S-H platelets showed a big overestimation of the percolation threshold (by 0.08 - 0.2). This was assigned to the model of outer (solid platelets made out of elementary bricks + gel and capillary porosity), which might have failed to capture the morphology of capillary porosity.

Pichler [56] showed that spherical hydrates are able to reproduce reasonable percolation thresholds. On the other hand, if acicular hydrates were considered, a non-zero stiffness of cement paste was predicted already at zero hydration degree. This seems to be a reasonable estimation, because the results only present the bounds for the percolation threshold and the reality will be somewhere in between.

Simplified efforts were made in order to compute percolation on a 2D-lattice by Torrenti and Benboudjema [76] 1000 x 1000 μm, with the resolution of 10 μm. Because the prediction of solid percolation was too low compared to Taplin's data, they defined an existence of another type of percolation threshold - mechanical percolation threshold. Unlike solid percolation threshold, which only requires contact between particles, mechanical percolation threshold requires a cohesion between particles and should therefore appear later. It is a moment, below which the strength of material is not zero but can be neglected and is an intersection of the regression line with the x-axis. Mechanical percolation threshold was modeled by interface

elements.

Ye et. al [81] compared the results of both solid and pore percolation threshold for w/c 0.4 for the HYMOSTRUC3D and CEMHYD3D microstructural models. The simulation was preformed for a CV of 100 μm. The simulations differed in the assumptions - in HYMOSTRUC psd ranged between 2 and 45 μm, while in CEMHYD3D only four sizes of particles 3, 9, 13, and 19 were used. The resolution for the percolation algorithm was 0.25 μm in HYMOSTRUC, while for CEMHYD3D it was 1 μm. Strangely, despite the differences in assumptions, both models produced a similar solid percolation threshold - between 0.02 and 0.03 degree of hydration. Significant differences were observed between the capillary pore percolation threshold - 0.035 from HYMOSTRUC, 0.22 from CEMHYD3D. The huge difference is associated with the difference in the simulation mechanisms and in the resolution.

2.2.8 Numerical prediction of mechanical properties of cement paste

The complexity of the microstructure and the computational cost associated with it requires a thourough thinking about the approaches and simplifications. The replacement of the 3D microstructure by 2D slices is tempting. However, Hain and Wriggers [26] showed on CT-scans that the plane stress and plane strain conditions in 2D are 30 % lower than from a 3D microstructure. The results suggests that the connectivity in 3D is very different and cannot be easily established through 2D microstructure.

Boundary conditions and size of the computational volume

Various sizes of computational volumes appear in the literature, mostly based on the size of the largest particle in the system. Bary used the size of a computational volume as 100 (115) μm - 5 times of the size of the largest particle. Smilauer used computational volumes between 20 and 75 μm [64]. Based on his results, he concluded that bigger CVs are needed for early ages. The smallest limit ever, was suggested by Hain and Wriggers [26], who used computational volumes between 4 and 72 μm on real microstructural images for fully hydrated cement paste. Similarly to Smilauer, using linear displacement boundary conditions they confirmed, that the

lower the CV, the higher the efffective properties. Since, their upper limit turned out to be not representative enough, they accounted for insufficient representativness by using about 10000 CVs with a size 64 μm.

Some boundary conditions, i.e. linear displacement boundary conditions, seem to violate the local equilibrium at the boundary of voxel meshes [26]. The microstructure has to be therefore embedded into a window of average stiffness and the boundary conditions have to be applied to this window. The method is similar to the Self-Consistent approach. The size of the window appears to influence the result, the bigger the window, the better the prediction. Hain [26] used windows between 0 and 16 μm (the size of the internal material is 64 μm), but a window of 4 μm yielded only by 5 % different values than a window of 16 μm micron. He also found out that the elastic properties of the window have an effect of the prediction and suggested to use the elastic properties from experiments. The effective properties of the microstructure in this case are obtained iteratively.

Static boundary conditions seemed to be the worst situation for an iterative solver. If not sufficient number of iterations were used, a highly non-isotropic response was obtained. Periodic boundary conditions have been shown to give a result quasi-independent of the size of computational volume [64].

Poromechanical boundary conditions

Two types of boundary conditions have been used to study effective elastic properties - drained (water is free to flow through the connected network of micropores, macroscopic loading does not activate significant pore pressures) and sealed (water cannot leave the volume of cement paste).

Pichler et al [56] showed that the sealed conditions follow the trends of the Boumiz experimental data significantly better than the drained conditions. He concluded that in the ultrasonics testing cell rather sealed conditions than drained conditions were present. However, the resonant-frequency measurements taken at very early ages of cement paste with w/c = 0.35 show the drained conditions were able to reproduce the measurements at early age better. This suggested that the resonant frequency tests might correspond to drained conditions rather than to sealed conditions.

Mesh

Very little seemed to be done for mesh generation for the cement paste level. Apart from a very recent effort of Bary et al.[4], almost exclusively voxel meshes have been used for the predictions.

A voxel mesh is an equally spaced, uniform grid, where one voxel corresponds to a brick element in the form of a cube. The use of voxel meshes is convenient, since it is a result of the use of digitally based microstructural model and X-ray tomography images. Simulations with the CEMHYD3D model revealed that the behavior of such a microstructure is too stiff at early ages, compared to the experimental data. The reason for that is the presence of artificial connnections. Because isolated clusters do not contribute to the shear stiffness, it is recommended that the isolated clusters are removed and replaced by water-filled porosity. This itself did not seem to be sufficient - the early age microstructure still seemed to be too stiff compared to the experimental data [64]. For CEMHYD3D model Smilauer reasoned that the reason lies in different contact type between percolation and FEM; while percolation takes into account a connection face-to-face, FEM takes into account displacements at nodes. That way it may have happened that two adjacent brick elements are in a spanning cluster, share the same nodes but belong to different cement grains. He tried to remove this effect by separating the displacement at that node and introduced so called split nodes, which replace to some extent the contact elements and relax concentrated stresses as well [64]. The use of this scheme sometimes resulted in even lower values of stiffness than the lower bound FFT method. So it seems, that the result is heavily dependent on the number of split nodes which are introduced.

An attempt to create a proper geometry-aligned mesh was made by Bary. Bary et. al [4] simulated hydrated cement paste using 800 - 2800 inclusions, with a maximum ratio in size 6, minimum distance 0.3 μm. This distance was the result of the computational cost. The corresponding mesh in the case of 2800 inclusions already contained 1.15 million nodes and 6.5 million tetrahedra. This points out a huge computational cost associated with microstructure-aligned geometries.

2.3 Summary

In the view of the literature review, it seems that mostly analytical approaches have been used for the prediction of elastic properties. The studies all come to a common conclusion, that analytical approaches are not suitable for high porosity ranges and early ages and overestimate the value of percolation threshold. Studies of the shape of the particles are common, and suggest that shape matters, especially for early age microstructures.

On the other hand, the Finite Element method as a prediction technique has not been studied very much, although it appears to provide a good interface for the prediction of early age mechanical properties, as it is able to capture to some extent the complex geometry. Some non-physical phenomena connected to the FEM have been pointed out and a corresponding treatment has been suggested. Very little work has been done on meshes for the FEM especially at early ages. There is almost no study of the effect of change of intrinsic properties of the phases, studies on the particle shape were only performed for later ages. Very few simulations have been performed with a microstructure from a vector microstructural model.

In the following chapters, our study is going to focus on the prediction of early age elastic properties, based on a 3-D microstructure. This is in order to come as close as possible to the phase arrangements which seem to be so influential for the mechanical properties. In the first instance, specific problems of FEM associated with early age microstructure will be addressed. These include resolution, mesh type, integration scheme, size of the computational volume. Later, FEM will be applied to different microstructural parameters, such as flocculation, different w/c ratios, particle size distributions and number of the hydrate clusters. In the last part of the study, we will focus on the experimental validation.

Chapter 3

Numerical modelling

Cement microstructure, as a result of complex interactions, is a whole world of poorly defined geometries. There is no universal method as to how such complex microstructures should be modelled. In the end, the best approach will depend on the property of interest and - specifically for cement - on the age.

The basic approach of this study is shown schematically in Fig.3.1. The microstructure is generated by a vector microstructural model, meshed and the effective elastic properties are computed by the Finite Element method.

The mesher and Finite Element solver were developed for the purpose of this study in Java. Object-oriented paradigm allowed to write easily portable, extensible and maintanable code, which was simultaneously optimised for structured meshes. The code can be used as standalone or with connection to faster mathematical solvers developed in C++ or Fortran.

From the complexity of the microstructure and the computational memory overhead connected with it, it is clear that we will not be able to capture all the geometrical features of the microstructure. For early ages, while the geometry should be preserved to the greatest possible extent, it is also important to conserve other aspects such as the overall volume fractions.

The methods used in this study aim at achieving a trade-off between capturing the geometrical features, preserving the most important factors for the prediction and keeping the computational cost at realistic values. The generation of microstructure is described in detail. Numerical homogenization and several meshing

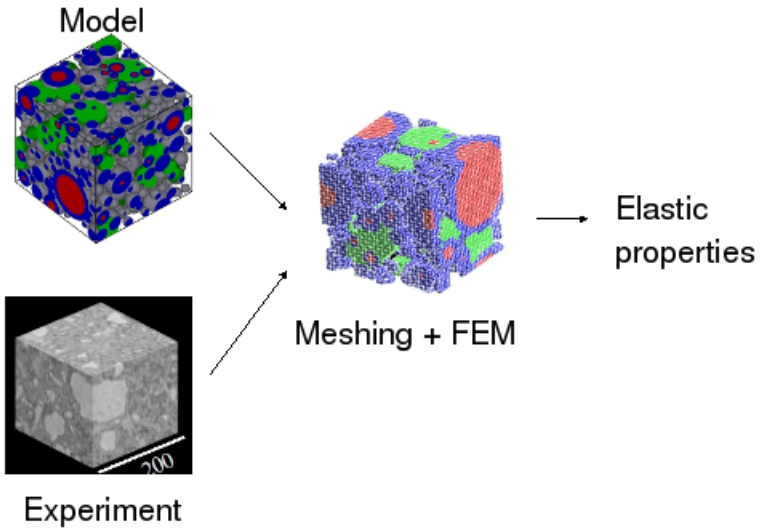

Figure 3.1: Process of the prediction

approaches were studied in order to better resolve material boundaries.

The treatment of capillary porosity, which causes specific problems in FEM is discussed. The sensitivity of the prediction of mechanical properties to the microstructural arrangement and mesh resolution were investigated. Rigorous bounds are used in order to deal with the multiple-phase elements in the Finite Element computation.

3.1 Generation of microstructure

The choice of a microstructural input limits or allows more flexibility in the prediction method. Input for a prediction can be provided from an experiment or a microstructural model. A vector microstructural model was chosen for our study. By modelling the microstructure as a set of vector objects (spheres) it is able to provide an input with no resolution limits and provide more flexibility in the next computational stages. This also allows microstructures to be generated quickly, so the study is not limited by the time for microstructural characterisation.

An alite microstructure, which dominates the setting and hardening process, was used to study the basic factors influencing the FEM prediction. This microstructure was obtained from a vector microstructural model μic developed at LMC EPFL [11], which derives its basics from the work of Navi and Pignat [52]. Reactants and

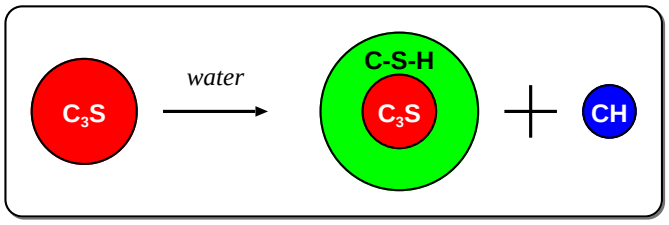

Figure 3.2: Alite hydration

products in this model are represented by spheres in a continuum space. The size of a representative volume, particle size distribution, w/c ratio and kinetic parameters are needed as an input for the model. The microstructure is generated by a random placement of the cement grains into the numerical volume. Two main hydration products are formed during the hydration, namely calcium-silicate-hydrate (C-S-H) mostly formed around cement grains and calcium hydroxide (CH) formed in the pore space in case of alite hydration - Fig.3.2.

In order to identify the main factors which play a role in the prediction of effective elastic properties, we decided to perform simulations on simple microstructures of C_3S. The span of the simulation is from 0 to 45 % of the degree of hydration. Only one type of C-S-H is considered for the prediction with the density 2.0 g/cm^3. This density is considered to be an average of what Jennings [38] considers to be LD and HD C-S-H.

The prediction is carried out for a w/c ratio 0.4 and a realistic particle size distribution (mean 8.1 μm), taken from the thesis of Boumiz [12], see Appendix. A narrow particle size distribution was chosen to keep the number of particles in the computational volume small. This approach allowed the study of basic problems before going to microstructures with a large number of particles. The number of portlandite (CH) clusters at the end of hydration was assumed to be 20 % of the total number of cement grains at the beginning [39]. This assumption has the purpose of creating cement-like computational volume. The number of CH clusters and their distribution is a direct input to the model - see Appendix. There are indications that during the hydration of alite only few but big portlandite clusters appear [18], [62]. We observed a presence of 'grains in a grain' - i.e. hydrating grains embedded in a big portlandite cluster. This would require much larger computational volume

and result in much lower resolution. Therefore cement-like proportional particle size distribution of CH was chosen. The microstructure generation did not require knowledge of the kinetics parameters, as the simulation considered only the degree of hydration which was then empirically related to time through experimental data (module Externally Defined Kinetics in the hydration model). The size of the computational volume varied between 3 - 5 times size of the biggest cement grain particle, resulting in 60 - 100 μm, respectively. The microstructure was firstly generated for a CV of 100 μm.

3.2 Finite Element method and numerical homogenization

The FEM has been extensively used to analyze computational volumes, to determine the mechanical properties and in the present work the FEM micromechanical analysis method is applied to periodic volumes of cement microstructure. Once the computational volume is proven to be representative, it is assumed that the average mechanical properties of a RVE are equal to the average properties of the heterogeneous material. The average stresses and strains in a RVE are defined by:

$$\overline{\sigma}_{ij} = 1/V \int \sigma_{ij} dV \tag{3.1}$$

$$\overline{\varepsilon}_{ij} = 1/V \int \varepsilon_{ij} dV \tag{3.2}$$

The output of the Finite Element simulation are the displacements of the nodes and the stresses and strains at the integration points of the elements. In order to obtain the stiffness (or compliance) matrix, average stresses and strains in the RVE are needed. These are obtained firstly as an average of the integration points in the element. In the second step, the element stresses are averaged proportionally to their volume over the whole microstructure. The stiffness matrix is obtained from the constitutive law between the averages of stresses and strains. Young's modulus and Poisson's ratio (or any other combination of elastic constants) are obtained from any two non-equal members of the stiffness (compliance) matrix.

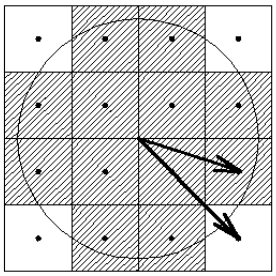

Figure 3.3: Assignment of a material to the voxel

3.2.1 Finite Element solver

Two types of solvers exist for systems of linear equations - direct solvers (based on Gauss elimination) and iterative solvers. When considering very large finite element systems, direct solvers can require a large amount of storage and computer time. The required storage is proportional to

$$neq\sqrt{neq} \tag{3.3}$$

,where neq is the number of equations. In practice, the storage on a computer frequently limits the size of the finite element problem. On the other hand, iterative solvers require much less storage because only the non-zero matrix elements under the skyline of the matrix and some arrays for preconditioner and iteration vectors need to be stored. Iterative conjugate gradient solver with preconditioning was used for our purpose.

3.2.2 Voxel mesh

The output of the microstructural model is a set of spheres, defined by their centre and radii and the order of their placing. The generation of the voxel mesh for spherical objects follows a simple rule. The radius of a sphere is compared with the distance of the sphere center and the voxel center. In case the radius is bigger, voxel is considered to lie inside the sphere and the material properties of the sphere are assigned to the voxel - Fig.3.3. In case of layers, the voxel centers need to be checked against all layers.

The problem with this method is that because the resolution of the mesh is limited, many particles are below the size of the resolution and will not be meshed.

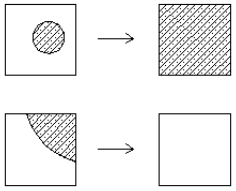

Figure 3.4: Assignment of a material to the voxel

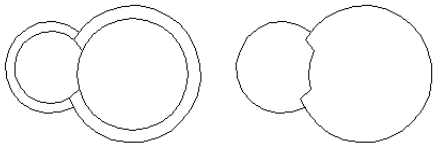

Figure 3.5: Non-spherical particle boundaries due to the presence of layers

We therefore used a method, which statistically preserves the volume fractions of the phases in the computational volume - if the centroid lies within a phase, it is assumed that the entire volume lies within the phase - Fig. 3.4. In practice, the material in the middle of the voxel cannot be easily determined by searching over the spheres. This is because the spheres and their layers overlap. Instead the voxels are subvoxelized and the material of the voxel is taken as the material of the middle subvoxel. This method has one disadvantage - the local information is not preserved anymore and the previously disordered voxels become one-phase isotropic media.

The generation of the mesh for a new time step is always based on the microstructure from the previous step. Since it is very awkward to transfer the information about jagged boundaries in terms of vectors - Fig. 3.5, because it requires a lot of processing and storage, the information is kept in the terms of voxels (the non-spherical boundary is voxelized).

Due to the limited resolution and the way we mesh the microstructure, the particle size distribution cannot be captured under the mesh resolution and an effect of two different particle size distributions will only be visible if there is a difference in the particle size distribution larger than the mesh resolution.

3.2.3 Elastic properties of the phases

The elastic properties assumed for the phases are listed in the table below and based on published nanoindentation data [17], [77]. The elastic properties of water are discussed in the section on Poromechanics boundary conditions. The phases themselves are assumed to have linear elastic behavior. Perfect bonding is assumed between the constituents. Linear hexahedral elements are used in case of the voxel mesh with standard number of 8 integration points.

Because only one type of C-S-H is considered, its properties are taken as an arithmetic average of the LD C-S-H and HD C-S-H. This is based on the assumption that the ratio of LD to HD C-S-H is 1:1 for w/c 0.4, once the hydration is complete [38]. This is not the case for early age, however because there is a lot of uncertainty in the data on C-S-H and indications that the density of C-S-H might be higher, we will use an average value throughout the studied range of hydration.

	Young's modulus [GPa]	Poisson's ratio[-]
alite	135	0.3
belite	130	0.3
aluminate	145	0.3
C-S-H	25.55	0.24
CH	38.5	0.305
ettringite	22.7	0.25
water	0.001	0.499924

3.2.4 Poromechanics boundary conditions

Two extreme cases of the macroscopic poromechanics boundary conditions are known - drained and undrained. Under drained conditions, water is free to flow through the connected network of micropores and the pressure state within the pore fluid is controlled by the conditions outside the CV. That means that macroscopic loading does not activate significant pore pressures. This behavior can be introduced by considering water as a phase with vanishing elastic properties.

In our computation, undrained conditions were considered. Under sealed conditions, water cannot leave CV of the cement paste and macroscopic loading activates

pore pressures. This refers to a problem of poro-micromechanics and a new degree of freedom - pore pressure - would have to be introduced. However, to keep the computational cost at minimum, we considered these undrained conditions within the framework of classical micromechanics of solid materials, by introducing water as a quasi-solid phase with a shear modulus of almost zero and a bulk modulus of 2.18 GPa. For later ages, it would be necessary to consider semi-drained state, knowing that water disappears earlier from larger capillary pores than from smaller ones.

3.2.5 Artificial connectivity in the microstructure, percolation threshold

A standard voxel mesh of 100 elements per side was generated for the above mentioned microstructures (for CV of 100 μm this corresponds to the resolution of 1 μm). In the first instance, mixed displacement boundary conditions were applied on the faces of the microstructure, assuming that they produce a result which we could call representative. By mixed boundary conditions we mean conditions which are applied in a compressive strength test. Two of the faces are constrained with a prescribed displacement - one zero, one non-zero displacement, other four faces are free.

Figures 3.6, 3.7 show elastic properties with age. Note that there is a big overestimation of the elastic properties at the beginning of hydration if full microstructure (microstructure as it comes from microstructural model) is used. This is something which has been observed previously [63] and is not coherent with the experimental observations - e.g.[65].

It is known, that the Young's and shear modulus of cement paste do not occur at the very start of hydration, but typically only after the setting time. This moment is known as a percolation threshold - a moment, when a spanning cluster occurs in the microstructure and a load can be transmitted from one part to the other. At the micrometer scale, this percolation threshold is considered to be a material property that is mainly affected by the w/c ratio and cement fineness.

The reason for the overestimation of elastic properties at the beginning of hydration is caused by the artificial connectivity in the mesh. Artificial connectivity can

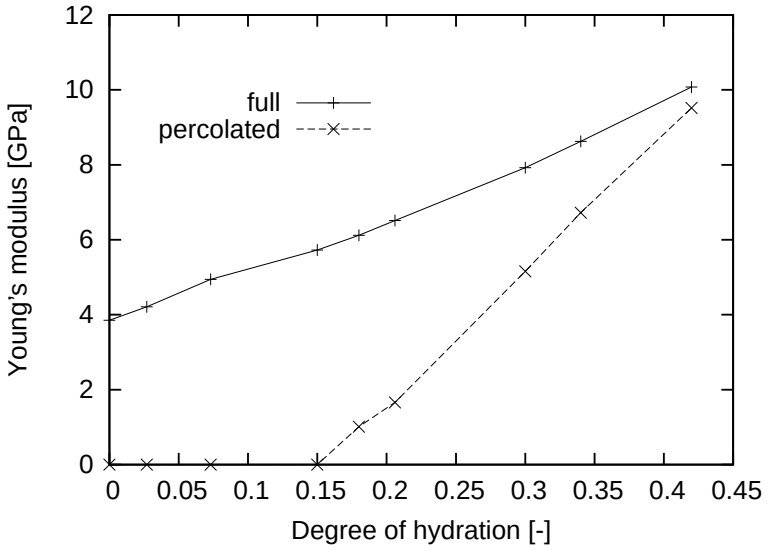

Figure 3.6: The effect of burning on Young's modulus, CV 100 μm

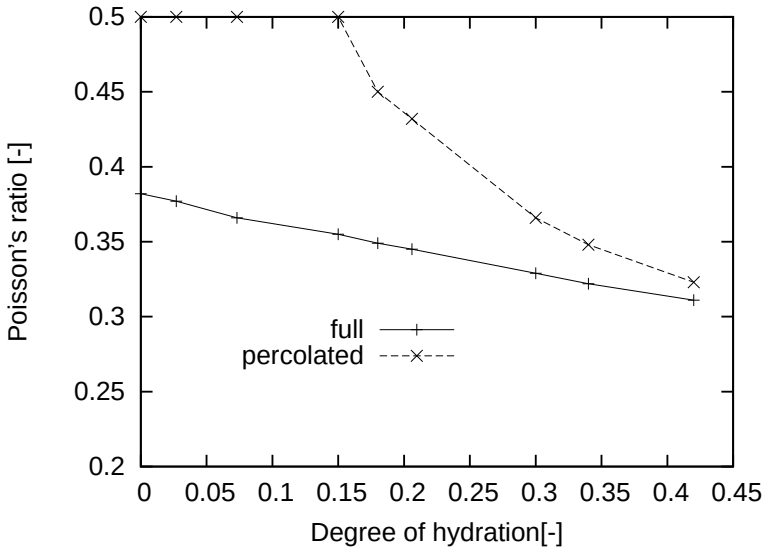

Figure 3.7: The effect of burning on Poisson's ratio, CV 100 μm

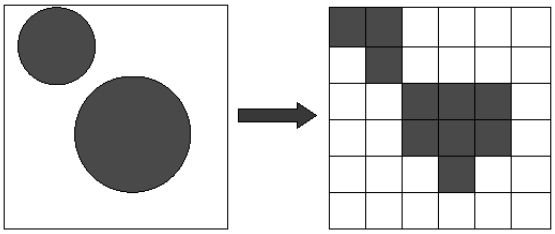

Figure 3.8: The origin of artificial connections

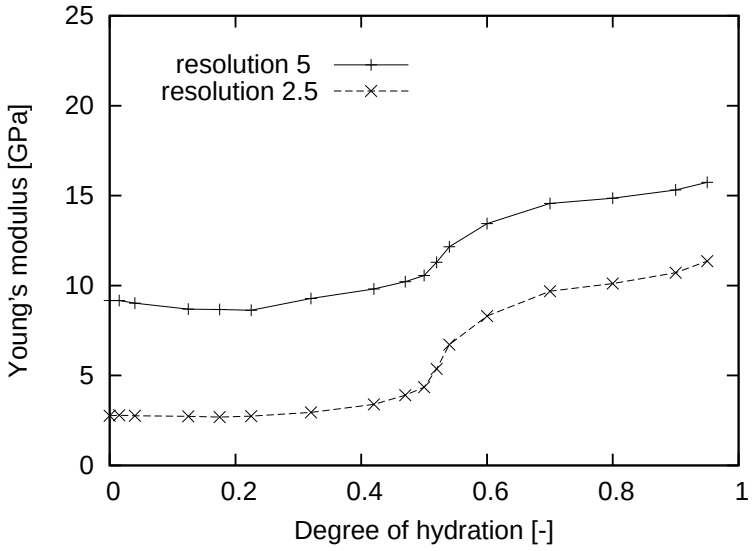

Figure 3.9: Effect of resolution on a simple microstructure

be seen by looking at the 2D or 3D image of the generated microstructure and is a result of insufficient resolution - Fig.3.8. If we achieved ideal resolution, which is due to computational reasons not possible, such an effect would not occur. The effect of resolution can be easily demonstrated on a simple microstructure of approximately 50 particles. Tested for two different resolutions (2.5 and 5 μm), Fig. 3.9, the effect on the Young's modulus is drastic and with the increase in resolution the simulated results come closer to what is observed experimentally with similar microstructures [65]. This is because the material boundaries are resolved better and simultaneously the FEM solution for the same geometry captured by more elements becomes softer. With real microstructures with a broad range of particle sizes, due to computational constraints, such a dramatic effect of the resolution on the convergence of numerical and experimental values is not apparent.

The artificial connectivity can be dealt with by application of a burning algorithm which is applied to the microstructure before meshing and is used for the study of percolation (the amount of the solid fraction connected).

The burning algorithm is based on the idea, that only spanning cluster can transfer mechanical properties and the isolated clusters can therefore be removed from the microstructure. Before the microstructure is meshed for FEM, the isolated clusters are eliminated by this algorithm - Fig.3.10, 3.11. Since at the beginning of hydration nothing is connected and the microstructure is therefore empty, only the microstructure after the percolation threshold is used for FEM computations.

Whether there are disconnected clusters in the microstructure at the beginning of hydration is questionable, however from a mechanics point of view the assumption of throwing away disconnected clusters seems reasonable.

Two groups of burning algorithm methods exist. The first group is based on a very fine voxelization of the microstructure. This is generally at least ten times finer than the FEM mesh. Occupied sites of the microstructure are labelled, each cluster with a different label. Percolation threshold is reached, when there is the same label at two opposite surfaces of the system [66]. The problem with this method is that the whole microstructure needs to be kept in memory and the resolution of the algorithm is therefore limited.

The second type of algorithms is based on a vector approach. Overlaps between the particles are checked by classical geometrical means. In order to avoid checking for overlaps between all the particles, particles in the CV are localized into several bounding boxes. This method is more cost-effective, especially when it is an inherent part of the vector microstructural model, which was used here.

The results for both full and depercolated microstructure of alite - Fig.3.6, 3.7 show that simulated elastic properties for microstructures which contain only the spanning cluster are much closer to experiments [65]. The difference between the two methods is remarkable at early age. In time, when, more and more clusters get connected, the difference becomes less. For the microstructure studied, the results are similar from approximately 35 % hydration - Fig 3.6. The Poisson's ratio starts from the value 0.5 and decreases, which very well corresponds to the elimination of water in the system in time. The percolation threshold appears at 15 % of hydration,

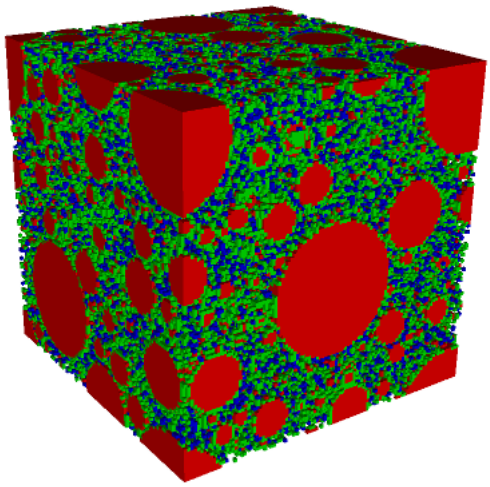

Figure 3.10: Complete microstructure from microstructural model, CV 100 μm, 20 % hydration

which seems to be high and might have to do something with the initial packing of the particles. This problem will be examined later.

3.2.6 Element type and numerical integration scheme

Another reason for overestimation might be hidden in what is in FEM known as locking and is caused by the presence of water in the capillary pores of the microstructure.

In the Finite Element analysis, the numerical integration is generally performed by the use of Gauss quadrature, in which the polynomial of order (2n - 1) is integrated exactly with n function evaluations. The choice of the order of the numerical integration is important because the cost of analysis increases when a higher-order integration is employed. Secondly, the result can be very much affected by the integration order used. A low order of the integration scheme can result in bigger number of zero eigenvalues than the number of physical rigid body modes. The result would be a singular stiffness matrix.

While the solid phases in the system do not pose a problem for the standard integration scheme, the water elements representing the capillary porosity do. Elements with a Poisson's ratio close to 0.5 experience a phenomenon called locking - underestimation of the displacement, resulting in the overestimation of stiffness.

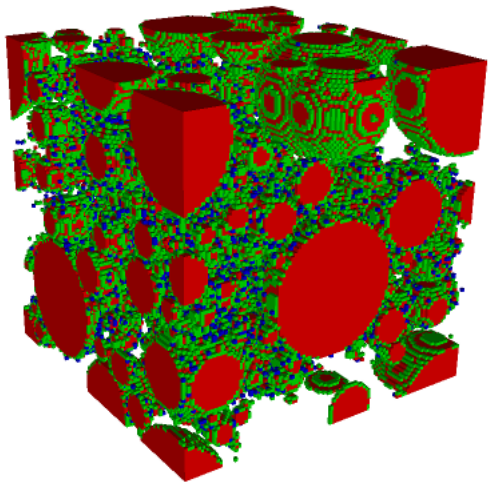

Figure 3.11: Spanning cluster (percolated microstructure), CV 100 μm, 20 % hydration

Locking phenomenon can be observed by evaluating eigenvalues and eigenvectors of the stiffness matrix of the water element. High eigenvalues with eigenvectors in the shape of a skirt suggest locking - Fig.3.12. Selective integration scheme needs to be used to solve this problem. The problematic volumetric part is evaluated by a lower number of integration points, while the shear part is integrated with the standard number of points.

Selective integration is based on the fact that the displacement formulation of the FEM yields a strain energy smaller than the exact strain energy of the mathematical model considered. Therefore we may expect that by not evaluating the displacement-based element stiffness matrices accurately in the numerical integration, a better overall solution can be obtained [5].

Therefore, before going on further with the analysis, the effect of locking was explored with a view of removing it.

Selective integration was employed for the studied microstructure. The shear part was integrated using the standard number of integration points (8), while the problematic volumetric part was integrated using only one integration point. The results from the two integration schemes can be seen in Fig.3.13, 3.14. The Young's modulus based on the selective integration is lower and qualitatively it can be seen, that the importance of the integration scheme is greater at early age. This is mostly

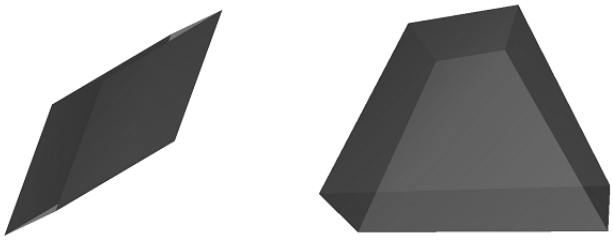

Figure 3.12: Standard shear mode and locking skirt mode, eigenvalues 0.333 and 731 respectively, deformed shape based on eigenvectors

because the amount of water decreases with time, so the selective integration does not improve the result so much. The Poisson's ratio shows higher values with the selective integration.

3.2.7 Effect of eliminated clusters

The burning algorithm, as it was applied so far, simply assumed that porosity does not transfer any mechanical properties. Under the condition, that the pores are filled with air, the burning algorithm should be valid, because the elastic properties of air are very close to zero and the disconnected clusters are redundant. However, this is not true in the case of water, which has a non-zero bulk modulus and is able to transfer some part of the load to disconnected clusters, as well. Discarded disconnected clusters should not be replaced by water alone, but by an effective medium of water and disconnected clusters.

We decided to evaluate the effect of the effective medium by an analytical homogenization scheme. Because the microstructure at the beginning of hydration has a particulate structure - cement grains embedded in a water matrix - we chose for the approximation the Mori-Tanaka [49] homogenization scheme. Although it is known that the method does not work very well for the microstructures with more than 30 % of particles, the solution is more reasonable than that which would be produced by a Self-Consistent scheme [31, 42], since the latter has an intrinsic perco-

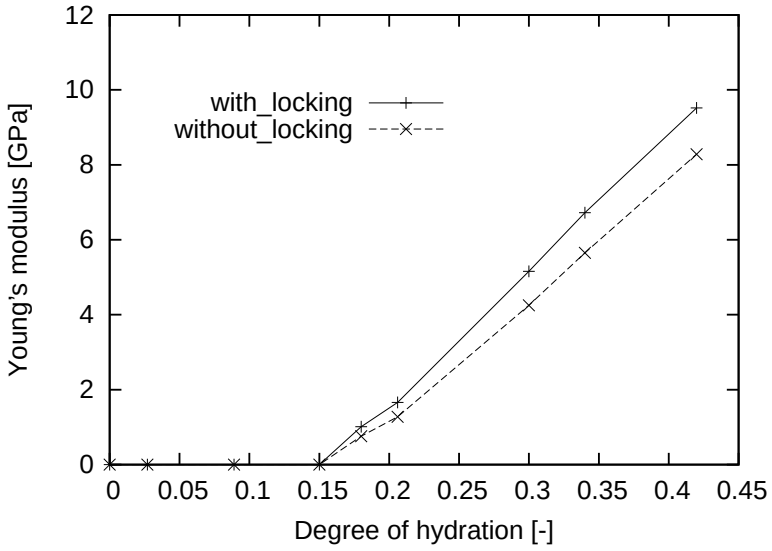

Figure 3.13: The effect of integration scheme on Young's modulus, CV 100 μm

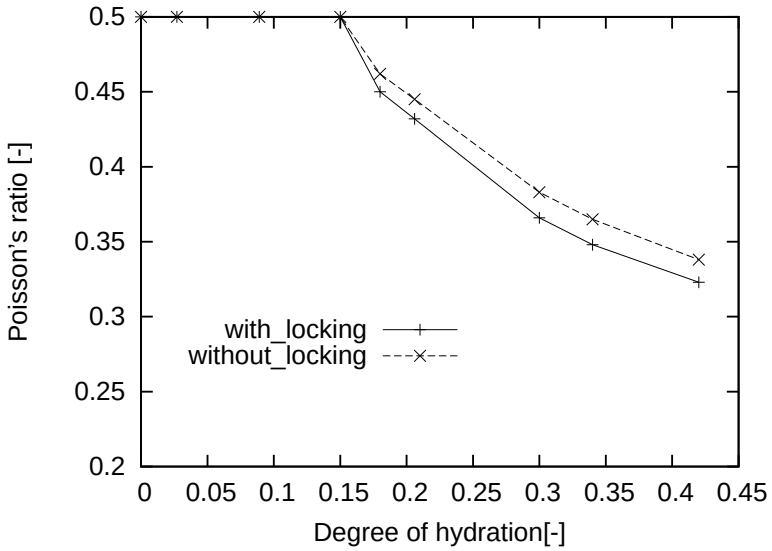

Figure 3.14: The effect of integration scheme on Poisson's ratio, CV 100 μm

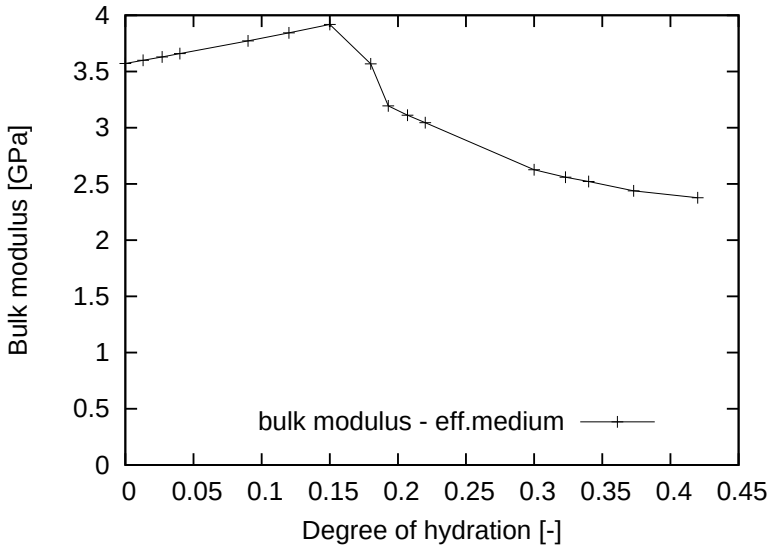

Figure 3.15: Bulk modulus of the effective medium, CV 100 μm

lation threshold. In our case, even if the volume fraction is higher than the intrinsic percolation threshold of the Self-Consistent scheme, we know that the medium of isolated clusters is not connected and the matrix phase is always water. Once the properties of the new medium are evaluated, its elastic properties are inserted into FEM computation instead of the properties of water.

The homogenization has shown that the bulk modulus of the medium is approximately twice that of water. The highest value of the bulk modulus is at the percolation threshold, because the amount of isolated volume fraction is the highest - Fig.3.15.

In the next step, the properties of the effective medium were inserted into the FEM scheme instead of water. The results can be seen in Fig.3.16 for the resolution 1 μm. There is no change in Young's modulus, while the Poisson's ratio is higher than what it was with the original scheme. The difference can be explained in terms of bulk modulus - Fig.3.17. At the start of hydration, the importance of the effective medium is higher, the disconnected solid clusters enhance bulk modulus more than in later ages - i.e. the disconnected clusters increase incompressibility of the microstructure at early ages.

In the subsequent work, simulations will be performed with the microstructure with spanning cluster embedded in the effective medium. The numerical integration

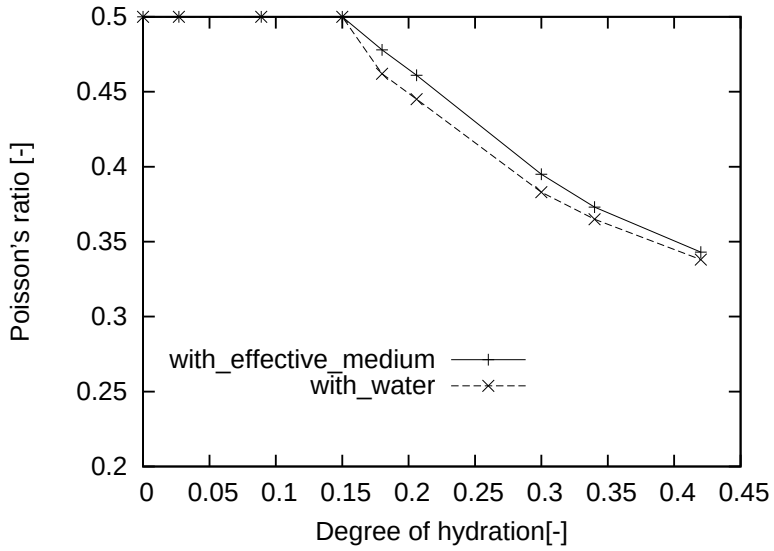

Figure 3.16: The effect of the effective medium on Poisson's ratio of the microstructure, CV 100 μm

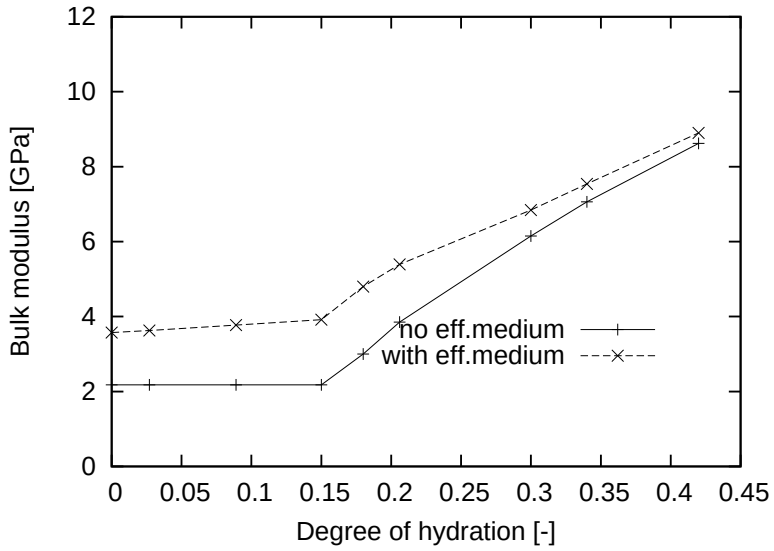

Figure 3.17: The effect of the effective medium on bulk modulus of the microstructure, CV 100 μm

will be performed with the use of a selective integration scheme.

3.2.8 Error of the Finite Element Method

The solution obtained by the Finite Element method is approximate and what is meant by the error of the Finite Element method is usually an error between the exact mathematical solution and the approximation, in sense of displacement and stresses or strains. The very act of subdividing the continuum provides the opportunity for discretization errors. The type of integration scheme used is a cause of 'elemental' errors [20].

Elemental errors are evaluated before they are applied to a specific problem and they are referred to as "a priori error analysis". In our study, this type of error is the volumetric locking phenomenon, which occured with water elements and is studied in the section Element type and numerical integration scheme. We do not expect the presence of other elemental errors such as parasitic shear, spurious zero-energy modes and shear locking, since they are mostly relevant to beam elements.

Discretization errors can only be evaluated after the problem is solved, and therefore they are known as a posteriori process. Discretization errors can be evaluated by refinement of the problem and can be seen explicitly in Finite Element results as discontinuities or jumps in the stresses or strains between elements. In our analysis, the discretization error is the error of the mesh resolution, therefore for the same CV size, several mesh resolutions were studied.

For the study of the discretization error, we chose a CV of 80 μm. This was in order to show a bigger range of resolutions - i.e. from 0.5 to 2.5 μm. The resolution of the voxel mesh seems to be highly important even on the microstructure containing only the spanning cluster - Fig.3.18, 3.19. This can be explained by the artificial connectivity in the spanning cluster, which appears because burning algorithm removed only part of the possible connection problems - Fig.3.20. The resolution problem does not seem to be significant till about 20 % of the hydration. This is most probably due to lower volumes of solid present in the spanning microstructure, simultaneously minimizing artificial connections.

The problem, especially at later ages, led to the investigation of advanced meshing techniques for the microstructure with a spanning cluster, such as tetrahedral

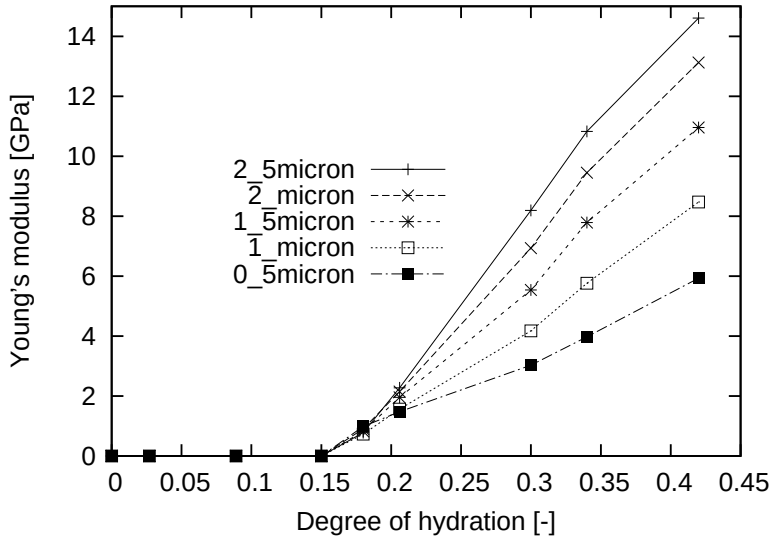

Figure 3.18: Resolution effect on Young's modulus, CV 80 μm

and octree refinement.

3.2.9 Octree refinement

In order to increase the accuracy of the discretization of the boundaries of the particles and decrease the number of artificial connections, octree-refinement was applied, which produces non-conforming elements - Fig.3.21. With this refinement, voxels are refined only to better resolve material boundaries, not to minimize the error estimates associated with the displacement solution fields as is commonly done in step-refinement procedures. Only one-level refinement will be used in this study in order to maintain the computational cost.

Because of the requirement of keeping the history of the previous hydration steps, classical octree refinement, based on the geometrical description, is not applicable here. Instead two or more regular meshes are created and merged together. The procedure consists of looking at the same location in the coarser and refined mesh. If the place in the finer mesh contains the same volume fraction of the phase as in the coarser mesh, the voxels are merged into one. In any other case, the location stays subdivided - Fig.3.22.

The octree mesh consists of non-conforming elements - Fig.3.21 and in order to perform FEM, consistency between the coarse and refined part must be ensured.

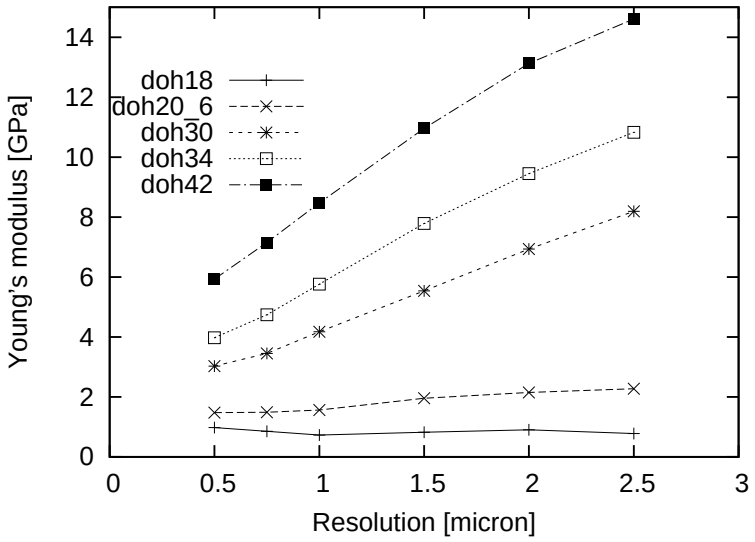

Figure 3.19: Resolution effect on Young's modulus for different hydration degrees, CV 80 μm

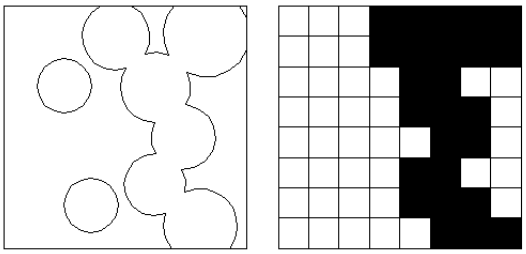

Figure 3.20: Artificial connections in the spanning cluster

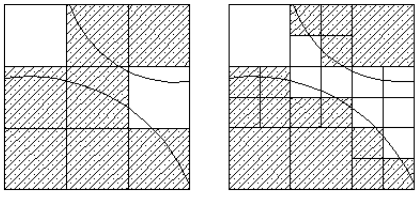

Figure 3.21: Octree refinement to resolve material boundaries

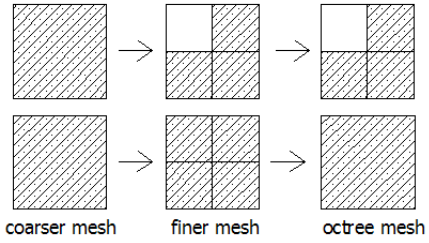

Figure 3.22: Merging procedure for the creation of the octree

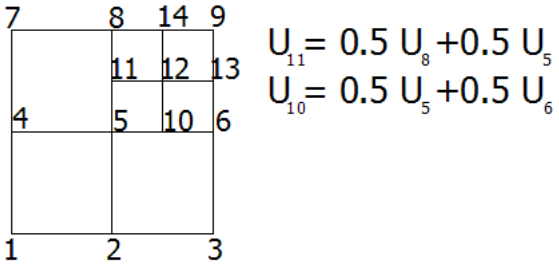

Figure 3.23: Hanging nodes consistency

Two options are available to solve this problem - transition elements [54] and a hanging node technique. Transition elements are rather awkward when it comes to complexities in the mesh. In order to allow further refinement in the future, we opted for the technique of hanging nodes. In the hanging node technique, additional algebraical constraints are added to the system of equations to ensure consistency. An additional matrix is created from the constraint equations and the constrained degrees of freedom are eliminated from the system of equations by static condensation. The technique can be illustrated on a simple example - hanging node 11 is not an unknown in the system of equations, instead its displacement is interpolated from nodes 8 and 5 - Fig.3.23. Although the presence of hanging nodes does not introduce additional computational requirements, the approach itself does. This is because the refinement of two neighbouring cell produces a standard, not a hanging node.

To show the effect of the refinement, four meshes - three structured meshes with the resolution 1, 0.75 and 0.5 μm and one octree mesh, containing both types of resolution. Detail of the generated mesh can be seen in Fig.3.24. The total number of elements in the refinement scheme is dependent on the age - i.e. at early ages

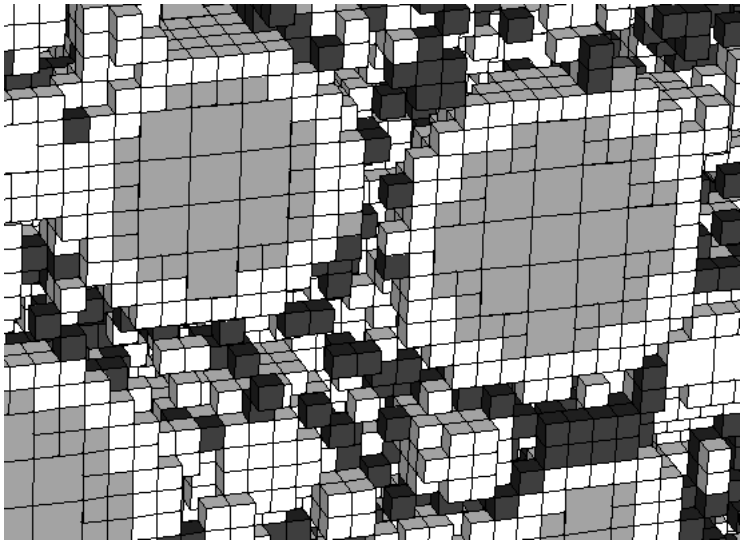

Figure 3.24: Detail of the generated octree mesh

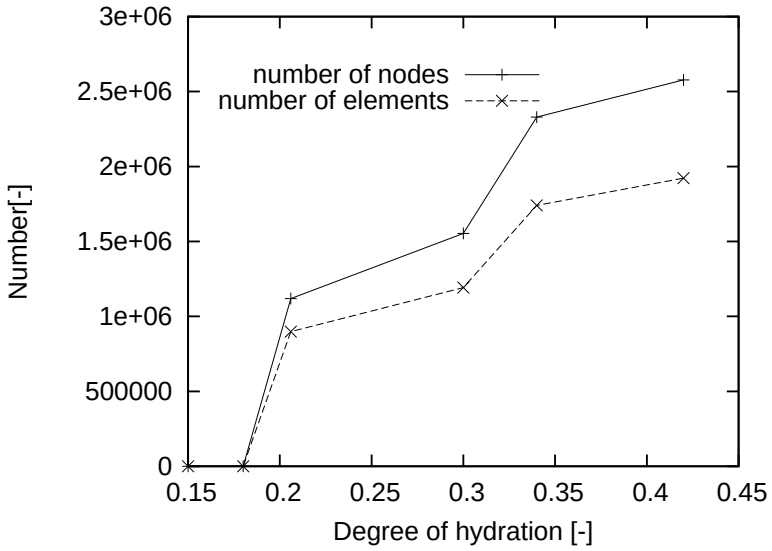

Figure 3.25: Number of elements and nodes for an octree with age

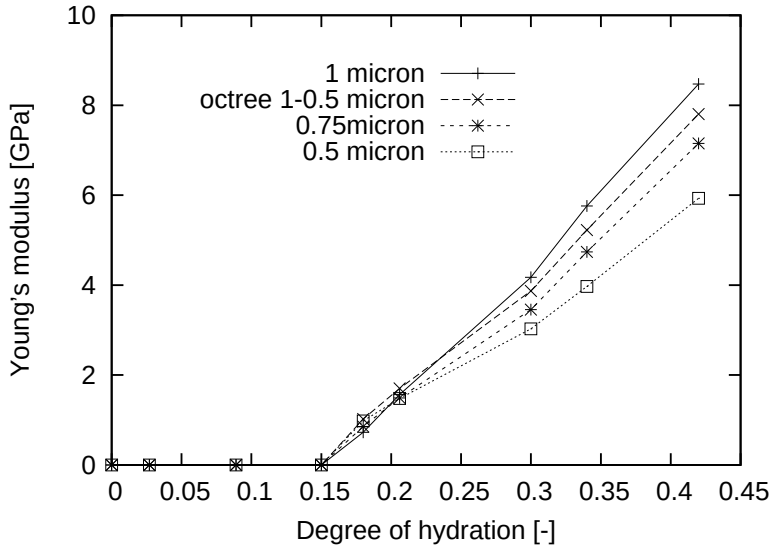

Figure 3.26: Effect of the refinement on Young's modulus

the number of elements is lower than for later ages - Fig.3.25. This is a result of the existence of bigger alite cores at the beginning of hydration, which do not need refinement.

As can be seen from the Fig.3.26, the refinement scheme decreases effective Young's modulus, but not dramatically. At early ages, the results are even higher than the original coarse mesh. This is perhaps due to numerical instabilities and with such small differences in elastic properties, it is difficult to draw conclusions. The results compared to a middle-sized regular mesh with the resolution 0.75 μm show, that it makes sense to strive for higher resolution on a regular mesh, rather than apply octree. This could be due to locking, which might not have been fully removed by the selective integration and became pronounced with additional constraints in the octree mesh.

What could be achieved by octree, can be demonstrated on a simple microstructure containing 50 particles. This is a full microstructure (spanning + isolated clusters) and it can be seen, that the method helps to decrease the properties significantly at later ages (after 50 % of hydration)- Fig.3.27. The early age effect is not highly improved, again, most probably due to the presence of locking (the number of problematic water elements is higher at early age).

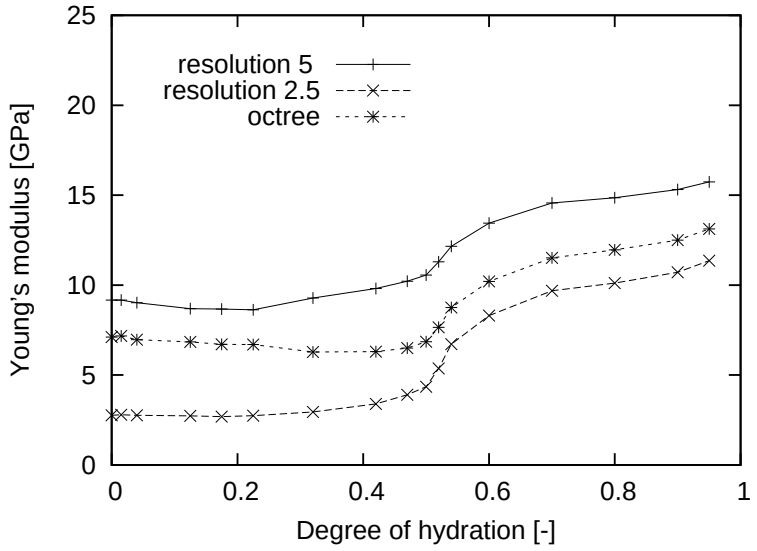

Figure 3.27: Effect of the refinement on Young's modulus on a simple full-cluster microstructure

3.2.10 Regular tetrahedral mesh

Another technique which could help with resolving the material boundaries is a regular tetrahedral mesh. A regular tetrahedral mesh is created by decomposition of cube into 5 or 6 tetrahedra. Smoothing is usually performed on this type of mesh, nevertheless this is not applicable for this study due to the complex overlapping and layered geometry.

There are several requirements for the decomposition. First, the new elements have to have a good geometrical aspect ratio for the FEM performed in the next stage. Secondly, in order not to increase the memory requirements, the decomposition should be performed in such a manner that the number of nodes is not increased. Thirdly, compatibility of the element walls, i.e. displacement field has to be preserved and therefore the orientation of tetrahedra cannot be random. Provided all these requirements are fulfilled, elements should also be able to fit the spherical geometry - Fig. 3.29. For all the above mentioned reasons, we chose a subdivision into 5 tetrahedra - Fig. 3.28, which was previously applied at the concrete level by Guidoum [24].

By performing the refinement on the chosen microstructure we found that the

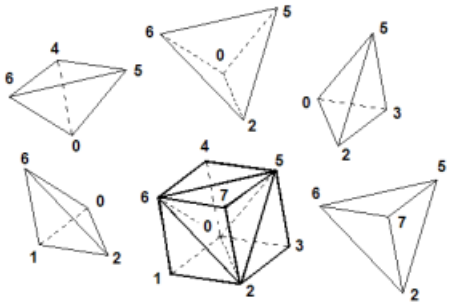

Figure 3.28: Decomposition of a cube into 5 tetrahedra

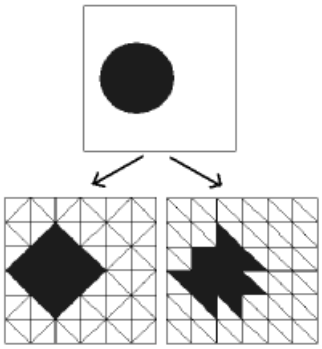

Figure 3.29: 2D section of a 5-tetrahedra (left) and 6-tetrahedra (right)

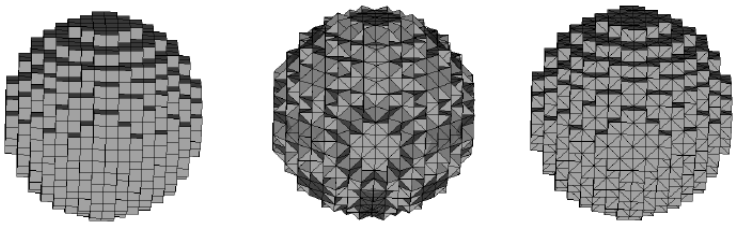

Figure 3.30: Voxel mesh, stand alone tetrahedral mesh, tetrahedral mesh with the same phase allocation as the voxel mesh

technique has just the opposite effect than the one expected - the Young's modulus increased with the tetrahedral refinement.

Before questioning, whether the technique resolved the material boundaries better, we tried to look at the effect of element type. To that end, we introduced a third type of mesh - with the same distribution of phases as the voxel mesh, but a different element representation - i.e. tetrahedral. This type of mesh can be seen in Fig.3.30, on the right.

Simulations with this third type of a mesh showed that the tetrahedral mesh with the same phase allocation as the voxel mesh is much closer to the stand-alone tetrahedral mesh - Fig.3.31, 3.32. This shows that the problem is associated with the type of element, not with a worse resolution of material boundaries. An explanation lies again in locking. Because the constant strain tetrahedral element is by standard integrated in one integration point, the effect of locking cannot be removed by reducing the integration order (as there would be no points to integrate over), unlike the hexahedral element, for which this option was used.

Since no improvement was observed with the tetrahedral refinement scheme, we opted for going back to the standard voxel mesh and tried to find the bounds on the FEM solution.

3.2.11 Bounds on the solution due to presence of multi-phase elements

Because of the uncertainty of the elastic properties of the multi-phase voxels remains, the suitability of the voxel mesh needs to be proven by the bounds of the FEM solution. In order to evaluate the bounds on the FEM solution for a particular

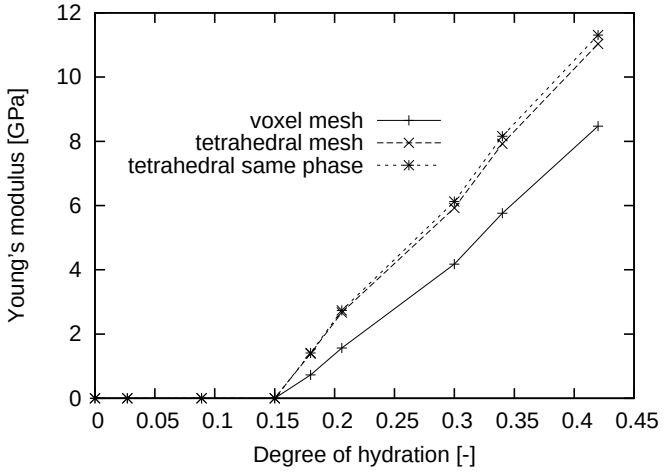

Figure 3.31: Young's modulus for voxel and tetrahedral mesh

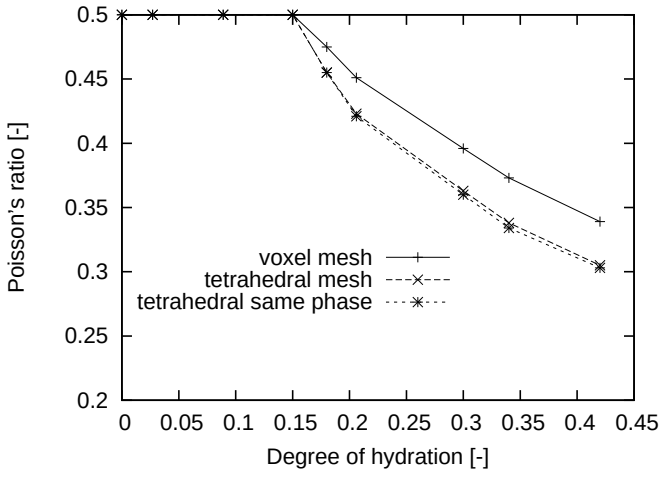

Figure 3.32: Poisson's ratio for voxel and tetrahedral mesh

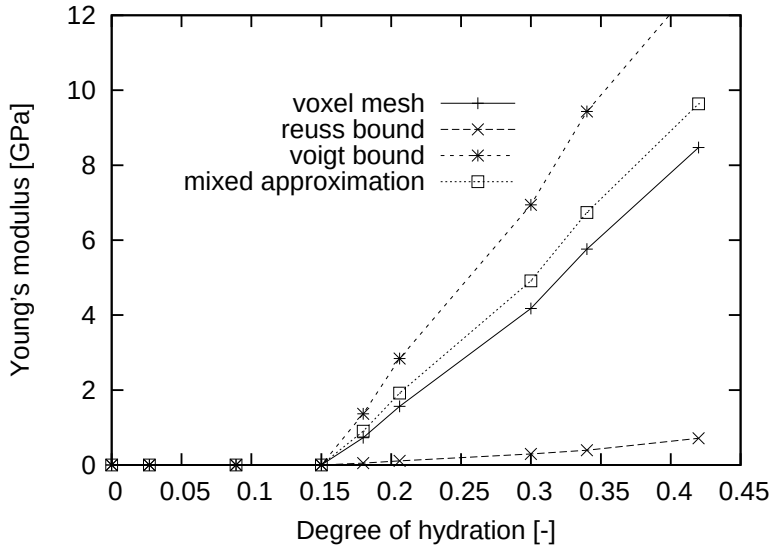

Figure 3.33: Bounds on Young's modulus

computational volume and resolution, we evaluated firstly lower Reuss and upper Voigt bound of the multi-phase voxels. After the evaluation we inserted one of the bounds of the mixed voxels into the FEM procedure. There is no point in applying the Hashin-Shriktman bounds, because the difference between the phase properties is too high - i.e. the voxels contain water - and the medium is not quasi-isotropic.

FEM computation was done first with all the voxels having their upper bound properties, secondly, with their lower bound properties. The properties of the one-phase voxels remain unchanged. As can be observed from Fig.3.33 the voxel mesh with spanning cluster goes between these two bounds. At later stages of hydration we can see a shift of the properties to the upper bound and is probably due to the artificial connectivity in the spanning cluster. It should however be stressed, that these are not overall bounds of the properties, as they are dependent on the resolution of the system. For real cement microstructures the sensitivity of the bounds should be tested against various resolutions.

3.2.12 Averaging scheme for multi-phase elements

Because of the limited mesh resolution, some of the voxels contain a disordered mixture of phases. The stiffness matrix of these elements could be potentially estimated from FEM, however, this is rather time-consuming and due to its character, it would

be difficult to say which boundary conditions to apply and what the result actually means.

Use of analytical schemes would be meaningless here. Firstly, because the voxels have a disordered non-isotropic geometry. Secondly, the periodic boundary conditions for the homogenization are not fulfilled, because the surrounding voxels do not have the same geometry as the voxel studied.

The assumption of the averaging procedure we use, is that in the CV the local properties will be changed in all the directions in the same manner and the result on the whole RVE might therefore be well in the bounds of the solution. Volume fractions of the phases in the voxel are obtained from the subvoxelization scheme described in the section Voxel mesh. To obtain the elastic properties of the mixed voxels we used an averaging scheme based on the work of Mishnaevsky [47]. This scheme obtains the properties of the mixed voxels by a combined Voigt-Reuss approach. The voxel is subvoxelized and the properties are evaluated firstly for individual rows by the Voigt rule, later all the rows are averaged by the Reuss rule into elastic properties of a voxel.

As can be seen in Fig.3.33 the mixed approximation does not seem to produce significantly higher values than the voxel approach. There is no reason to assume that the mixed approximation will always be higher than the classical voxel approach, based on author's experience it seems to be dependent on the particular microstructure and the resolution.

3.2.13 Statistical fluctuation of the microstructural representation

Statistical fluctuation is a result of a random placing of the grains at the beginning of hydration and is a major factor influencing the size of the computational volume. Microstructures, which are small, compared to the size of the biggest grain in their particle size distribution, can suffer greatly from non-isotropicity due to the concentration of big grains in one part of the microstructure. For concrete samples the minimum size of a CV is suggested to be at least three times bigger than the size of the biggest aggregate. We try to apply the suggestion for the cement paste level.

In order to find out the representativeness of the computational volume, five microstructures were generated for three sizes of computational volumes, namely

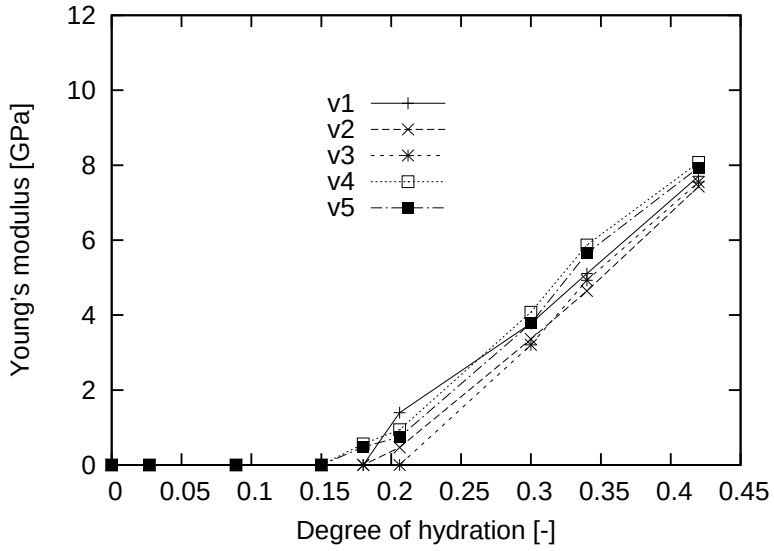

Figure 3.34: Fluctuation of Young's modulus - CV 60 μm

60, 80 and 100 μm. From the results (average from three directions)- Fig.3.34, 3.35 we can see, that the size of the microstructure is very important at early age - i.e. 0 - 30 % of hydration. Afterwards, the results fall within a maximum error of 25 % and clearly the computational volume does not have to be so big at this stage. Based on the statistical fluctuation of the elastic properties and the resolution problems, we can conclude, that for later ages of hydration - i.e. 30 - 50 %, it is reasonable to invest more computational resources into resolution increase rather than into the size of the computational volume. On the other hand, early age between 0 - 30 % is not very much resolution dependent, but requires bigger computational volumes due to statistical fluctuations.

3.2.14 Boundary conditions and RVE size

If the microstructure is not big enough to be representative, finite size effects occur. There is no way to tell whether the microstructural volume is representative, unless the property of interest is tested. In case of effective elastic properties, this means trying different sizes of computational volumes and applying different types of boundary conditions. Generally, three types of boundary conditions can be applied on the CV, namely, displacement boundary conditions, periodic boundary conditions and static conditions. Displacement boundary conditions mean all the microstruc-

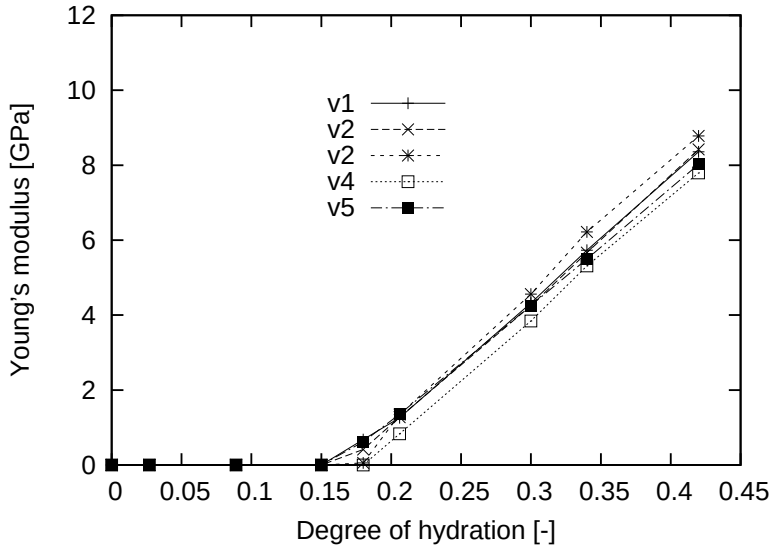

Figure 3.35: Fluctuation of Young's modulus - CV 100 μm

tural faces constrained in their normal and shear direction. Five of the faces have a zero displacement prescribed, while one of them has a non-zero displacement. Pure static boundary conditions are difficult to achieve because of the iterative character of the solver. For this reason, mixed static boundary conditions are used - one of the faces constrained in the normal direction, the opposite face being statically loaded.

Periodic boundary conditions prescribe the movement of the opposite sides of the microstructure. No real displacement is prescribed, only the difference in the position of the opposite nodes. Periodic boundary conditions create a need for displacement compatibility on opposing exterior faces of the unit cell. Beyond that, it is also necessary that the meshing of the corresponding external faces is identical. For this reason, we do not apply this type of boundary conditions for the octree mesh. As the CV approaches the representative size, the various boundary conditions should converge to the same result.

Although the above mentioned boundary conditions can be applied for most heterogeneous materials, due to the existence of water filled porosity this is not the case here. The character of the static boundary conditions, i.e. prescribed force results in a node-pullout effect - i.e. nodes belonging to soft pore elements are going to have a much bigger displacement than the nodes belonging to solids. This is very different from what we see with displacement boundary conditions, where the

displacement	7.21	7.1
mixed displacement	6.82	6.63
static	6.13	6.15

Table 3.1: Bulk modulus - 60 vs. 100 μm, 30 % hydration

displacement	1.71	1.68
mixed displacement	1.34	1.31
static	1.04	1.05

Table 3.2: Shear modulus - 60 vs. 100 μm, 30 % hydration

displacement is generally the same for all the nodes.

Because static boundary conditions constitute the lower bound of the elastic tensor, with the standard approach it would be impossible to say whether the computational volume is representative. For this reason a quasi-embedded approach was introduced. The microstructure is embedded into a medium (window) of effective properties. This is similar to the Self-Consistent approach. The effective medium's properties and the properties of the microstructure are obtained iteratively. The starting point for the effective properties of the window could be taken as the properties obtained from experiments. This approach is much more time-costly than the standard approach, but since the medium is a solid, it does not suffer from the node pullout.

The computation was performed on two boundary sizes of computational volume - i.e. 60 μm and 100 μm for three types of boundary conditions i.e. displacement, mixed displacement and static boundary conditions. Because of an iterative character of the procedure, the computation was limited to two degrees of hydration for time reasons, namely 0.3 and 0.42. The procedure is approximately 5 times more time costly than the traditional one.

We list the results in the Tab. 3.1, 3.2, 3.3 for clarity. Bulk and shear modulus were chosen to represent the results, because all the references about the order of the boundary conditions apply to elastic tensor, i.e. bulk and shear modulus rather than Young's modulus and Poisson's ratio.

displacement	7.1	9.7
mixed displacement	6.63	9.4
static	6.15	8.9

Table 3.3: Bulk modulus - 100 μm, in time

As can be seen, application of displacement boundary conditions resulted in the highest values, followed by mixed displacement and static boundary conditions. The mixed displacement boundary conditions are slightly closer to the displacement boundary conditions than static (6 vs 10 % for bulk modulus at hydration degree 30 %). It is however not very obvious, that the bigger computational volume would result in closer bounds than the smaller computational volume (normally the computational volume of 100 μm should converge to the representative volume). This can however be caused by statistical fluctuation. The difference between the boundary conditions changes in time. While for 100 μm it is about 14 % at the degree of hydration 0.3, for the later degree of hydration the difference is only 9 %. This leads to a similar conclusion as with the statistical fluctuation - i.e. that the size of the computational volume is more important at early ages.

3.3 Summary

In this chapter we presented the results of a numerical study on a simple cement-like microstructure, which resulted into identification of the most significant factors influencing the prediction of elastic properties.

- The most important factor is artificial connectivity, which is a result of insufficient mesh resolution. It causes a big overestimation of elastic properties - at the beginning of hydration in full microstructures and in burned-out microstructures at later ages. The problem is clearly more pronounced with higher amounts of solids present.

- The current burning algorithm was improved by taking into account the presence of disconnected clusters embedded in water which are able to transfer normal loads. This was achieved by application of the homogenization scheme.

The scheme resulted in higher values of the overall bulk modulus, mainly at the beginning of hydration.

- Water-filled porosity is the second most significant factor, causing numerical overestimation of the properties in form of locking. The effect was to a great extent removed by application of the selective integration scheme.

- The effect of the resolution was studied on the microstructure with spanning cluster. The resolution turned out to have a significant effect on the results in the range 30 - 50 % hydration. Octree and tetrahedra refinement was applied. Octree refinement improved the values only mildly, tetrahedra refinement resulted in even higher values of Young's modulus, because its current integration scheme could not account for locking.

- Bounds on the FEM solution were established, the solution was closer to the upper bound, partially because of the artificial connectivity. An averaging scheme was applied to the mixed voxels, but did not result in better overall values.

- The representativeness of the computational volume was studied in terms of statistical fluctuation and boundary conditions. The size of the computational volume is very important in range 0 - 30 % hydration, when there is high porosity and therefore a big effect of the position of the biggest grain. A study on statistical fluctuation and resolution suggests that it is sensible to invest in larger computational volumes at early ages, at the expense of the resolution, while the opposite is true for the later ages.

In the next chapter we will apply the knowledge on the numerical factors on the simulation of microstructural variations.

Chapter 4

Numerical prediction on the virtual microstructure

In this chapter the effect of different microstructural parameters on the prediction of effective elastic properties is determined. This study indicates which features are in reality more likely to impact the elastic properties of a material. Examples include flocculation, number of portlandite clusters, density of C-S-H, different w/c ratios and particle size distributions.

While the differences between the w/c ratios and density of C-S-H can be explained by analytical schemes, the influence of other factors, such as flocculation, distribution of portlandite clusters and particle size distribution is best approximated by numerical methods.

In view of the results of the previous chapter dealing with the numerical aspects, we still have to bear in mind that the precision of the prediction is limited by the resolution, i.e. the connectivity effect and the results have to be considered with this in mind.

4.1 Effect of flocculation

The first factor studied is the flocculation. It is generally considered, that cement particles on the addition of water flocculate, i.e. form clusters rather than move disconnected in water, as was assumed in the previous simulations.

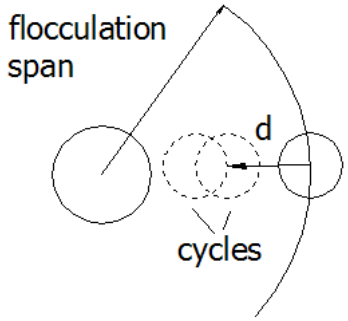

Figure 4.1: Scheme of the flocculation parameters

Flocculation was chosen as the first parameter due to the fact, that the spatial position of the grains can highly influence the percolation threshold and finally decide as what should be considered as the best approximation of the real microstructure.

Computations were mostly performed on the microstructure from the previous chapter - w/c 0.4, CV 80 μm and a cement-like distribution of portlandite clusters following proportional approximation - i.e. having 20 % of the number alite grains at the end of hydration.

The vector microstructural model allows us to study the effect of flocculation by bringing particles closer to each other from their original locations. The initial position of particles is a result of surface chemistry, yet very little is known on this problem in cementitious systems. The model allows study of flocculation in terms of the affected neighbour area of a particle (flocculation span radius), distance by which they are brought closer to each other (flocculation factor) and number of flocculation cycles - Fig.4.1.

Currently, the percolation threshold found from the non-flocculated microstructure is too high (around ca. 0.15 degree of hydration), which brings us to the conclusion that the initial random packing might not be representative of the real microstructure. The initial trials with flocculation of the microstructure were therefore done to study the effect on the percolation threshold. The computations were all performed with one cycle, the particles were all affected by the flocculation and the range of the particle's neighbours was set to be 10 μm. The distance factor was varied between 0.1 - 0.7 of the original distance.

As can be seen from Tab. 4.1, the higher the distance factor, by which we

distance factor	0.0	0.1	0.3	0.5	0.7
doh at percolation threshold	0.15	0.09	0.073	0.065	0.056

Table 4.1: Percolation threshold for various flocculation distance factors

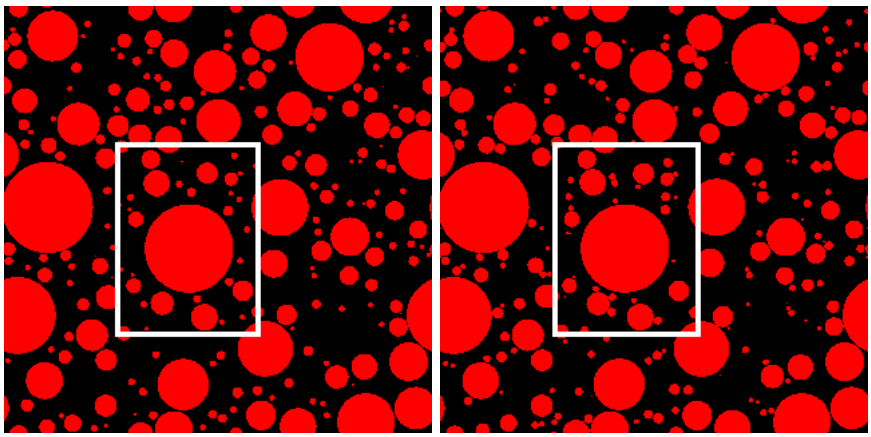

Figure 4.2: Original vs. flocculated microstructure - 2D slice, distance factor change 0.7

bring the particles closer, the lower the degree of hydration at which the percolation occurs. The algorithm in this case did not work beyond the 0.7 factor of the original distance. This is due to simplicity of the algorithm which is not able to handle the overlaps, occuring with high distance changes.

The effect of the flocculation can be observed in Fig.4.2 and it can be seen that the algorithm changed the microstructure from regularly spaced to an irregular flocculated.

While this is a good result in terms of percolation threshold, we still need to find the effect of the resolution, which might be rather different from what we observed with the original random packing. For the computation we preserved the original size of the computational volume. This might a reasonable assumption, because although the capillary pores become bigger with this change in packing, they will not change their size to such an extent that a change of the computational volume would be needed. The resolution of the volume was varied between 0.5 and 1.5 μm.

The results - Fig.4.3, 4.4 show a big resolution dependency, similarly to the non-flocculated microstructure, which is higher at later ages. However, unlike the non-

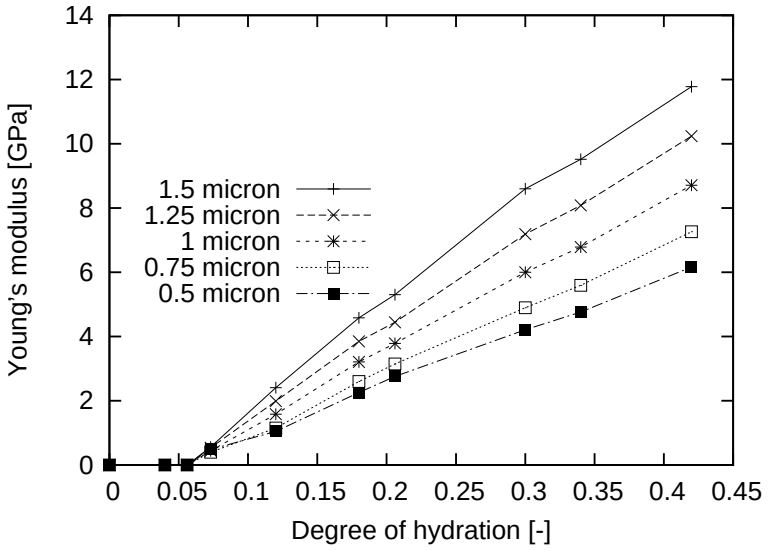

Figure 4.3: Young's modulus for different resolutions - flocculated microstructure

flocculated microstructure, the dependency seems to be asymptotic (visibly asymptotic at the earlier ages) rather than linear. If the data was extrapolated to the zero resolution in limit, there would still be a difference of ca. 20 % at later ages between the resolution 0.5 μm and the perfect resolution.

If we talk in terms of the smallest particle in the particle size distribution, we might conclude that achieving the resolution, which equals to the half of the particle size, still causes an error of ca. 20 % in the range of the degree of hydration 0.2 - 0.4.

Another effect to study is the effect of the number of the cycles of the flocculation algorithm. The outcome should be a similar final distance, nevertheless achieved by a different number of cycles. For the study, factor 0.7 was chosen (the particles will be by 70 % closer than originally), which was performed in three different ways - 1 cycle and distance factor 0.7, 3 cycles and distance factor 0.3 and 5 cycles and distance factor 0.1.

The results from the simulation can be seen in Fig.4.5, the number of flocculation cycles has some effect, however that is rather insignificant when compared to the non-flocculated microstructure. The difference between the number of the flocculation cycles is well in the resolution error of the solution itself, slight differences could be attributed to the randomness and to the fact, that the algorithm behaves differently

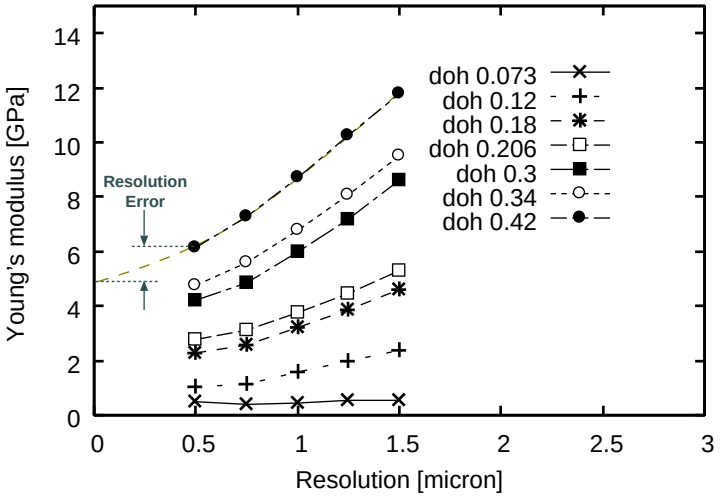

Figure 4.4: Effect of the resolution on Young's modulus - flocculated microstructure

when done in cycles. The non-monotonic trends between the various distance factors are only an artifact of the algorithm, in which the achieved final distances are close but not identical.

The differences in the percolation threshold and the early age elastic properties of the flocculated and non-flocculated microstructure are significant. The flocculated microstructure has very different values of the elastic properties in the range of the degree of hydration 0.05 - 0.3, which is a result of a different initial particle packing.

Last, the particle shape might have an influence on the percolation threshold, as well as the final elastic properties. However, at the moment it is not possible to simulate different particle shapes in the vector microstructural model.

4.2 Effect of C-S-H density and elastic properties

The types, densities and elastic properties of C-S-H are a subject of controversy due to its amorphous nature and subsequent difficult determination. So far, we explored one type of C-S-H with an average density of $2.0\,\mathrm{g/cm^3}$ and an average Young's modulus of $25.55\,\mathrm{GPa}$. This value was taken as an average between what is considered to be LD and HD C-S-H by [77], [17] (w/c 0.4 is considered to consist of LD and HD C-S-H in ratio 1:1 in the J-T model [73]).

Here we tried to determine the bounds on the solution in terms of unknown

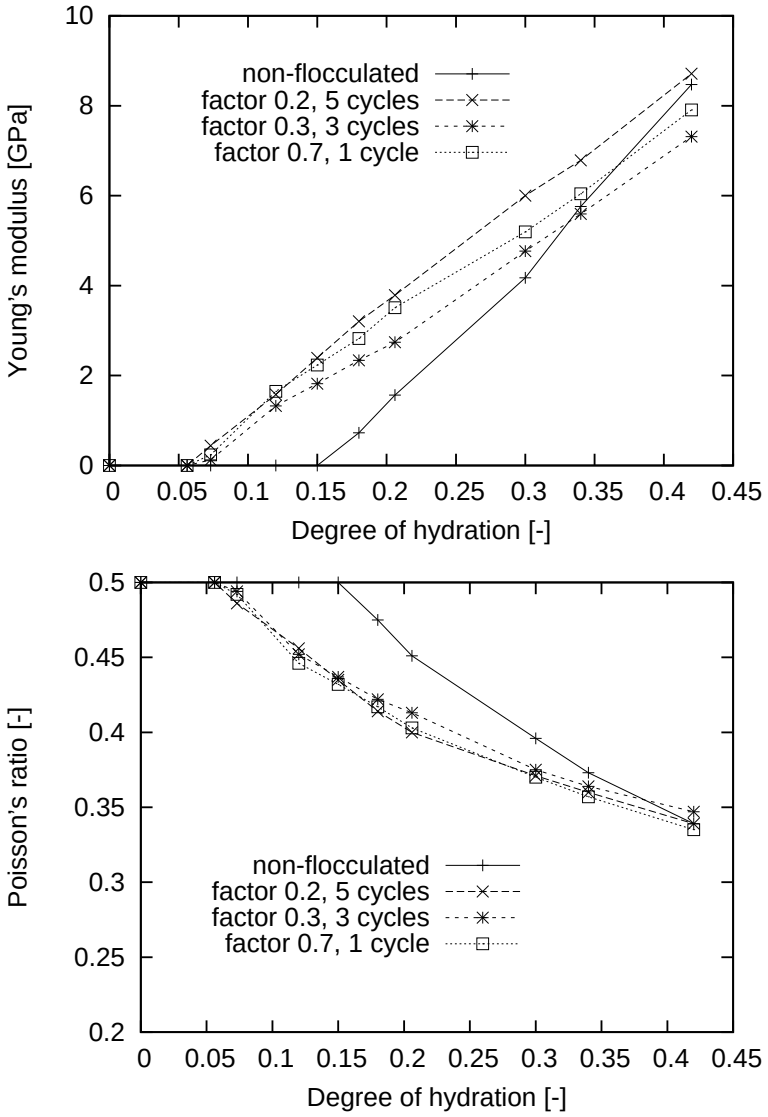

Figure 4.5: Young's modulus and Poisson's ratio for flocculated and non-flocculated microstructure

density and elastic properties. We assumed two other microstructures - one filled only with a low-density C-S-H, i.e. having the density of 1.9 g/cm^3 and the effective Young's modulus 21.7 GPa, as well as a microstructure filled with only high-density C-S-H with the density 2.1 g/cm^3 and the Young's modulus of 29.4 GPa. The mass of C-S-H is for a particular microstructure in all the cases the same, the volume changes due to the change in density. In case of LD C-S-H the volume is higher, while for HD C-S-H, the volume is lower than with the original microstructure.

Due to the heavy dependency of the result on the resolution, we strived for a higher resolution - i.e. 0.75 μm. The flocculation was performed with a final distance 0.7 of the original one.

The results performed on microstuctures with different C-S-H densities can be seen in Fig.4.6. The microstructures give very similar values in terms of Young's modulus and Poisson's ratio. The difference is all within the error of statistical fluctuation and resolution error.

The percolation threshold however does change, this is due to different volume fractions for a particular hydration degree. While for low density C-S-H, the value of percolation is the lowest - i.e. 4.6 %, followed by the average density C-S-H microstructure with 5 % and 7.3 % for the HD C-S-H.

In this case, it is reasonable to compare the results to an analytical scheme, because the volume fractions in all the cases differ. However, as can be seen from Fig. 4.7, the Self-Consistent approach did not predict any difference between the various cases of C-S-H densities either. In terms of the values of the Young's modulus, SCS predicted higher values than the FEM.

4.3 Effect of the number of portlandite clusters

The connectivity of the microstructure is a critical factor in the prediction of the elastic properties and therefore not just the total volume of the hydrates, but also the character of the hydrate clusters, might be very influential in the prediction. Although this concerns all hydrates, here we solely concentrated on portlandite.

In cements, portlandite is usually considered to form clusters in large numbers, based on the work of Jennings - 20 % of the total number of alite grains at the end

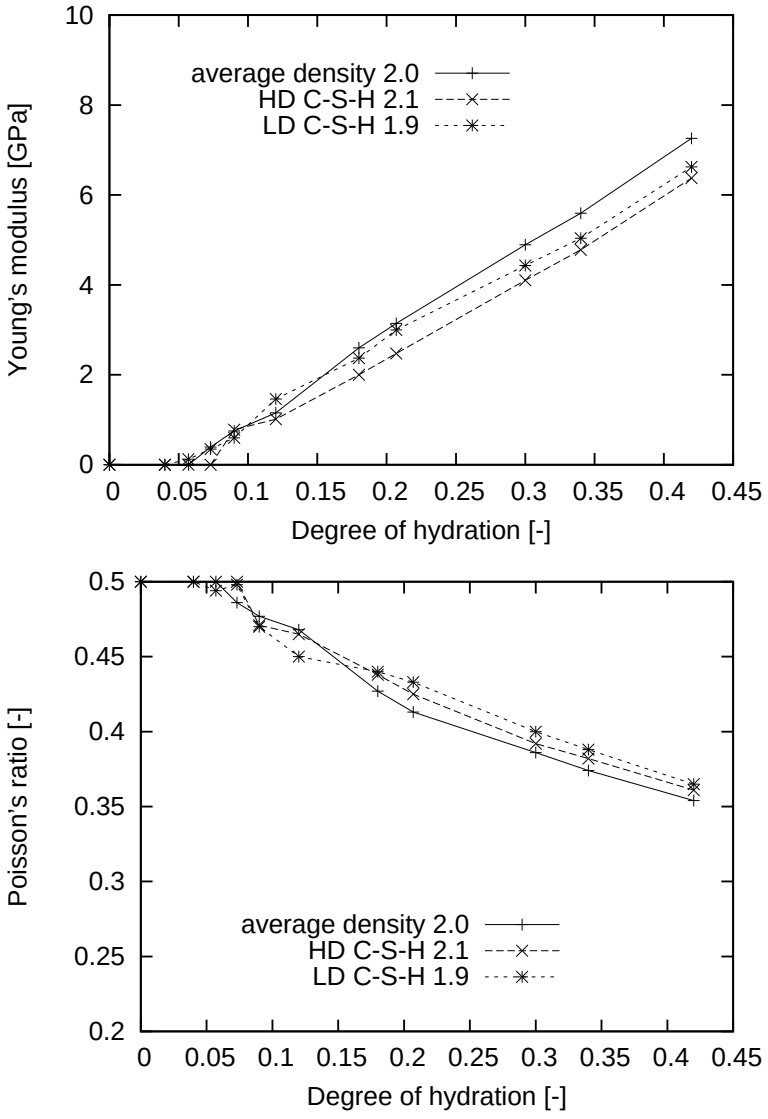

Figure 4.6: Young's modulus and Poisson's ratio for different C-S-H densities

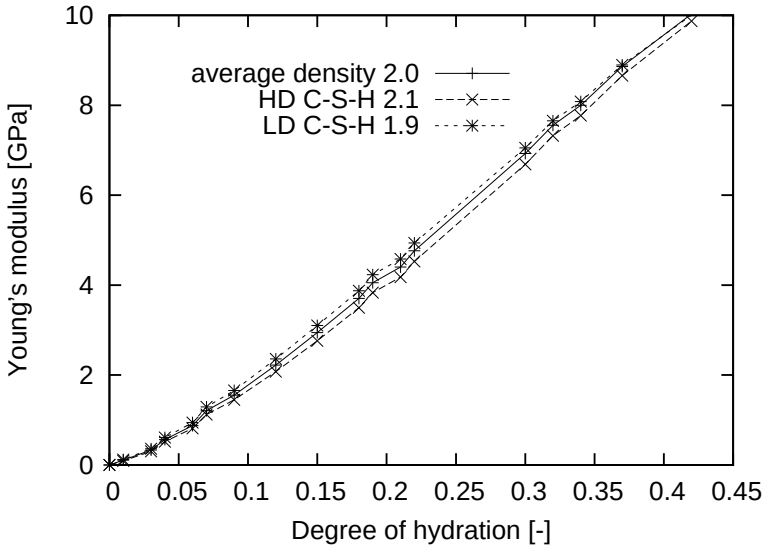

Figure 4.7: Young's modulus from SCS

of hydration [39]. An influence of their number can therefore have implications on the prediction of cements.

In order to see the effect of the number of the portlandite clusters, we generated a microstructure with the same initial placing of the particles, but a different number of portlandite clusters. For the given microstructure, we varied the number of portlandite clusters - 100, 500, 1000 and 2000 clusters, which corresponds to 1, 5, 10, and 20 % of the initial number of the alite grains, respectively - Fig.4.8. The number of portlandite clusters is constant - i.e does not change with the progressing hydration. This approach was chosen in order not to introduce additional parameters into the computation.

As can be seen from Fig.4.9 the results of the computation are dependent on the number of portlandite clusters, with higher number of the clusters the effective Young's modulus of the microstructure increases. This is due to the extra connections the clusters provide. Smaller clusters create more connections with the rest of the microstructure. It can be also noticed, that the number of portlandite clusters matters highly only in the range from 1 - 5 % of the original number of the alite grains.

There seems to be no effect on percolation threshold, which means that it is primarily C-S-H causing percolation to occur.

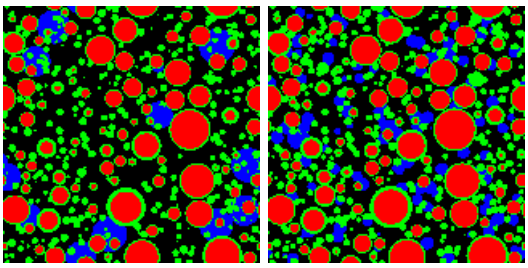

Figure 4.8: Microstructure with 100 CH and 2000 CH clusters, CH (blue)

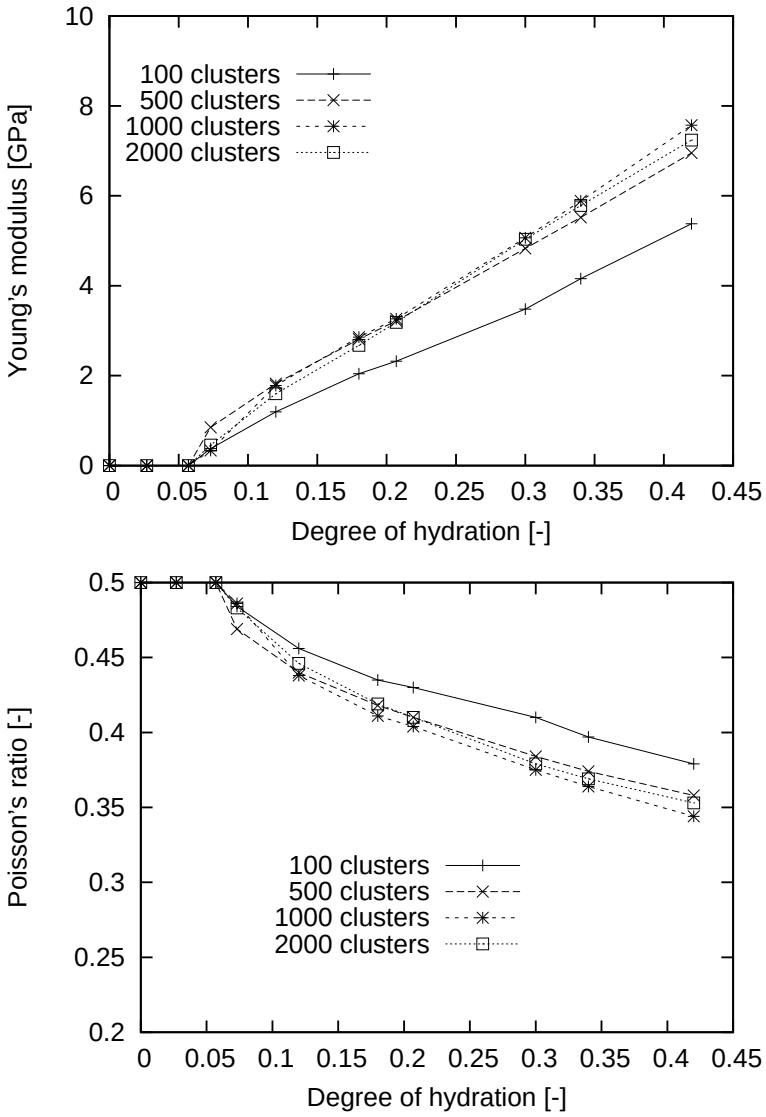

Figure 4.9: Young's modulus and Poisson's ratio for different number of portlandite clusters

4.4 Effect of the w/c ratio

The effects of the w/c ratio are known from many previous works, either performed by analytical estimations or numerical predictions and this section serves only to check the validity of the numerical technique on different w/c ratios.

In order to see the effect of the w/c ratio, microstructures with three different w/c ratios were generated - namely 0.35, 0.4, 0.45. The CV for all of them is the same (i.e. $80\,\mu$m, resolution $0.75\,\mu$m). It is worth mentioning, that higher w/c results in bigger capillary porosity. If the size of the capillary porosity changes to a big extent, then it would be worth considering a change in the CV. In this study, the original size of the computational volume was preserved. The distribution of portlandite clusters was considered proportional to the number of alite grains - i.e. final number of CH clusters equals to 20 % of the original number of the alite grains.

One type of C-S-H is used, however, its densities and elastic properties do change, according to the J-T model. For w/c ratio 0.35, the ratio between HD and LD C-S-H is 0.6 : 0.4, while for w/c 0.45 the ratio is 0.4 : 0.6. The density of C-S-H for the w/c 0.35 is $2.02\,\mathrm{g/cm^3}$, while for w/c 0.45 it is $1.98\,\mathrm{g/cm^3}$. In terms of Young's modulus, this results in average values 26.32 and 24.78 GPa for C-S-H, respectively.

Results from the simulations - Fig.4.10 confirm a known trend, that for the same degree of hydration, the lower w/c ratio results in higher values of Young's modulus than the higher w/c ratios. The opposite is true for the Poisson's ratio. This is the effect of bigger pores in case of higher w/c ratios, resulting in a softer microstructure. The difference between the w/c 0.4 and 0.35 is not as large as the difference with the w/c 0.45. This might be partially intrinsic, partially due to the resolution (connectivity) error. Lower w/c ratios contain originally more solid and have therefore higher resolution dependency than the higher w/c with less solid. The overestimation will be greater for the low w/c.

4.5 Effect of the particle size distribution

Particle size distribution is a factor, which has a high impact on the development of mechanical properties of the cement paste with time. The effect of particle size

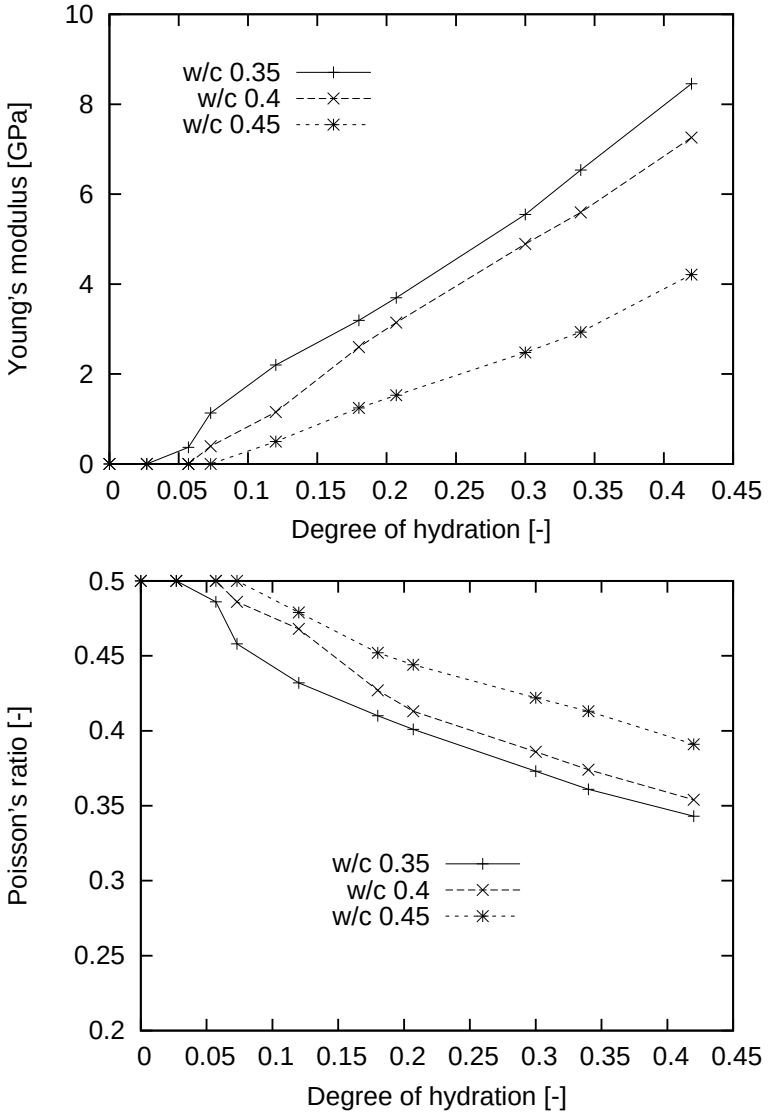

Figure 4.10: Young's modulus and Poisson's ratio for different w/c ratios

distribution in terms of hydration degree, i.e. amount of solid fraction present, has not been studied extensively.

In order to see the effect of fineness, we chose three different particle size distributions - namely in the spans 0 - 11, 0 - 24 (PSD 8.1 [12], see Appendix), 0 - 40 μm - Fig.4.11. The upper limit indicates only the size of the largest particle, but does not tell anything about the distribution. The computational volumes were chosen to be approximately 3 - 3.5 times higher than the largest grain in the microstructure - i.e. 35, 80 and 120 μm. The particle size distribution was cut under 0.46 μm, which is slightly less than the resolution, as it is assumed that the particle grows by a factor of 1.3 of its original size towards the end of hydration.

The resolution was in all cases the same - i.e. 0.75 μm. The microstructures can be seen in Fig.4.13, 4.14, 4.15. Preliminary look at the microstructures suggests that the lowest result in terms of Young's modulus will be the case of the psd 0 - 24, because of the big capillary porosity.

As the result suggests - Fig.4.12 this indeed happened. The microstructure for psd 0 - 24 shows the lowest value of Young's modulus and the highest value in terms of Poisson's ratio. This is followed by the psd 0 - 40 and 0 - 11. Particle size 0 - 11 has the highest values of Young's modulus due to smaller capillary porosity and wider particle size distribution, when compared to the case of psd 0 - 40. The development of Young's modulus of the psd 0 - 11 is non-linear, unlike the other particle size distributions. The reason for this is not clear, probably the number of elements, by which the microstructure was captured introduced some artificial effects. Nevertheless, the results show that the method is able to differentiate between the particle size distributions at a particular hydration degree to the extent of the resolution limits.

4.6 Summary

Several comparative numerical predictions were carried out in order to observe the effect of flocculation, C-S-H density, number of portlandite clusters, w/c ratio and particle size distribution.

Initial flocculation of the microstructure is necessary in order to ensure rea-

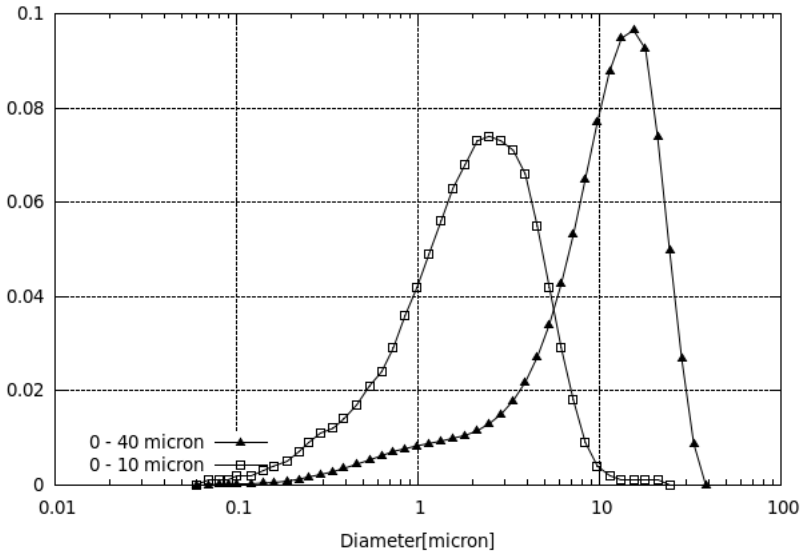

Figure 4.11: Simulated particle size distributions

sonable values of the percolation threshold. The value of percolation threshold is influenced by the distance, by which the particles are brought closer. As long as the final distance is the same, the number of flocculation cycles does not have a significant effect on the final elastic properties. The early age elastic properties are significantly different for a flocculated and non-flocculated microstructure.

Calculations with different C-S-H densities showed similar values of effective elastic properties for the microstructures of several densities of C-S-H. The same result was obtained by SCS scheme. The density of C-S-H nevertheless had an impact on percolation threshold, with LD C-S-H resulting in the lowest percolation threshold.

Simulations on portlandite showed that number of portlandite clusters seems to have significant effect on the final elastic properties. For flocculated microstructures the range of 1 - 5 % of the original number of the alite grains seems to be important.

With the presence of higher capillary porosity and reasonable resolution of the fine grains, the method seems to predict well for different w/c ratios and particle size distributions.

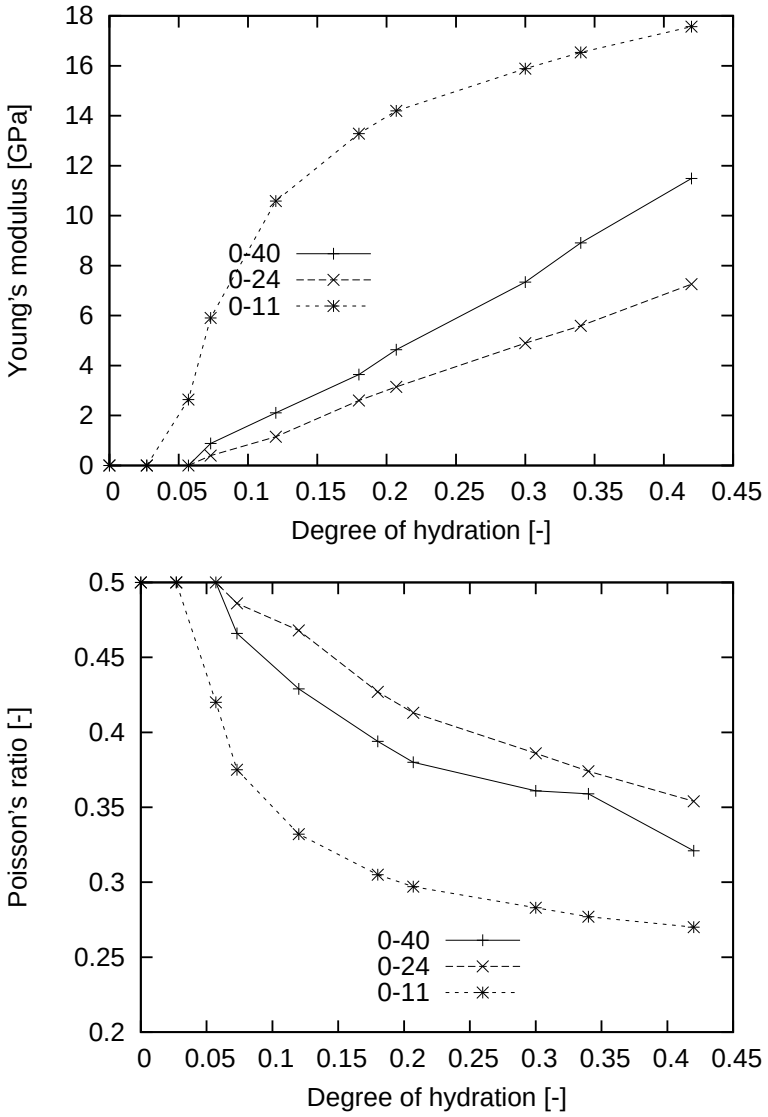

Figure 4.12: Young's modulus and Poisson's ratio for different particle size distributions

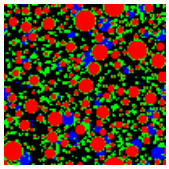

Figure 4.13: CV 35, psd 0 - 11

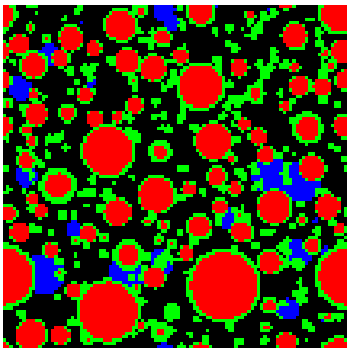

Figure 4.14: CV 80, psd 0 - 24

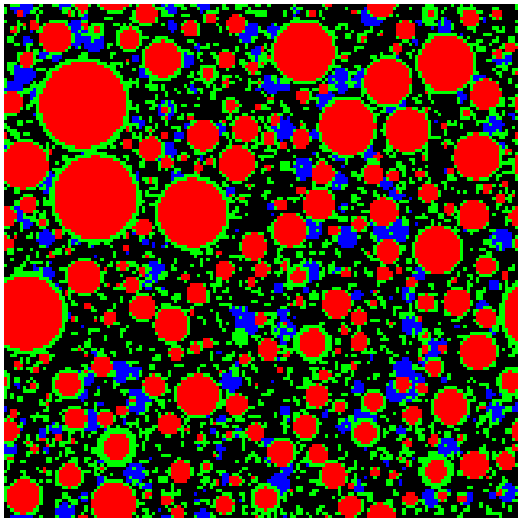

Figure 4.15: CV 120, psd 0 - 40

Chapter 5

Experimental verification

One of the critical points of the model is its validation with experiments, which will confirm or lead to an adjustment of the parameters used so far. Moreover, it might result in observation of other significant input parameters for the prediction.

In this chapter, preliminary validation of the numerical technique is shown on the experimental data of Boumiz [12], later, experiments and numerical predictions on four white cement pastes are presented.

5.1 Experimental validation for alite

Experimental validation of the numerical technique was conducted for white alite paste of Boumiz, with mean particle size distribution of 8.7 μm (see Appendix). This is a different particle size distribution than the one from previous chapters and it was chosen because of the access to the experimental data, which was not available for the particle size distribution of 8.1 μm.

The computation was performed on the microstructure with an average density C-S-H - i.e. 2.0 g/cm^3 and 25.55 GPa. Two possible distributions were assumed for portlandite, 20 % of the initial number of alite grains and secondly 25 clusters in the whole CV. This value was chosen based on the observation of alite microstructures from other works [18], [62] showing the existence of big but few portlandite clusters in alite. The number was chosen as an interpolation between the values provided by Costoya [18] and adapted to the computational volume of 160 μm. The size of the computational volume was chosen to be about 3 times the size of the biggest

grain. The computation was performed with several flocculation distance factors, namely 0.2, 0.5 and 0.7. The simulation with a big number of portlandite clusters was carried out only for the highest flocculation distance factor.

As can be seen - Fig.5.1 the computation performed with a big number of CH clusters results in higher values of Young's modulus and overestimates the experimental values. With lower number of portlandite clusters, the results are still overestimated especially in lower hydration degrees, however not so greatly as with the higher number of the clusters. In the first instance, that could mean that the flocculation algorithm puts the particles too close to each other.

However, computations performed with various flocculation distance factors do not show big differences - Fig.5.2, only very mild difference can be seen between factor 0.2 and 0.5. In this regard, for further computations on cement, it makes more sense to employ higher values of the distance factor in order to obtain lower percolation threshold.

5.2 Experimental validation on cement

Due to the lack of availibility of alite in large amounts, the experimental validation of the numerical technique was performed on white cement pastes. White cement was chosen, because its hydration resembles that of alite. Moreover, it does not contain ferrite, whose reaction is slow and not well known so there is less inprecision brought into the prediction in terms of hydration degree. The measurements were performed for the hydration degree in range 0.17 - 0.4. In this range the comparison with the numerical data is out of the range of the biggest error caused by statistical fluctuation and non-isotropicity of the generated microstructure.

The w/c ratios were chosen so that the artificial connectivity effect is not very large - i.e. low w/c ratios were excluded. However, due to bleeding the study could not be done on high w/c ratios either. For that reason, w/c ratios 0.4 and 0.45 were chosen.

The mixes were prepared for two finesses of white cement, the particle size distribution can be seen in Fig.5.3. The difference between the amounts of various phases between the fine and coarse cement is negligible (see Appendix).

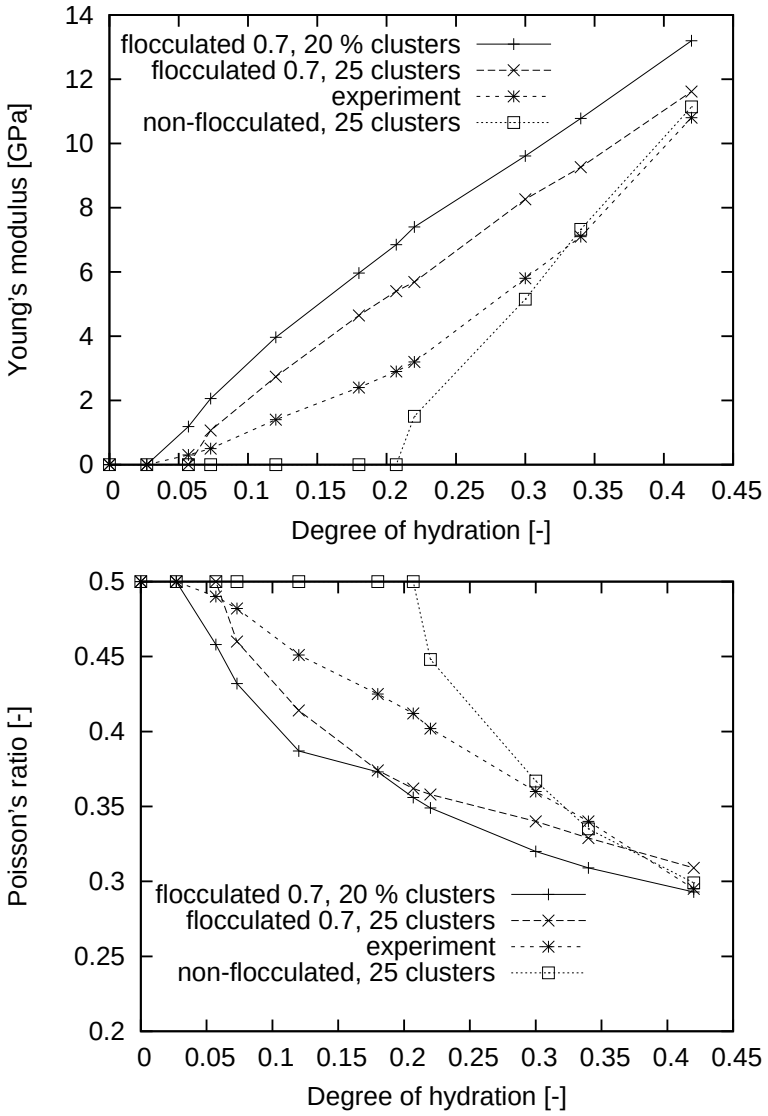

Figure 5.1: Young's modulus and Poisson's ratio for PSD 8.7 for different number of portlandite clusters

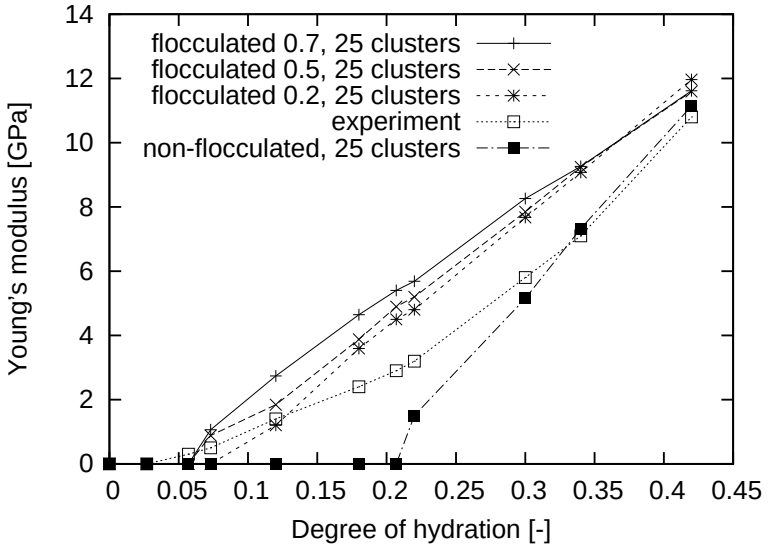

Figure 5.2: Young's modulus for PSD 8.7 for different flocculation factors

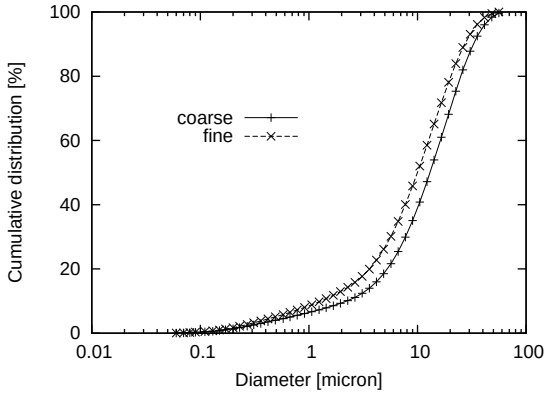

Figure 5.3: Cumulative particle size distribution for coarse and fine cement

Three samples were prepared for each testing time for all 4 mixes. The samples were prepared according to EN 196-1 in the standard mortar-bar size 40x40x160 mm. The mixing procedure followed 60s low, 30s high speed, 90s stand-by and 60s high speed (coherent with the standard, except for the part when the sand would come in). The samples were stored in moulds in 100 % RH until the time of the testing. The amount of bleed water was measured in the first hour after moulding to enable the real w/c to be calculated.

Static test and dynamic resonant frequency tests were performed for 12, 18, 24 and 36 hours.

The static test was performed in compression on the bars in vertical position according to SIA 262-1/G. The bars were loaded and unloaded in three cycles. The Young's modulus was taken from the unloading part of the last cycle. The duration of the whole test was cca 180s. The peak load was assumed to be about 1/3 of the ultimate strength. The device allows to measure only the displacement in one direction, that is why only Young's modulus could be determined - Fig.5.5.

The resonant frequency test was performed on cement paste bars in their horizontal position. The procedure is described in ASTM E 1876-01. A wave is initiated in the bar with a stick in three possible modes - torsional, transversal and longitudinal. Only torsional and transversal modes were determined, as it was very difficult to estimate the centre of the smallest side of the sample for the longitudinal mode. Weight and dimensions of the specimens were measured. Once the torsional and transversal frequencies were obtained, the Young's and shear modulus were determined according to ASTM E 1876-01. Shear modulus was determined from the torsional mode directly, however Young's modulus was computed only afterwards - by iteration with the knowledge of the shear modulus. This is because the flexural mode is highly dependent on the dimensions - i.e. on the Poisson's ratio. The device can be seen in Fig.5.4.

Total degree of hydration was obtained by isothermal calorimetry. The degree of hydration for the individual phases was determined by X-ray diffraction. For this technique, samples were prepared by mixing 5 minutes at 500 rpm, three samples were prepared for each time cured saturated. Because the system is generally not closed, a correction for the dilution effect was made by the loss on ignition measure-

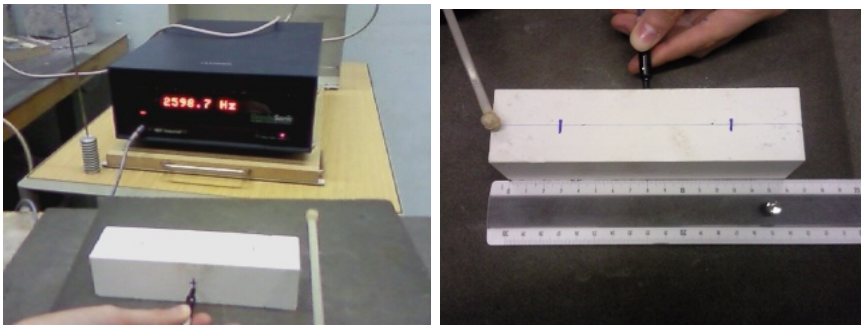

Figure 5.4: Resonant frequency test, flexural mode

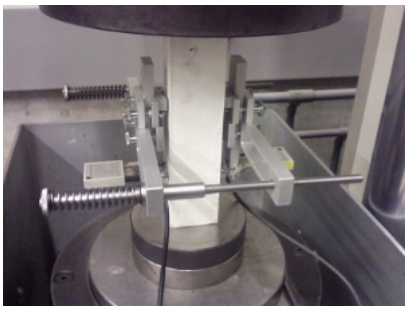

Figure 5.5: Static compression measurement

ment.

5.2.1 Modelling

Computational volume of 100 μm and a resolution of 0.75 μm was used. The size of the computational volume was chosen to be about 3 times bigger than the largest grain. Aluminate and belite were not considered as discrete, instead they were embedded in alite. The same is valid for ettringite, which was embedded in C-S-H. Belite was considered to be unreactive for the time of prediction - i.e. first thirty hours of hydration. Two main hydration reactions were considered - alite hydration and aluminate hydration. In alite hydration, 1.0 hydrating alite produces 1.57 C-S-H and 0.596 CH. In aluminate hydration, 1.0 Aluminate and 2.0681 gypsum produces ettringite, which is distributed into ettringite embedded in grain, pore C-S-H and inner C-S-H. The distribution between them is not very clear, but due to the fact that ettringite properties are very similar to C-S-H, the distribution between them does not matter very much.

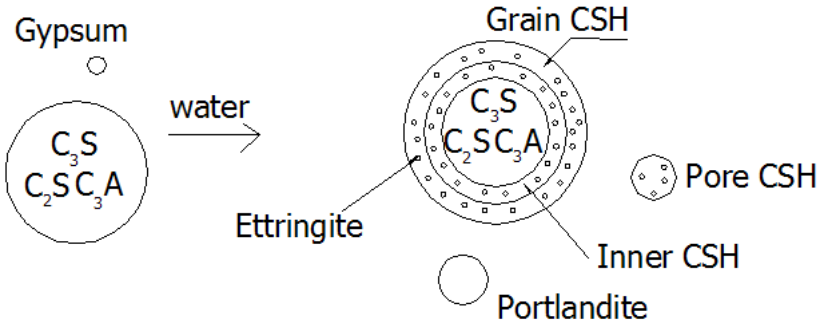

Figure 5.6: Distribution of the phases in the model

For intermixed phases, Mori-Tanaka homogenization scheme was used, i.e. the phases in smaller fractions were considered as inclusions (e.g. aluminate, belite, ettringite), while the other (alite, C-S-H) were considered to be the matrix. Because the properties of the matrix and inclusion of the phases are very similar, a simple averaging would be sufficient as well.

Selective integration scheme was used with the phases of the microstructure with spanning cluster. The elastic properties of the phases were considered as follows:

	Young's modulus [GPa]	Poisson's ratio[-]
alite	135	0.3
belite	130	0.3
aluminate	145	0.3
C-S-H	25.55	0.24
CH	38.5	0.305
ettringite	22.7	0.25
water	0.001	0.499924

C-S-H was assumed to exist in three forms - inner C-S-H, grain C-S-H and pore C-S-H. The density was considered to be an average of $2.0\,\mathrm{g/cm^3}$ for all of them, similarly the Young's modulus was considered to be 25.55 GPa. The distribution between pore and grain C-S-H was controlled by a virtual material - outer C-S-H buffer - Fig.5.6. Since no knowledge on how grain and pore C-S-H was distributed, existed, they were created in ratio 1:1. This ratio is later adjusted by the model based on the available surface area. The number of pore C-S-H clusters was considered

to be about 20 % of the alite grains at the end of hydration. This number is not considered to cause similar problems as portlandite, because it only exists in small volume fractions. The amount of portlandite, was chosen to be 1 % of the alite grains at the end of hydration. This is because visibly the generated microstructure with higher number of CH clusters does not correspond to the SEM images - Fig.5.10. Later on, for one of the mixes, variation of the number of portlandite clusters is performed - tested on 20 % of the number of alite grains, as well.

The particle size distributions were cut under the size of 0.42 μm, since the computational cost prevents us from modelling particles smaller than the mesh resolution. A particle above the size of 0.42 μm will grow by a factor of 1.3 towards the end of hydration, i.e. particles with this size will still be captured with high probability with the current resolution. It is important to say, that this approach leads to a slightly different distribution of the hydration products, than it would be with the full fraction. This will not result in a big change for elastic properties because of their partial dependency on overall volume fractions and current computational unavailability to handle higher resolution.

The microstructure was flocculated before hydration. The factor of the distance change was chosen to be 0.5 in the first instance, based on the preliminary experimental comparison to the microstructure of Boumiz. Later on, for one of the mixes, a variation 0.5 and 0.7 of the distance factors was tested.

The degree of hydration was enforced by the $ExternallyDefinedKinetics$ plugin, based on the X-ray diffraction data and was therefore not the object of the study of the output of the hydration model.

5.2.2 Experimental results

Experimentally, the samples made from coarser cement mixes showed higher amount of bleeding than the fine cement ones. The w/c ratios after the correction can be seen in the table below.

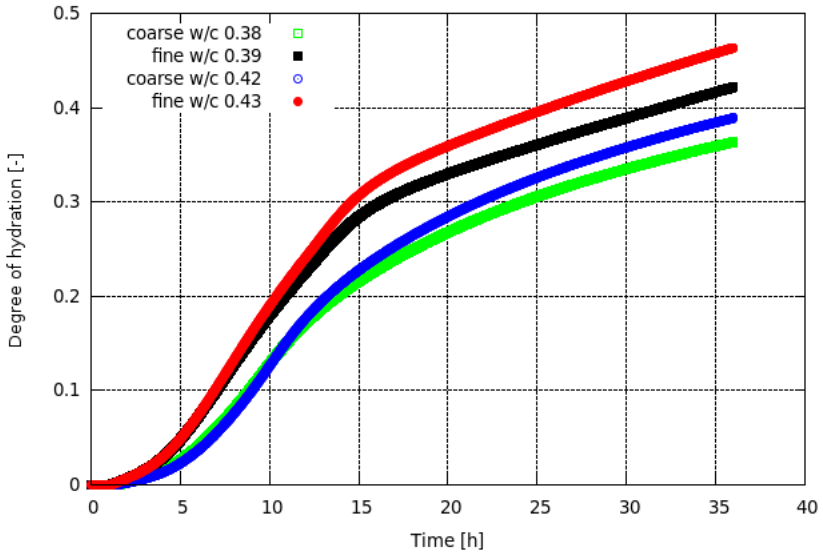

Figure 5.7: Experimental degree of hydration for various mixes - calorimetry

	original	after correction
fine	0.4	0.39
fine	0.45	0.43
coarse	0.4	0.38
coarse	0.45	0.42

Calorimetry, used to obtain the overall hydration degree, showed the highest degree of hydration for the fine mixes. For both fine and coarse mixes, the higher w/c ratio resulted in slightly higher values of the hydration degree for a particular time.

The results of the static and dynamic Young's modulus measurement can be seen in Fig.5.8. The error of the static measurement is approximately $\pm$ 2.5 %, the error of the resonant frequency test $\pm$ 3 % in terms of Young's modulus (error bars not plotted in order not to mix the results close to each other). If the measurements are related to time, then for both types of fineness a difference in elastic properties can be observed in terms of w/c ratio - the properties are higher for the lower w/c ratio.

The conclusion on the relationship between elastic properties with time for similar w/c ratio but different fineness has to be made with the effect of bleeding in

mind. It seems that the static measurement gives only mildly higher values for the fine mix w/c 0.45 (0.43) than coarse w/c 0.45 (0.42), although it has a higher degree of hydration. Nevertheless, if correction after bleeding is taken into account, the fine cement has a higher w/c ratio and that is why the difference between the fine and coarse is not very big. In one case, the dynamic test seems to show higher value for the coarse 0.4 (0.38), than for the fine 0.4 (0.39), this might again be the effect of bleeding - Fig.5.8.

The differences between static and dynamic modulus have been observed many times. In all of the cases, the dynamic values are higher than the static ones, which is generally claimed to be the effect of an instanteneous loading in the dynamic test and a creep inducing non-instaneous strain in the static case. Moreover, although the bar should be loaded in the elastic range, it is possible that cracks were induced in the static compression test. The difference, nevertheless changes in time for all of the mixes. While at 12 hours, the difference between static and dynamic modulus is about 30 %, at 30 hours the difference between the moduli is about 20 %. This might be the result of hardening and loss of viscoelasticity - Fig.5.9.

Hardly any conclusion can be drawn on Poisson's ratio, as the only method which could measure it, is the resonant frequency measurement. Poisson's ratio, however, does not seem to exhibit any change in time and its value is about 0.24 ± 0.03.

5.2.3 Numerical results

Based on X-ray diffraction input, particle size distribution and w/c, 4 types of microstructures were generated. Coarser microstructures were generated with 434043 and 410551 grains for w/c 0.38 and 0.42, finer microstructures with 558287 and 528395 grains for w/c 0.39 and 0.43, respectively - i.e. the microstructure was generated with the effect of bleeding in mind. The comparison of real and generated microstructure for fine mix, w/c ratio 0.39 can be seen in Fig.5.10. Apart from the shape, it seems that in reality there might have been even less clusters of portlandite than generated.

The results from the simulation show almost no difference between the two particle size distributions for the given hydration degree. Mild difference can only be seen at the very beginning of hydration, but is most probably caused by the statistical

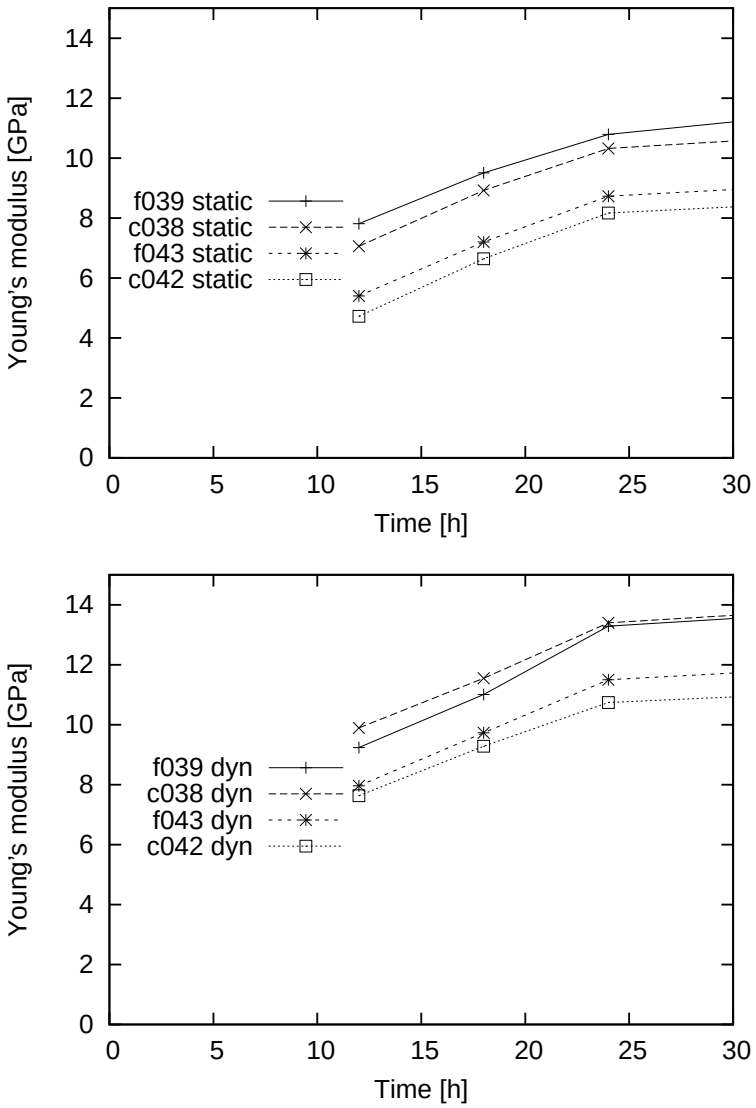

Figure 5.8: Development of Young's modulus - static test (above), dynamic test (below)

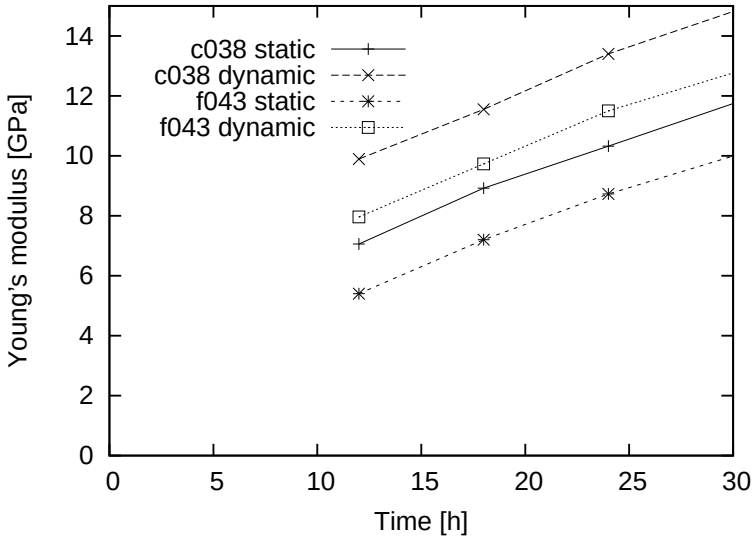

Figure 5.9: Comparison of the development of Young's modulus - static vs. dynamic test

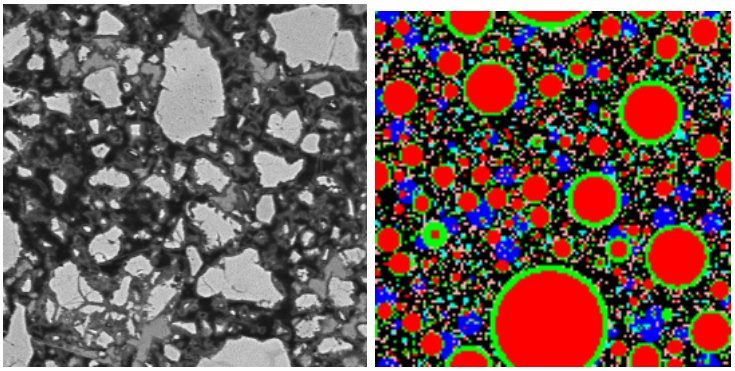

Figure 5.10: Fine mix, w/c 0.39, SEM image (V.Kocaba) vs. generated microstructure - alite(white → red), C-S-H (dark gray → green), CH (light gray → blue), porosity (black → black)

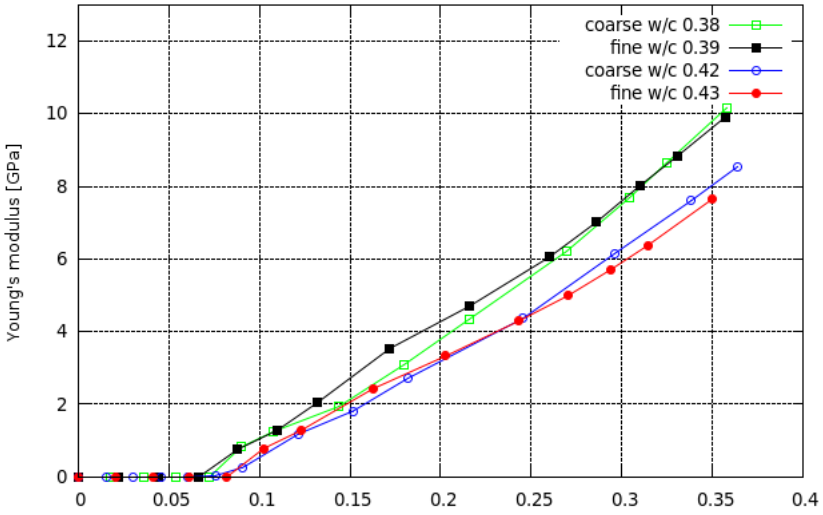

Figure 5.11: Young's modulus for all mixes - simulation

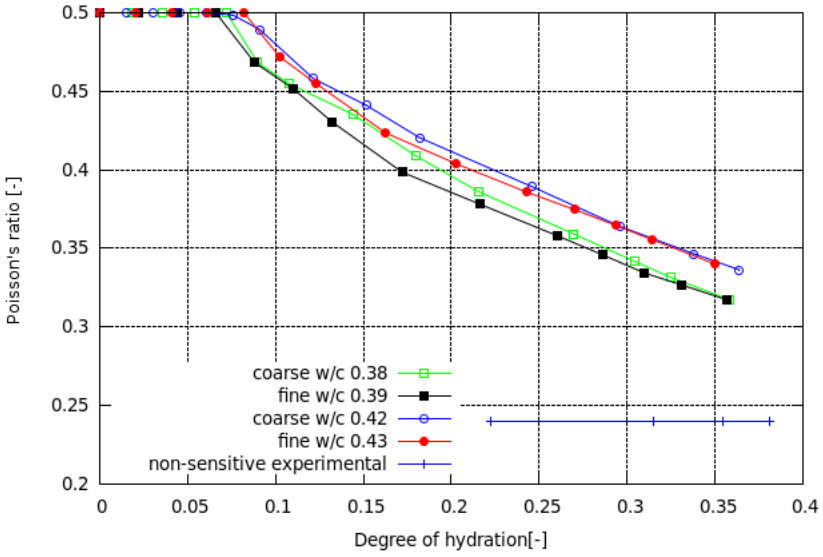

Figure 5.12: Poisson's ratio for all mixes - simulation

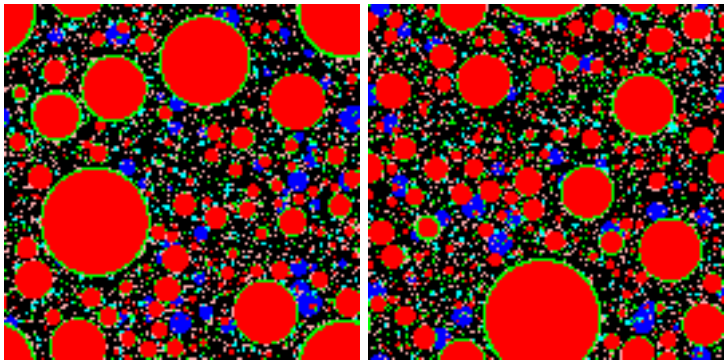

Figure 5.13: Coarse and fine mix, same hydration degree - 21.5 %

fluctuation. A clear difference can only be seen in terms of w/c ratios - Fig.5.11, 5.12. In terms of percolation threshold, the values for the higher w/c is around 8 %, lower w/c around 6 %.

It is not really clear whether the prediction should approach the static or dynamic measurements. If we consider that the model does not account for viscoelastic behavior, the results should be closer to the dynamic modulus. However, if we consider that the input values of the elastic properties of the phases come from a drained state (nanoindentation), then the values of the predicted properties should be certainly lower than what was observed with the dynamic measurement, which probably behaves more like an undrained test.

Overall, the prediction seems to underestimate the static modulus - Fig.5.14 (the data is plotted with the degree of hydration obtained from calorimetry). This might be more an effect of an underestimated hydration degree from the experiment. Indeed, other studies performed with the fine cement of w/c 0.4, seem to obtain a degree of hydration of around 40 % at 24 hours, while about 35 % was obtained based on the calorimetry. Assuming linear behavior, this might result in a change of about 2 - 3 GPa. Overall, the result seems to be good from 25 % hydration on. Before drawing the final conclusion, results on the variation of the flocculation distance factor and number of portlandite clusters are presented in Fig.5.15 for coarse cement mix w/c 0.42. It seems, that the change of the flocculation factor did not have a significant effect on the results. In one case higher flocculation distance factor actually resulted in mildly lower values of the Young's modulus. On the other hand, the increase in the number of portlandite clusters caused an increase of about

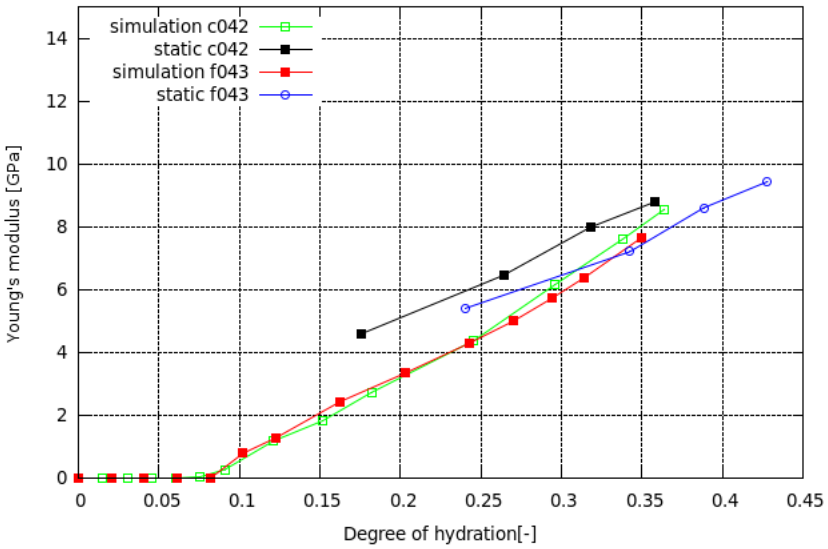

Figure 5.14: Comparison of the experimental values and simulation

17 % in terms of Young's modulus. The result shows that a proper knowledge of the microstructural arrangement is needed to interpret any results.

Poisson's ratio from the resonant frequency test - Fig.5.12, compared to the simulation is completely off the range of early age values. This problem was already reported by Haecker [25], who realised that an error of 5 % in Young's and shear modulus resulted in a substantial difference in Poisson's ratio.

5.3 Summary

In this chapter, an experimental validation of the numerical technique was shown. Firstly, comparison with an alite microstructure of Boumiz was performed and showed an overestimation of Young's modulus and underestimation of Poisson's ratio for a microstructure flocculated with a final distance factor 0.7. This was a reason to change the flocculation range for the next simulations.

Later, predictions on four types of cement mixes were performed - fine and coarse white cement and two different w/c ratios 0.4 and 0.45. The degrees of hydration were obtained experimentally by calorimetry and X-ray diffraction, corrections for bleeding were made. The simulation showed no difference between the microstruc-

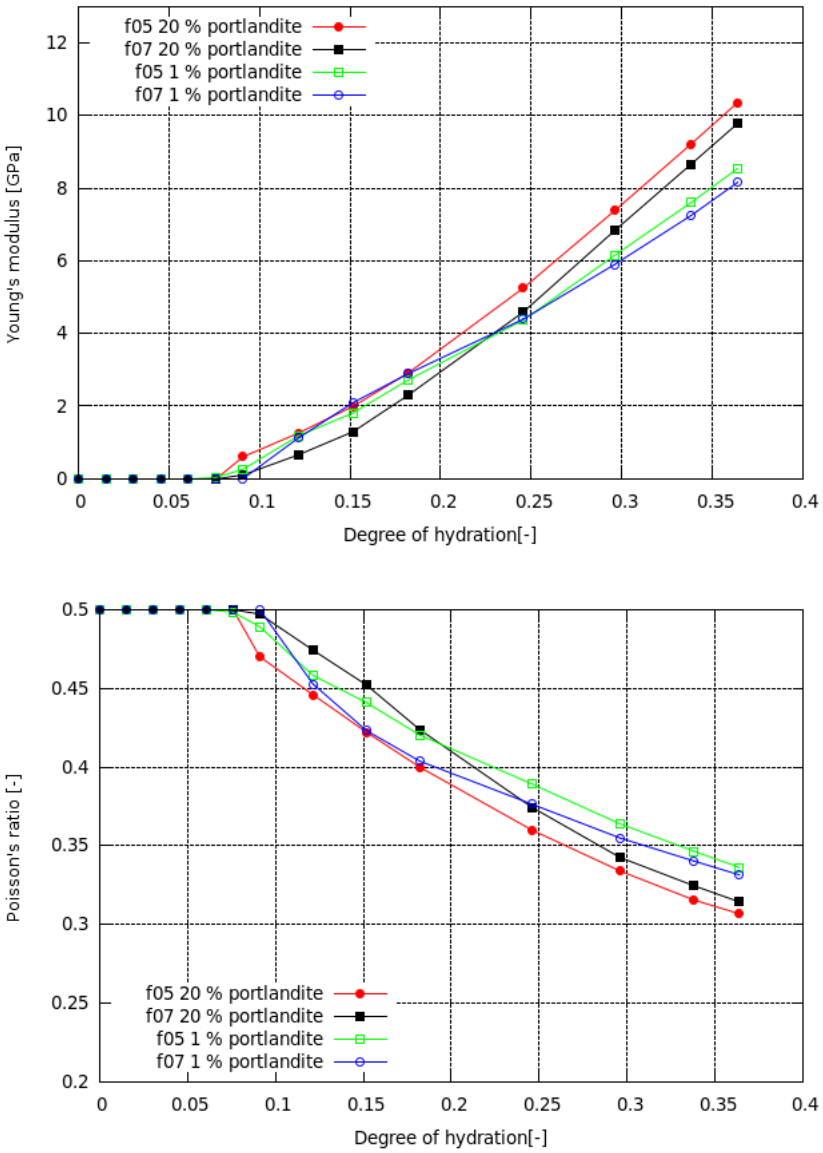

Figure 5.15: Coarse 0.42 - variations of the flocculation factor and number of portlandite clusters

tures of different fineness and very similar w/c ratio.

Static test produced lower values of Young's modulus than the one obtained from resonant frequency test, which is a result of viscoelastic behavior under static loading. The simulations seem to be slightly lower than the static test. This could be the result of an underestimated hydration degree or insufficient flocculation. Poisson's ratio was only obtained from the resonant frequency test and did not change its value in time, which might signalize a large dependency of its value on the dimensions of the specimen.

Overall, this study showed the importance of the knowledge of the microstructural details, so that a thorough validation could be made.

Chapter 6

Discussion

The goal of this study was to explore the effective elastic properties of cement paste at early age by means of Finite Element method. Specific problems related to early age microstructure and the sensitivity of the FEM method to the microstructural parameters were investigated.

The microstructure was generated by a vector microstructural model developed at LMC EPFL and the effective elastic properties were computed by a FEM code, specifically developed for this work.

The discussion will focus on three parts:

- Problems specific to modelling of cement microstructure by FEM at early age
- The sensitivity of FEM to microstructural parameters
- Perspectives on the resolution issues

6.1 Problems specific to modelling of cement microstructure by FEM at early age

In the first part of the study a simpler alite microstructure was generated. This enabled us to concentrate on the specifics of FEM, before going to more complex systems. Early age microstructure is complex and poses a big challenge for the generation of unstructured meshes. This is due to big particle gradations and very thin layers. For this reason, in the first instance, voxel mesh was generated.

The Young's modulus at zero hydration degree is known to be very close to zero. However, the simulations based on the voxel mesh predicted a high value of Young's modulus ($\sim 5\,\mathrm{GPa}$) already at this point. It was observed that, it was possible to reduce this artifact by increasing the mesh resolution. Unfortunately, unacceptably large artifacts (larger than 1 GPa) still remained even with mesh resolutions bordering on the computational limits. Closer investigation of the microstructure revealed artificial connectivity between particles. This effect occurs when the particles are too close to each other and the mesh resolution is insufficient.

Burning algorithm was used to address this problem. Although significant improvement was observed at very early age, continuing resolution dependency suggested that artificial connectivity was removed only to some extent and still remained in the microstructure with spanning cluster.

Additional source of overestimation was found to be associated with finite elements representing water. The water elements are the cause of locking - i.e. underestimating the displacements and overestimating the stiffness as a result of the full integration scheme. Selective integration scheme was therefore used to improve the result, i.e. the volumetric part was integrated with a reduced integration scheme.

Generally, improving resolution yields better results. However, every increase in resolution simultaneously increases the memory and computation requirements cubically. More efficient representations of the same geometry could alleviate this problem, therefore two different refinement schemes have been implemented.

Simpler regular and octree-based techniques were found to be of none or very mild improvement to the resolution problem. Regular tetrahedral mesh did not improve the solution at all, this was due to the integration scheme, which could not be reduced unlike in the case of the hexahedral element. Octree refinement allowed only a mild improvement at later ages. This could indicate that the removal of locking on octree mesh was not fully effective due to additional constraints introduced by the octree mesh. From computational point of view, it makes more sense to use a regular mesh with slightly higher resolution, than the octree mesh.

The size of the computational volume seems to be of big importance in range 0 - 30 % hydration due to larger statistical fluctuation, the same was found to be valid for the boundary conditions. The error in the resolution, on the other hand seems to

be more important in the later stages - 30 - 50 % hydration, and the results suggest that care must be taken with the interpretation of the results for higher solid volume fractions. This also indicates that lower w/c ratios will generally suffer from higher overestimation of effective properties than higher w/c ratios.

6.2 The sensitivity of FEM to microstructural parameters

The issues of FEM associated with the early age microstructure, such as resolution, still affect the precision of the prediction of the microstructural parameters. The general trends and differences between microstructural variations will nevertheless stay, even after the resolution correction.

Sensitivity of FEM was explored on flocculation, several w/c ratios, particle size distributions, number of hydrate (portlandite and pore C-S-H) clusters and density of C-S-H.

The first problem adressed was the value of the percolation threshold, which was found to be too high in the preliminary simulations compared to experiments. That indicated that the initial random packing might not be representative of the real packing. Flocculation algorithm was used to decrease the values of the percolation threshold. The simulations showed that upon application of flocculation algorithm, the values of the percolation threshold can be improved to a large extent.

The flocculation distance factor, by which the particles are brought closer, seems to affect both percolation threshold and the values of effective elastic properties. It is however not completely clear what the distance factor should be in general and it seems to be dependent on the particle size distribution.

The method distinguishes well between different sizes of capillary porosity for a particular hydration degree. This was found to be true for both w/c ratios and particle size distributions. Because the same hydration degree means equal amounts of solid in the microstructure, the method has a big potential to respond to anomalies.

Variations of the C-S-H density and its elastic properties do not seem to cause a big difference in the effective elastic properties. However, it was discovered to have an effect on the percolation threshold. The lowest percolation threshold was

predicted when LD C-S-H was used.

The method was found to be sensitive to connectivity also in terms of the number of clusters of hydration products. The number of portlandite clusters seems to be of high importance. This could also be observed upon the experimental comparison, in which the change from 1 to 20 % of the number of the clusters changed the results by 15 %.

Experimental validation showed generally a good agreement between experimental and numerical data. However, the final conclusion whether the method actually predicts well compared to experiments could be done, only if the microstructural parameters - i.e. mainly the number of portlandite clusters, were known. Another important factor is the hydration degree. Inaccuracies in the hydration degree most probably do not result in any substantial changes when comparing the simulations from various cement mixes between themselves, however it could be important when comparing the simulations to the experiments. The change of hydration degree by 0.05 can cause a change in the results by 25 %.

It should be noted, that the effective elastic properties predicted by FEM in this study strongly depend on the output of the microstructural model. The microstructural model is a complex tool and is still under development. As such, any potential inaccuracies of the model will be directly reflected on the FEM results.

6.3 Perspectives on the resolution issues

One of the big limitations of the FEM prediction on early age cement microstructure is its computational cost. The question as how far it is necessary to go with the computational resources, remains.

Use of a computer cluster for the prediction of elastic properties with respect to other properties might sound like shooting a fly with a cannon. However, results could be obtained quickly because the problem represented by voxel mesh can be easily parallelized. Yet, the problem scales cubically and while for the moment we have been dealing with ratio of particle sizes 1 : 100, much higher resolution would be actually required for very fine particle size distributions.

For early age prediction of elastic properties, desktop computers, together with

thorough resolution convergence studies seem to be a very good alternative. The positive news is that the memory and speed of computers double every 18 months following the so called Moore's Law. The bad news is that increasing the resolution of the CV increases the requirements cubically, in other words, to increase the resolution two-fold, we need to increase the computational resources eight-fold.

This makes it even more difficult for the prediction of nonlinear material properties on cement paste scale. Moreover, unstructured meshes still have a long way ahead before they could be used for complex overlapping microstructures. Voxel mesh causes undesired problems, such as artificial stress concentrations on the jagged boundaries. From this point of view, it is necessary to consider other options, such as lattice models.

6.4 Conclusions and Perspectives

In this work a methodology based on the numerical homogenization by Finite Element method was developed and tested for the cement paste at early age. Based on numerous simulations, verified by the experimental data, it has been shown, that the model is able to predict effective elastic properties with reasonable accuracy.

We have understood that cement paste microstructure at early age imposes intrinsic limitations for the Finite Element method because of its complex geometry. Nevertheless, the model demonstrated the capability to produce results in accordance with the change of the microstructural parameters.

I believe that the method could be used for predicting anomalies, such as higher porosity resulting in higher mechanical properties which occur on addition of SCMs into cementitious systems. To achieve that, in future, more focus should be put on the influence of the resolution on the convergence of the results. Simultaneously, a larger range of experiments should be done on plain and blended cement mixes, in order to verify the methodology.

Appendix A

Additional Tables and Figures

A.1 List of abbreviations

C-S-H	calcium-silicate hydrate (main hydration product),
CH	calcium hydroxide, portlandite (main hydration product),
CV	computational volume,
doh	degree of hydration,
FEM	Finite Element method,
HD	high-density,
IDD	Interaction Direct Derivative,
ITZ	Interfacial Transition Zone,
LD	low-density,
MT	Mori-Tanaka,
psd	particle size distribution ,
RVE	representative volume element ,
SC	Self-Consistent,
SCS	Self-Consistent scheme,
w/c	water to cement ratio

A.2 Particle size distributions

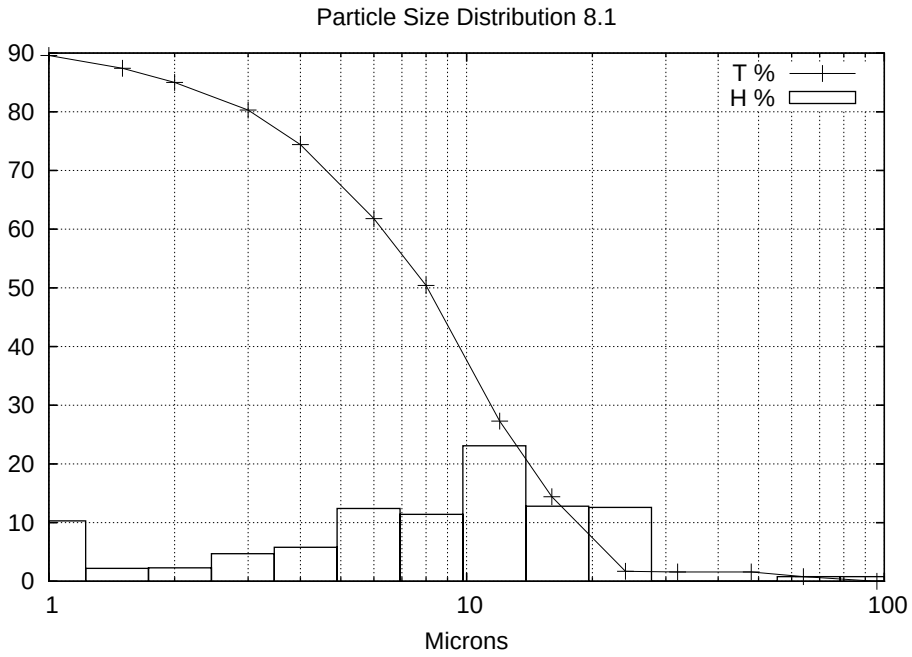

D	1	1.5	2	3	4	6	8	12
T%	89.6	87.4	85.0	80.3	74.4	61.8	50.4	27.3
H%	10.3	2.2	2.3	4.7	5.8	12.4	11.4	23.1
D	16	24	32	48	64	96	128	192
T%	14.4	1.7	1.6	1.6	0.8	0	0	0
H%	12.8	12.6	0	0	0.8	0.8	0	0

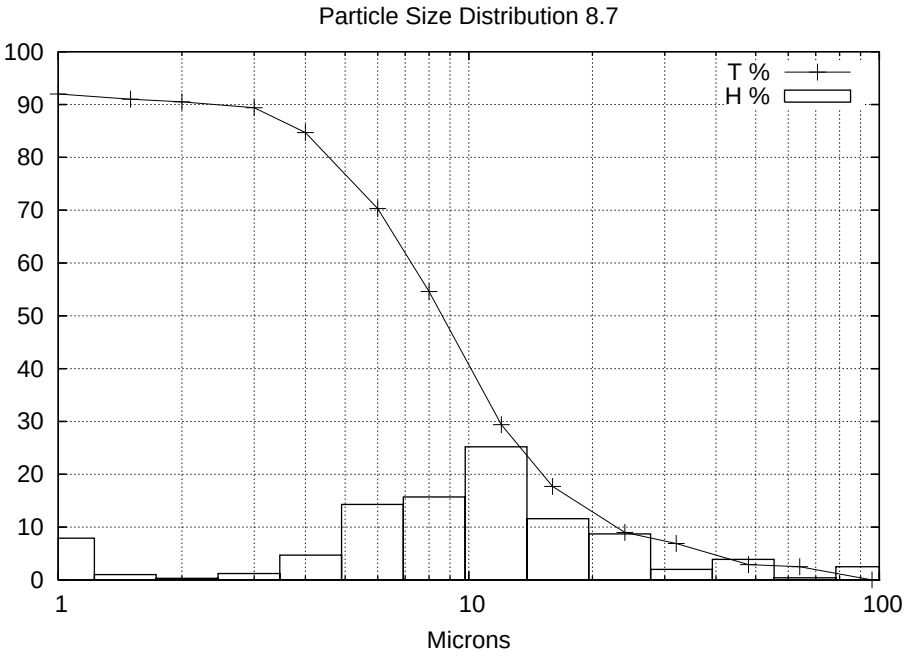

D	1	1.5	2	3	4	6	8	12
T%	92.0	91.0	90.5	89.4	84.7	70.3	54.6	29.4
H%	7.9	1.0	0.3	1.2	4.7	14.3	15.7	25.2
D	16	24	32	48	64	96	128	192
T%	17.7	9.0	6.9	2.9	2.5	0	0	0
H%	11.6	8.7	2.0	3.9	0.4	2.5	0	0

A.3 Mori-Tanaka

$$k_{eff} = \left(k_m + \frac{4}{3}\mu_m \sum_{j=1}^{n} v_j \frac{k_j - k_m}{k_j + \frac{4}{3}\mu_m}\right)\left(1 - \sum_{j=1}^{n} v_j \frac{k_j - k_m}{k_j + \frac{4}{3}\mu_m}\right)^{-1} \quad \text{(A.1)}$$

$$\mu_{eff} = \left(\mu_m + \kappa_m \sum_{j=1}^{n} v_j \frac{\mu_j - \mu_m}{\mu_j + \kappa_m}\right)\left(1 - \sum_{j=1}^{n} v_j \frac{\mu_j - \mu_m}{\mu_j + \kappa_m}\right)^{-1} \quad \text{(A.2)}$$

$$\kappa_m = \frac{\mu_m(\frac{3}{2}k_m + \frac{4}{3}\mu_m)}{k_m + 2\mu_m} \quad \text{(A.3)}$$

A.4 Quantitative analysis of the white cement

Name	Formula	Fine	Coarse
Alite	C_3S	67.5	68.2
Belite	C_2S	23.6	23.1
Ferrite	C_4AF	-	-
Aluminate	C_3A	3.8	3.6
Lime	C	0.9	0.6
Periclase	M	0.3	0.0
Gypse	$CaSO_4 - 2H_2O$	0.0	0.0
Hemihydrate	$CaSO_4 - 0.5H_2O$	1.0	0.7
Anhydrate	$CaSO_4$	1.4	2.7
Portlandite	$Ca(OH)_2$	0.5	0.6
Quartz	S	0.0	0.0
Calcite	$CaCO_3$	0.0	0.0
Arcanite	K_2SO_4	0.8	0.5

Taken from [37]

A.5 Selective Integration

New Strain-Displacement Matrix Representation. Numbers 1,2,3, represent the standard derivatives. The tensors with the overline represent evaluation by a reduced integration scheme here in the middle of the hexahedral element.

$$B_4 = \left[\begin{array}{ccc} B_5 & B_6 & B_8 \\ B_4 & B_7 & B_8 \\ B_4 & B_6 & B_9 \\ \hline 0 & B_3 & B_2 \\ B_3 & 0 & B_1 \\ B_2 & B_1 & 0 \end{array}\right] \tag{A.4}$$

$$B_4 = \frac{\overline{B}_1 - B_1}{3} \tag{A.5}$$

$$B_5 = B_1 + B_4 \tag{A.6}$$

$$B_6 = \frac{\overline{B}_2 - B_2}{3} \tag{A.7}$$

$$B_7 = B_2 + B_6 \tag{A.8}$$

$$B_8 = \frac{\overline{B}_3 - B_3}{3} \tag{A.9}$$

$$B_9 = B_3 + B_8 \tag{A.10}$$

Taken from [36].

A.6 Sample xml file for alite hydration for the vector microstructural model

In the following the most important parts of the input for the model will be summarised in the order they appear in the xml file. The tags in the xml file have generally more options, only the relevant ones will be explained here. More can be found on *www.micthemodel.org*.

```
<setup>
   <material id="2" name="CSH">
       <density>2.0</density>
       <diffusivity>0.002</diffusivity>
       <inner>false</inner>
       <universal>false</universal>
       <discrete>true</discrete>
       <hasVariant>false</hasVariant>
       <initialAmount>0.0</initialAmount>
       <color>-16711936</color>
   </material>
   <material id="1" name="Alite">
       <density>3.15</density>
       <diffusivity>0.0</diffusivity>
       <inner>false</inner>
       <universal>false</universal>
       <discrete>true</discrete>
```

```
    <hasVariant>false</hasVariant>
    <initialAmount>0.4425</initialAmount>
    <color>-65536</color>
</material>
<material id="3" name="CH">
    <density>2.24</density>
    <diffusivity>0.0</diffusivity>
    <inner>false</inner>
    <universal>false</universal>
    <discrete>true</discrete>
    <hasVariant>false</hasVariant>
    <initia lAmount>0.0</initialAmount>
    <color>-16776961</color>
</material>
<modelGrain name="cementGrain">
    <layer>Alite</layer>
    <layer>CSH</layer>
    <filePSD>psd81.txt</filePSD>
</modelGrain>
<modelGrain name="CHGrain">
    <layer>CH</layer>
    <filePSD>undefined</filePSD>
</modelGrain>
<reactor name="alitehyd">
    <size>160.0</size>
    <pixelSize>1.0</pixelSize>
    <fileFolder>./aliteExample</fileFolder>
    <resourceFolder>./aliteExample</resourceFolder>
    <timeStepFile>timesteps.txt</timeStepFile>
    <backgroundColor>-16777216</backgroundColor>
    <maxOccupancyPixels>100</maxOccupancyPixels>
    <minOccupancyPixels>1</minOccupancyPixels>
    <flocculate value="true">
        <duringDistribution>false</duringDistribution>
        <range>10.0</range>
        <factor>0.3</factor>
        <cycles>1</cycles>
        <maxTrials>10000</maxTrials>
    </flocculate>
    <sphereSamplingPoints>92</sphereSamplingPoints>
    <checkIndividualArea>false</checkIndividualArea>
    <checkNoArea>false</checkNoArea>
    <findCoveringSphere>false</findCoveringSphere>
    <saveHydout>true</saveHydout>
    <savePorein>false</savePorein>
    <saveGrains>true</saveGrains>
    <saveDeepImages depth="128">false</saveDeepImages>
</reactor>
<reaction name="AliteHydration">
    <order>1</order>
    <reactant>
        <materialName>Alite</materialName>
        <ratio>1.0</ratio>
    </reactant>
    <product>
        <materialName>CSH</materialName>
        <ratio>1.57</ratio>
    </product>
    <product>
        <materialName>CH</materialName>
        <ratio>0.593</ratio>
    </product>
    <discrete>false</discrete>
</reaction>
<plugin type="kinetics">
    <classPath>precompiled</classPath>
    <className>plugins.kinetics.ExternallyDefinedKinetics</className>
    <parameter type="file">
        <name>./aliteExample/dohc.txt</name>
    </parameter>
    <parameter name="Order of implementation" type="number">
        <class>int</class>
        <value>1</value>
```

```
        </parameter>
        <parameter type="reactant">
            <hostReaction>AliteHydration</hostReaction>
            <name>Alite</name>
        </parameter>
        <parameter type="reaction">
            <name>AliteHydration</name>
        </parameter>
        <parameter type="reactor">
            <name>alitehyd</name>
        </parameter>
    </plugin>
    <plugin type="nucleiGenerator">
        <classPath>precompiled</classPath>
        <className>plugins.nucleiGenerator.ExponentialNucleiGenerator</className>
  <parameter name="Initial number of nucleii" type="number">
            <class>int</class>
            <value>25</value>
        </parameter>
        <parameter name="Maximum number of Nucleii" type="number">
            <class>int</class>
            <value>25</value>
        </parameter>
        <parameter name="Coefficient" type="number">
            <class>float</class>
            <value>0.0</value>
        </parameter>
        <parameter name="Starting time" type="number">
            <class>float</class>
            <value>0.0</value>
        </parameter>
        <parameter name="End time" type="number">
            <class>float</class>
            <value>-1.0</value>
        </parameter>
        <parameter type="modelGrain">
            <name>CHGrain</name>
        </parameter>
    </plugin>
    <plugin type="materialDistributionProfile">
        <classPath>precompiled</classPath>
        <className>plugins.materialDistributionProfile.SurfaceDistributionProfile</className>
        <parameter type="material">
            <name>CH</name>
        </parameter>
        <parameter name="Minimum radius" type="number">
            <class>float</class>
            <value>0.1</value>
        </parameter>
    </plugin>
    <command>hydrate</command>
    <command>saveElements</command>
    <command>noBurning</command>
    <command>markPores</command>
    <command>noContact</command>
    <command>noPixels</command>
</setup>
```

Materials are defined by their:

density

diffusivity - in this study, the diffusivity is redundant, as no kinetics which would need diffusivity, was defined

inner - true, if the material can be formed only in the bounds of the original particle

universal - true, if material is not present in any layer of any particle, it is a buffer, which can be redistributed to other materials, (in case of cement, universal OuterCSH is redistributed to GrainCSH and PoreCSH)

discrete - false, if material is considered to be diffused in another material (for cement system Aluminate can be considered to be diffused in Alite)

hostName - has to be defined if material is not discrete, e.g. Aluminate has a host Alite

hasVariant - true, if the phase exists in various forms, e.g. InnerCSH can have a variant OuterCSH

initialAmount - volume occupied by the phase at the start of the simulation

color - color for image output

Next, **modelGrains** have to be defined by their layers and particle size distributions. In this example, cementGrain has one layer of Alite, another layer of CSH and a particle size distribution defined in a file. CHgrain has only one layer - CH and undefined particle size distribution, i.e. the grains are all going to be of the same size.

The computational volume is defined in the **reactor** by its size and resolution. The *timesteps* file determines for which times the microstructure will be generated. If **flocculation** of the reactor is set *true*, the following parameters should be defined:

during distribution - false, if the flocculation should be performed only after the initial placing is done

range - area, in which the nearest particle is going to be located

factor - distance factor, by which the particles are brought closer to each other

cycles - in how many cycles the flocculation is done

Other important tags include in the **reactor** include:

saveGrains - should be set true if you want to reuse the initial placing in the next simulations

saveHydout - should be set true if you want to reuse the initial placing and the placing of hydration products

Reaction tag is self-explanatory and contains stochiometric coefficients of the reactions. The **discrete** tag of the reaction was set to *false* in this study in order to use *ExternallyDefinedKinetics* as **kinetics**. That means that the kinetics is defined in a file containing [time - degree of hydration] relationship, usually based on experiments. The products are distributed proportionally to the initial Alite grain sizes. The original grain changes in size by a factor of 1.3 towards the end of hydration. The distribution of CH is controlled by the stochiometry and **nucleiGenerator**, in which number of the CH grains can be set (in this case the number of grains is constant during the hydration).

The **materialDistributionProfile** controls the distribution of newly produced material to different particles, default values are provided by the model.

Other important tags are **command** tags.

hydrate - creates the initial particle placing and hydrates. The value of this tag can be replaced by restartHydration or redoPixels.

restartHydration - initial placing stays the same, distribution of hydration products changes, *saveGrains* needs to be set true in the previous simulations.

redoPixels - initial placing and distribution of hydration products stays the same, only the mesh size changes, *saveGrains* and *saveHydout* need to be set true in the previous simulations.

noBurning - full microstructure, can be replaced by doBurning

doBurning - percolated microstructure

saveElements - true, if the material of the voxels should be determined and stored in a ASCII file

markPores - true, if also the pore voxels should be stored

Bibliography

[1] Aboudi, J. *Mechanics of Composite Materials. A Unified Micromechanical Approach.* Elsevier Science Publishers, Amsterdam, 1991.

[2] Adams, D., and Doner, D. Transverse normal loading of a unidirectional composite. *J. Comput. Mat. 1* (1967), 152.

[3] Anthoine, A. Derivation of the in-plane elastic characteristics of masonry through homogenization theory. *International Journal of Solids and Structures 32*, 2 (1995), 137–163.

[4] Bary, B., Ben-Haha, M., Adam, E., and Montarnal, P. Numerical and analytical effective elastic properties of degraded cement pastes. *Cement and Concrete Research 39*, 10 (2009), 902–912.

[5] Bathe, K. *Finite Element Procedures.* Prentice Hall, Pearson Education, 2006.

[6] Beaudoin, J. Comparison of mechanical properties of compacted calcium hydroxide and portland cement paste systems. *Cement and Concrete Research 13*, 3 (1983), 319–324.

[7] Belytschko, T., and Black, T. Elastic crack growth in finite elements with minimal remeshing. *International Journal for Numerical Methods in Engineering 45*, 5 (1999), 601–620.

[8] Bentz, D. Three-dimensional computer simulation of portland cement hydration and microstructure development. *Journal of the American Ceramic Society 80*, 1 (1997), 3–21.

[9] Benveniste, Y. A new approach to the application of mori-tanaka's theory in composite materials. *Mechanics of Materials 6*, 2 (1987), 147–157.

[10] Bernard, O., Ulm, F., and Lemarchand, E. A multiscale micromechanics-hydration model for the early-age elastic properties of cement-based materials. *Cement and Concrete Research 33*, 9 (2003), 1293–1309.

[11] Bishnoi, S., and Scrivener, K. uic: A new platform for modelling the hydration of cements. *Cement and Concrete Research 39*, 4 (2008), 266–274.

[12] Boumiz, A. *Etude comparee des evolutions mecaniques et chimiques des pates de ciment etmortiers a tres jeune age. Developpement des techniques acoustiques.* PhD thesis, Universite Paris 7, Paris, 1995.

[13] Boumiz, A., Vernet, C., and Tenoudji, F. Mechanical properties of cement pastes and mortars at early ages : Evolution with time and degree of hydration. *Advanced Cement Based Materials 3*, 3-4 (1996), 94–106.

[14] Brockenbrough, J., Wienecke, H., and Suresh, S. Deformation of metal-matrix composites with continuous fibers: Geometrical effects of fiber distribution and shape. *Acta Metallurgica et Materialia 39*, 5 (1991), 735–752.

[15] Budiansky, B. On the elastic moduli of some heterogeneous materials. *Journal of the Mechanics and Physics of Solids 13*, 4 (1965), 223–227.

[16] Byfors, J. *Plain Concrete at Early Age.* PhD thesis, Swedish cement and Concrete Research Institute, 1980.

[17] Constantinides, G., and Ulm, F.-J. The effect of two types of c-s-h on the elasticity of cement-based materials: Results from nanoindentation and micromechanical modelling. *Cement and Concrete Research 34*, 1 (2004), 67–80.

[18] Costoya, M. *Effect of Particle Size on the Hydration Kinetics and Microstructural Development for Tricalcium Silicate.* PhD thesis, École Polytechnique Fédérale de Lausanne, 2008.

[19] De-Schutter, G., and Taerwe, L. Degree of hydration-based description of mechanical properties of early age concrete. *Materials and Structures 29* (1996), 335 – 344.

[20] Dow, O. *A Unified Approach to the Finite Element Method and Error Analysis Procedures*. Academic Press San Diego, 1999.

[21] Drugan, W., and Willis, J. A micromechanics-based nonlocal constitutive equation and estimates of representative volume element size for elastic composites. *Journal of the Mechanics and Physics of Solids 44*, 4 (1996), 497–524.

[22] Eshelby, J. The determination of the elastic field of an ellipsoidal inclusion, and related problems. *Proceedings of the Royal Society of London Series A-Mathematical and Physical Sciences 241*, 1226 (1957), 376–396.

[23] Ghosh, S., and Moorthy, S. Elastic-plastic analysis of arbitrary heterogeneous materials with the voronoi cell finite element method. *Computer Methods in Applied Mechanics and Engineering 121*, 1-4 (1995), 373–409.

[24] Guidoum, A. *Simulation Numérique 3D des Comportements des Bétons en Tant que Composites Granulaires*. PhD thesis, École Polytechnique Fédérale de Lausanne, 1994.

[25] Haecker, C.-J., Garboczi, E., Bullard, J., Bohn, R., Sun, Z., Shah, S., and Voigt, T. Modeling the linear elastic properties of hydrating cement paste. *Cement and Concrete Research 35* (2005), 1948–1960.

[26] Hain, M., and Wriggers, P. Numerical homogenization of hardened cement paste. *Comput Mech 42* (2008), 197–212.

[27] Hashin, Z. On some variational principles in anisotropic and nonhomogeneous elasticity. *Journal of the Mechanics and Physics of Solids 10*, 4 (1962), 335–342.

[28] Hashin, Z., and Shtrikman, S. A variational approach to the theory of the elastic behaviour of multiphase materials. *Journal of the Mechanics and Physics of Solids 11*, 2 (1963), 127–140.

[29] Hazanov, S. Hill condition and overall properties of composites. *Archive Appl. Mech. 68* (1998), 385–394.

[30] Hazanov, S., and Huet, C. Order relationships for boundary conditions effect in heterogeneous bodies smaller than the representative volume. *Journal of the Mechanics and Physics of Solids 42*, 12 (1994), 1995–2011.

[31] Hershey, A. The elasticity of an isotropic aggregate of anisotropic cubic crystals. *ASME J. Appl. Mech. 21* (1954), 226–240.

[32] Hill, R. Elastic properties of reinforced solids: Some theoretical principles. *Journal of the Mechanics and Physics of Solids 11*, 5 (1963), 357–372.

[33] Hill, R. Theory of mechanical properties of fibre-strengthened materials: I. elastic behaviour. *Journal of the Mechanics and Physics of Solids 12*, 4 (1964), 199–212.

[34] Hollister, S., and Kikuchi, N. A comparison of homogenization and standard mechanics analysis for periodic porous composites. *Computational Mechanics 10* (1992), 73–95.

[35] Hori, M., and Nemat-Nasser, S. On two micromechanics theories for determining micro-macro relations in heterogeneous solids. *Mechanics of Materials 31*, 10 (1999), 667–682.

[36] Hughes, T. *The Finite Element Method, Linear Static and Dynamic Finite Element Analysis*. Prentice-Hall, Englewood Cliffs, NJ, 1987.

[37] Jaouadi, I. *Etude Numerique et Experimentale du retrait Endogene de la Pate de Ciment a Jeune Age*. PhD thesis, École Polytechnique Fédérale de Lausanne, 2008.

[38] Jennings, H. A model for the microstructure of calcium silicate hydrate in cement paste. *Cement and Concrete Research 30* (2000), 101–116.

[39] Jennings, H., and Parrot, L. Microstructural analysis of hydrated alite paste, part 2: Microscopy and reaction products. *Journal of Materials Science 21* (1986), 4053–4059.

[40] Kamali, S., Moranville, M., Garboczi, E., Prene, S., and Gerard, B. Hydrate dissolution influence on the young's modulus of cement paste. *Proc. Fracture Mechanics of Concrete Structures, Vail* (2004).

[41] Kim, H., and Swan, C. Voxel-based meshing and unit-cell analysis of textile composites. *International Journal for Numerical Methods in Engineering 56* (2003), 977–1006.

[42] Kroner, E. Berechnung der elastischen konstanten des vielkristalls aus der konstanten des einkristalls. *Zeitschrift fur Physik 151* (1958), 504–518.

[43] Ma, H., Hu, G., and Huang, Z. A micromechanical method for particulate composites with finite particle concentration. *Mechanics of Materials 36*, 4 (2004), 359–368.

[44] Manzano, H., Dolado, J., and Ayuela, A. Elastic properties of the main species present in portland cement pastes. *Acta Materialia 57*, 5 (2009), 1666–1674.

[45] Mehta, P., and Monteiro, P. *Concrete: Microstructure, Properties, and Materials*. McGraw-Hill, 2006.

[46] Mesarovic, S., and Padbidri, J. Minimal kinematic boundary conditions for simulations of disordered microstructures. *Philosophical Magazine 85*, 1 (2005), 65–78.

[47] Mishnaevsky, L. *Computational Mesomechanics of Composites*. John Wiley and Sons, 2007.

[48] Monteiro, P., and Chang, C. The elastic moduli of calcium hydroxide. *Cement and Concrete Research 25*, 8 (1995), 1605–1609.

[49] Mori, T., and Tanaka, K. Average stress in matrix and average elastic energy of materials with misfitting inclusions. *Acta Metallurgica 21*, 5 (1973), 571–574.

[50] Moulinec, H., and Suquet, P. A fft-based numerical method for computing the mechanical properties of composites from images of their microstructure.

In *Microstructure-Property Interactions in Composite Materials*, R. Pyrz, Ed. Kluwer Academic Publishers, Zurich, Switzerland, 1995, pp. 235–246.

[51] Moulinec, H., and Suquet, P. A numerical method for computing the overall response of nonlinear composites with complex microstructure. *Computer Methods in Applied Mechanics and Engineering 157*, 1-2 (1998), 69–94.

[52] Navi, P., Scrivener, K., and Pignat, C. Simulation of cement paste microstructure hydration, pore space characterisation and permeability determination. *Materials and Structures 38* (2005), 459–466.

[53] Needleman, A., and Tvergaard, V. Comparison of crystal plasticity and isotropic hardening predictions for metal-matrix composites. *Journal of Applied Mechanics 60*, 1 (1993), 70–76.

[54] Nikishkov, G. Finite element algorithm with adaptive quadtree-octree mesh refinement. *ANZIAM J. 46 E* (2005), C15–C28.

[55] Ostoja-Starzewski, M. Lattice models in micromechanics. *Applied Mechanics Reviews 55* (2002), 35–60.

[56] Pichler, B., Hellmich, C., and Eberhardsteiner, J. Spherical and acicular representation of hydrates in a micromechanical model for cement paste: Prediction of early-age elasticity and strength. *Journal Acta Mechanica 203*, 3-4 (2008), 137–162.

[57] Reuss, A. Berechnung der fliessgrenze von mischkristallen auf grund der plastizitatsbedingung fur einkristalle. *Zeitschrift fur Angewandte Mathematik und Mechanik 9* (1929), 49–58.

[58] Rigby, G., and Swamy, N. Dynamic properties of hardened paste, mortar and concrete. *Materiaux et Constructions 4*, 1 (1971), 13–40.

[59] Rossler, M., and Odler, I. Investigations on the relationship between porosity, structure and strength of hydrated portland cement pastes i. effect of porosity. *Cement and Concrete Research 15* (1985), 320 – 330.

[60] Sanahuja, J., Dormieux, L., and Chanvillard, G. Modelling elasticity of a hydrating cement paste. *Cement and Concrete Research 37*, 10 (2007), 1427–1439.

[61] Sanchez-Palencia, E. *Non-homogeneous Media and Vibration Theory.* Springer-Verlag, Berlin, 1980.

[62] Scrivener, K., and Gallucci, E. Crystallisation of calcium hydroxide in early age model and ordinary cementitious systems. *Cement and Concrete Research 37* (2007), 492–501.

[63] Smilauer, V. *Elastic Properties of Hydrating Cement Paste Determined from Hydration Models.* PhD thesis, Czech Technical University Prague, 2005.

[64] Smilauer, V., and Bittnar, Z. Microstructure-based micromechanical prediction of elastic properties in hydrating cement paste. *Cement and Concrete Research 36* (2006), 1708–1718.

[65] Sorrentino, D., Vernet, C., Tenoudji, F., and Boumiz, A. Modelling the development of the elastic moduli as a function of the hydration degree of cement pastes and mortars. In *Hydration and Setting, Why does cement set? An interdisciplinary approach* (1997), A. Nonat, Ed.

[66] Staufer, D., and Aharony, A. *Introduction to Percolation Theory, 2nd Edn.* Taylor & Francis, London, 1992.

[67] Stora, E., He, Q., and Bary, B. Influence of inclusion shapes on the effective linear elastic properties of hardened cement pastes. *Cement and Concrete Research 36*, 7 (2006), 1330–1344.

[68] Sun, C., and Vaidya, R. Prediction of composite properties from a representative volume element. *Composites Science and Technology 56* (1996), 171–179.

[69] Sun, Z., Ye, G., and Shah, S. Microstructure and early-age properties of portland cement pasteeffects of connectivity of solid phases. *ACI Materials Journal 102*, 2 (2005), 122–129.

[70] Suquet, P. Elements of homogenization theory for inelastic solid mechanics. In *Homogenization techniques for Composite Media*, E. Sanchez-Palencia and A. Zaoui, Eds. Springer-Verlag, Berlin, pp. 194–275.

[71] Taplin, J. A model for following the hydration reaction in portland cement paste. *Australian Journal of Applied Science 10* (1959), 329 – 345.

[72] T.C.Powers, T. B. Studies of the physical properties of hardened portland cement paste. *J. Amer. Concr. Inst. 43* (1946).

[73] Tennis, P., and Jennings, H. A model for two types of calcium silicate hydrate in the microstructure of portland cement pastes. *Cement and Concrete Research 30*, 6 (2000), 855–863.

[74] Terada, K., Hori, M., Kyoya, T., and Kikuchi, N. Simulation of the multi-scale convergence in computational homogenization approaches. *International Journal of Solids and Structures 37*, 16 (2000), 2285–2311.

[75] Thomson, W. Measuring changes in physical properties of concrete by the dynamic method. *Proc. ASTM 40* (1940).

[76] Torrenti, J., and Benboudjema, F. Mechanical threshold of cementitious materials at early age. *Materials and Structures 38*, 3 (2005), 299–304.

[77] Velez, K., Maximilien, S., Damidot, D., Fantozzi, G., and Sorrentino, F. Determination by nanoindentation of elastic modulus and hardness of pure constituents of portland cement clinker. *Cement and Concrete Research 31* (2001), 555–561.

[78] Voigt, W. Uber die beziehung zwischen den beiden elastizitatkonstanten isotroper korper. *Wiedemanns Annalen der Physik and Chemie 38* (1889), 573–587.

[79] Wittmann, F. Estimation of the modulus of elasticity of calcium hydroxide. *Cement and Concrete Research 16*, 6 (1986), 971–972.

[80] Ye, G., Sun, Z., Voigt, T., Shah, S., and van Breughel, V. A micromechanical model for characterisation of cement paste at early age validated with

experiments. *International Symposium: Advances in Concrete through Science and Engineering, Evanston* (2004).

[81] Ye, G., van Breugel, K., and Fraaij, A. Three-dimensional microstructure analysis of numerically simulated cementitious materials. *Cement and Concrete Research 33*, 2 (2003), 215–222.

[82] Zheng, Q.-S., and Du, D.-X. An explicit and universally applicable estimate for the effective properties of multiphase composites which accounts for inclusion distribution. *Journal of the Mechanics and Physics of Solids 49*, 11 (2001), 2765–2788.